UNIVERSIDAD COMPLUTENSE DE MADRID
FACULTAD DE CIENCIAS QUÍMICAS

TESIS DOCTORAL

Nuevas estrategias farmacológicas para el tratamiento de infecciones bacterianas: proteína FtsZ y anticuerpos conjugados con antibióticos

New pharmacological strategies for the treatment of bacterial infections: FtsZ protein and antibody-drug conjugates

MEMORIA PARA OPTAR AL GRADO DE DOCTOR

PRESENTADA POR

Ana Andrea Escobar Peña

Directoras

María Luz López Rodríguez
María del Mar Martín-Fontecha Corrales

Madrid

UNIVERSIDAD COMPLUTENSE DE MADRID

FACULTAD DE CIENCIAS QUÍMICAS

NEW PHARMACOLOGICAL STRATEGIES FOR THE TREATMENT OF BACTERIAL INFECTIONS: FtsZ PROTEIN AND ANTIBODY-DRUG CONJUGATES

NUEVAS ESTRATEGIAS FARMACOLOGICAS PARA EL TRATAMIENTO DE INFECCIONES BACTERIANAS: PROTEÍNA FtsZ Y ANTICUERPOS CONJUGADOS CON ANTIBIÓTICOS

PhD candidate

Ana Andrea Escobar Peña

Advisors:

Dra. María Luz López Rodríguez

Dra. María del Mar Martín-Fontecha Corrales

MADRID, 2023

“Science is not only a disciple of reason but, also, one of romance and passion”

Stephen Hawking

A mi familia

El presente trabajo ha sido realizado en el Laboratorio de Química Médica del Departamento de Química Orgánica de la Facultad de Ciencias Químicas de la Universidad Complutense de Madrid, bajo la supervisión de la ***Catedrática María Luz López Rodríguez*** *y la* ***Prof. María del Mar Martín-Fontecha Corrales*** *a quienes deseo expresar mi afecto y mi más profundo agradecimiento por su acogida en este grupo de investigación, por sus continuas enseñanzas a lo largo de todo este tiempo, y muy especialmente, por todo el ánimo, apoyo y confianza depositados en mí. Gracias por ser mis guías durante este camino y ayudarme a llegar tan lejos.*

Asimismo, quiero expresar mi agradecimiento:

Al Dr. José Manuel Andreu del Centro de Investigaciones Biológicas (CIB) del Centro Superiores de Investigaciones Científicas (CSIC) y a su grupo de investigación, por llevar a cabo la evaluación biológica de los compuestos sintetizados en esta tesis doctoral.

Al Prof. Rafael Prados de la Universidad Autónoma de Madrid por la cálida acogida en su laboratorio y por llevar a cabo los experimentos con M. tuberculosis. Asimismo, quiero hacer extensivo este agradecimiento a todas las personas del grupo de investigación, por hacerme sentir como un miembro más. En especial, a mis amigas biólogas Laura y Vivi, por su infinita paciencia y ayuda para con esta química.

Al Ministerio de Educación de mi país de origen, El Salvador, por darme la oportunidad de estudiar en España y a todas las personas que lo hicieron posible. Al Ministerio de Educación y Formación Profesional (España) por permitirme continuar mi formación científica gracias a su beca predoctoral FPU.

A las Profesoras Silvia Ortega Gutiérrez, Bellinda Benhamú Salama, Henar Vázquez Villa y Ángeles Canales Mayordomo por su cercanía y su constante ayuda e interés.

Al Prof. Carlos Seoane Prado por contagiarme su pasión por la Química Orgánica durante mis estudios de grado y por su recomendación para entrar en el grupo de Química Médica.

A Lola, Elena, Marga y Ángel del Centro de Apoyo a la Investigación (CAI) de Resonancia Magnética Nuclear y a Cristina y Estefanía del CAI de Espectrometría de Masas de la UCM, por su inestimable asesoramiento.

A todos los compañeros de laboratorio con quienes he tenido la suerte de coincidir, con los que tan buenos momentos he compartido y de quienes he aprendido tanto durante estos años. A los que ya estaban cuando llegué y que han contribuido a crear los lazos tan importantes en el funcionamiento de este grupo, Javi, Paco, Ana, Fernando, Sergio y en especial a Débora por toda su ayuda durante mi TFG. A los que llegaron después y han sabido mantener el espíritu de compañerismo y de trabajo en equipo, Iván, Mónica, Nora, Beatriz, Benedetta, Víctor, Anabel, Estefanía, Román, Verónica, Paola, Bea, Daniel F., Daniel T. y Friederike. A mi confidente y buen amigo Jon, "el falso vasco" por tantos buenos momentos vividos, y por escucharme, apoyarme y ayudarme

en los momentos complicados. A Adrián, Stephen y Angie cuyos proyectos he tenido el honor de supervisar.

A todos mis compañeros y amigos de los diferentes grupos de investigación (los Sánchez, los Segura, los Nazario, los Sierra, los Cembe y los Orellana) con quienes he compartido muchos buenos momentos y nos hemos apoyado en los no tan buenos. A mis amigos, viejas y nuevas glorias, Cristina, Paloma, Sara, Ana V., Sergio, Elena, Jorge, Canario, Matías, Marcos, los Manus y Sergy, por tantos momentos inolvidables, por haber hecho más llevaderos los momentos difíciles y por el apoyo incondicional.

A mis eternos compañeros de aventura, Gaby, Nacho, Karla, Leo y Chave, quienes a pesar de la distancia me siguen demostrando que la amistad no entiende de fronteras. Gracias por estar siempre ahí. Los quiero.

A mi pequeña familia en Madrid, Patry y Alfonso, gracias por ser los mejores compis de piso que he podido tener, y por apoyarme y animarme siempre a seguir adelante. Nena, mil gracias por animarme en cada etapa y por asegurarte que comiera durante la recta final de la tesis. A mis incondicionales, Cris, Robert y Carlos, por tantos buenos momentos compartidos a lo largo de estos años de amistad.

A Dani, mi compañero de vida, ya que, sin todo su cariño, apoyo, ayuda y sobre todo, confianza en mí durante todos estos años no me hubiera sido posible llegar hasta aquí.

Finalmente, a toda mi familia, especialmente a mi madre, mi abuela y mis hermanos que, junto con Dios, constituyen los pilares de mi vida. Gracias por ser unos luchadores, por enseñarme a no darme nunca por vencida y, por ayudarme y animarme a cumplir mis sueños, incluso cuando eso implicaba alejarme de casa. Todo lo que soy y lo que llegue a ser se los debo a ustedes. GRACIAS

TABLE OF CONTENTS

ABBREVIATIONS AND ACRONYMS

Throughout this manuscript, abbreviations and acronyms recommended by the American Chemical Society in the Organic Chemistry and Medicinal Chemistry areas have been employed (revised in the *Journal of Organic Chemistry* and *Journal of Medicinal Chemistry* in December 2022; https://pubs.acs.org/userimages/ContentEditor/1218717864819/joceah_abbreviations.pdf and http://pubsapp.acs.org/paragonplus/submission/jmcmar/jmcmar_abbreviations.pdf). In addition, those indicated below have also been used.

AAC	Antibody-antibiotic conjugate
ADC	Antibody-drug conjugate
B. subtilis	*Bacillus subtilis*
BBC	*tert*-Butyl *N,N*-dibromocarbamate
BsFtsZ	FtsZ of *Bacillus subtilis*
CAI	Centro de Apoyo a la Investigación
Cl-NBD	4-Chloro-7-nitro-2,1,3-benzoxadiazole
DAR	Drug-to-antibody ratio
dhAA	Dehydroascorbic acid
DIAD	Diisopropyl azodicarboxylate
DIPEA	*N,N*-Diisopropylethylamine
E. coli	*Escherichia coli*
EDC	1-Ethyl-3-(3-dimethylaminopropyl)carbodiimide
EEDQ	2-Ethoxy-1-ethoxycarbonyl-1,2-dihydroquinoline
EMA	European Medicines Agency
FAR	Fluorophore-antibody ratio
FtsZ	Filamenting temperature-sensitive mutant Z
FtsZ-GFP	FtsZ fused to a green fluorescent protein
GAD	C-terminal GTPase activation domain
HATU	1-[bis(dimethylamino)methylene]-1H-1,2,3-triazolo[4,5-b]pyridinium 3-oxide
HEK 293 cells	Human Embryonic Kidney 293 cells
HEPES	4-(2-Hydroxyethyl)-1-piperazineethanesulfonic acid
HOBt	1-Hydroxybenzotriazole
K. pneumoniae	*Kleibsella pneumoniae*
M. tuberculosis x	*Mycobacterium tuberculosis*
mAb	Monoclonal antibody
mant-GTP	2'/3'-*O*-(*N*-methylanthraniloyl)-GTP
MDC	Minimal division inhibitory concentration
MW	Microwave
NBD	N-terminal nucleotide-binding domain

NHS	*N*-Hydroxysuccinimide
P. aeruginosa	*Pseudomona aeruginosa*
PABOH	*p*-Aminobenzyl alcohol
S. aureus	*Stahylococcus aureus*
SaFtsZ	FtsZ of *Staphylococcus aureus*
TBME	*tert*-Butylmethyl ether
TCEP	Tris(2-carboxyethyl)phosphine
UCM	Universidad Complutense de Madrid
VREF	Vancomycin-resistant *Enterococcus faecium*
WHO	World Health Organization

RESUMEN

RESUMEN

NUEVAS ESTRATEGIAS FARMACOLÓGICAS PARA EL TRATAMIENTO DE INFECCIONES BACTERIANAS: PROTEÍNA FtsZ Y ANTICUERPOS CONJUGADOS CON ANTIBIÓTICOS

El descubrimiento y desarrollo de antibióticos puede considerarse el avance médico más significativo del siglo XX. Sin embargo, la resistencia bacteriana supone una gran amenaza para la salud pública mundial en el siglo XXI y pone de manifiesto la necesidad de desarrollar nuevos tratamientos frente a las infecciones bacterianas.[1]

En este contexto, el objetivo principal del presente trabajo de investigación es el desarrollo de dos nuevas estrategias farmacológicas para el tratamiento de infecciones bacterianas resistentes basadas en la inhibición de la proteína de división bacteriana FtsZ y en el desarrollo de anticuerpo conjugados con antibióticos para el tratamiento de infecciones de alta incidencia, como la tuberculosis.

CAPÍTULO 1: INHIBICIÓN DE LA PROTEÍNA DE DIVISIÓN BACTERIANA FtsZ

FtsZ ha sido propuesta como una interesante diana terapéutica para el desarrollo de nuevos antibióticos ya que se encuentra en la mayoría de las bacterias conocidas y juega un papel clave en el proceso de división celular.[2-4] Por tanto, moléculas capaces de inhibir su actividad interrumpirán la viabilidad de las bacterias. Hasta el momento, se han identificado dos zonas en la proteína para la unión de moléculas pequeñas: el sitio de unión del nucleótido y un bolsillo alostérico situado entre la hélice 7 y el dominio C-terminal, al que se unen los inhibidores derivados de benzamida como PC190723 (Figura 1A).[5-7]

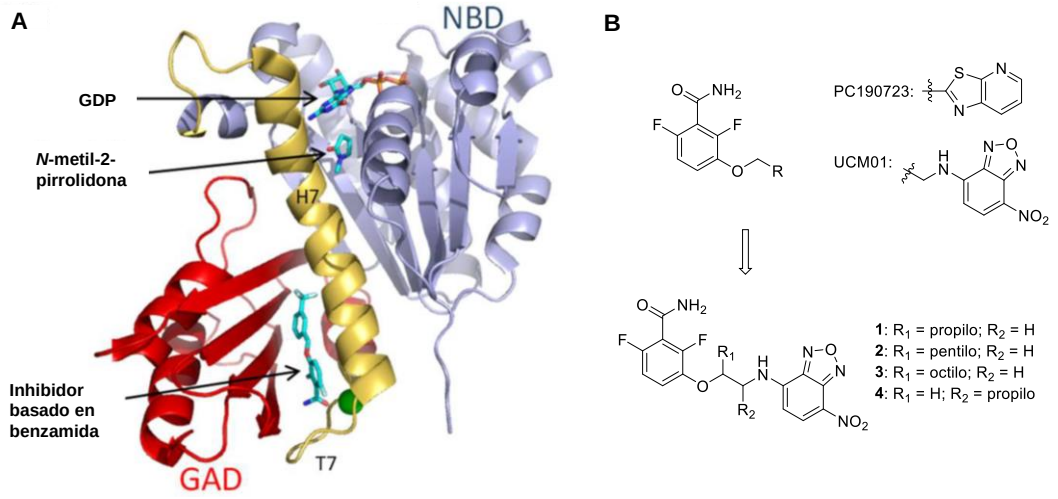

Figura 1. Diseño de las sondas fluorescentes con alta afinidad por el sitio de unión alostérico de FtsZ. (A) Estructura de FtsZ de *Staphylococcus aureus.* El dominio N-terminal de unión al nucleótido (NBD, nucleotide-binding domain) está coloreado en azul, la hélice central H7 y sus bucles flanqueantes en amarillo, y el dominio C-terminal de activación GTPasa (GAD, GTPasa activation domain) en rojo. Se muestran el nucleótido GDP, una molécula de co-disolvente de *N*-metil-2-pirrolidona y un inhibidor alostérico derivado de benzamida unidos a la proteína (PDB 6YD6). (B) Estructuras químicas de los derivados fluorescentes **1**-**4**.

La unión de moléculas pequeñas al sitio de unión alostérico de FtsZ afecta a la función de la proteína y eventualmente inhibe la división bacteriana.[8] De hecho, PC190723 (Figura 1B), el inhibidor más estudiado hasta la fecha, ha demostrado su eficacia al proteger a ratones frente a dosis letales de *S. aureus* en un modelo de infección, validando así a FtsZ como una interesante diana para el desarrollo de antibióticos.[9] Sin embargo, el perfil farmacocinético moderado de este inhibidor, junto con la rápida aparición de mutaciones, han impedido su desarrollo clínico. Además, la falta de un ensayo de unión frente a este bolsillo ha dificultado el descubrimiento de nuevos ligandos con afinidad por este sitio. En este contexto, el principal objetivo de este trabajo es el desarrollo de un ensayo de unión competitivo basado en sondas fluorescentes derivadas de PC190723 para la identificación de nuevos inhibidores alostéricos de FtsZ.

Por tanto, tomando la sonda previamente desarrollada en el grupo de investigación UCM01[10] como punto de partida, se han introducido cadenas alquílicas de diferente longitud en el espaciador entre la benzamida y el fluoróforo nitrobenzoxadiazol (NBD) para intentar mejorar la afinidad de los compuestos por FtsZ, dando lugar a los derivados fluorescentes **1**-**4** (Figura 1B). El estudio de las propiedades fluorescentes de estos derivados en presencia y ausencia de la proteína permitió evaluar su potencial como sondas químicas para desarrollar un ensayo de afinidad frente al sitio de unión a PC en *Bacillus subtilis* (*B. subtilis*). De entre los derivados analizados, destacan (*S*)-**1** y (*R*)-**4** que presentan la mayor variación de anisotropía de fluorescencia (*r*) en presencia de polímeros de FtsZ con respecto a la sonda libre (*r* = 0.172 y 0.227, respectivamente,

Figura 2A) y este parámetro recupera sus valores iniciales cuando se añade un exceso de PC190723 para desplazar la sonda (*r* = 0.065 y 0.052, respectivamente). Además, (*S*)-**1** y (*R*)-**4** son los derivados fluorescentes que presentan mayor afinidad por FtsZ (K_D = 8 y 1.9 µM, respectivamente, Figura 2B) e inhiben la división bacteriana produciendo el alargamiento de la bacteria ante su imposibilidad de dividirse a 100 y 25 µM (Figura 2C).[11]

A

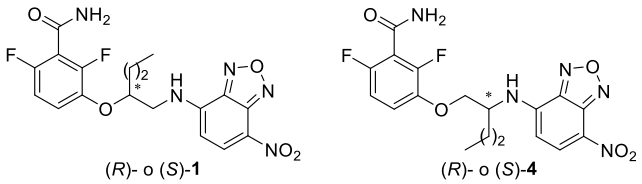

	Valores de anisotropía (*r*)					
Condiciones	**1**	**(*R*)-1**	**(*S*)-1**	**4**	**(*R*)-4**	**(*S*)-4**
Sonda libre (10 µM)	0.037	0.037	0.037	0.031	0.029	0.030
+ Bs-FtsZ (10 µM)	0.039	0.046	0.041	0.034	0.041	0.042
+ GMPCPP (0.1 mM)	0.046	0.050	0.044	0.036	0.040	0.041
+ $MgCl_2$ (10 mM)	0.157	0.081	0.172	0.203	0.227	0.096
+ PC190723 (10 µM)	0.053	0.051	0.065	0.055	0.052	0.038

B

Comp	K_D (µM) BsFtsZ	MDC (µM) *B. Subtilis*	MIC (µM) *B. Subtilis*
(*S*)-**1**	8 ± 1	100	250
(*R*)-**1**	N.D.	>100	>250
(*S*)-**4**	15 ± 2	>50	250
(*R*)-**4**	1.9 ± 0.6	25	25

C

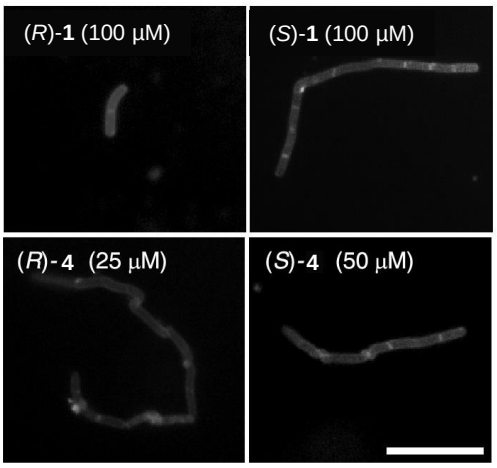

Figura 2. Caracterización de los dos enantiómeros de las sondas **1** y **4**. (A) Valores de anisotropía de fluorescencia de los nuevos derivados **1** y **4** (10 µM). (B) Valores de afinidad de unión y actividad de las sondas fluorescentes **1** y **4** en *B. subtilis*. (C) Imágenes de microscopía de fluorescencia de células de *B. subtilis* tratadas con ambos enantiómeros de **1** y **4**. Barras, 10 µm.

El ensayo de afinidad por el bolsillo alostérico de FtsZ se puso a punto con estas dos sondas y el uso de inhibidores previamente identificados como PC190723 y DFMBA permitió validar la metodología. A continuación, el ensayo de unión competitivo se

empleó en el cribado de una serie de derivados sencillos de benzamida (**19**-**28** y **33**-**41**, Figura 3) con objeto de identificar nuevos inhibidores de FtsZ. De entre todos los compuestos sintetizados, **35**, **40** y **41** mostraron las afinidades más elevadas por FtsZ [K_D(**35**) = 0.7 µM, K_D(**40**) = 1.9 µM y K_D(**41**) = 1.1 µM], siendo (*R*)-**41** el inhibidor que presentó la mayor afinidad de unión de toda la serie (K_D = 0.2 µM).

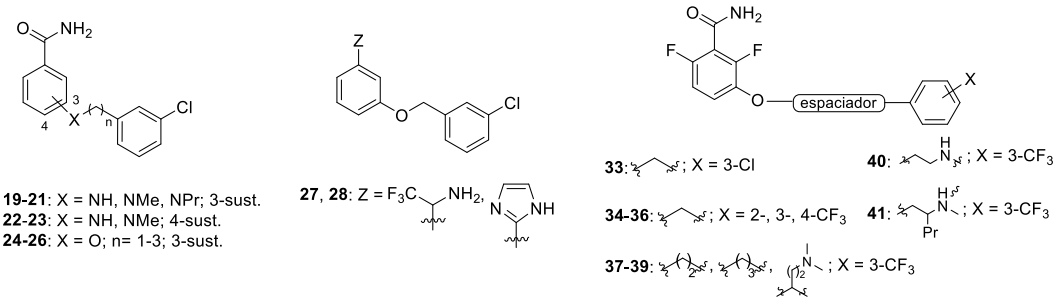

Figura 3. Estructuras de los derivados de benzamida **19**-**28** y **33**-**41** sintetizados y evaluados como inhibidores de FtsZ.

El tratamiento de *B. subtilis* con (*R*)-**41** (1 µM) produce la inhibición de la división bacteriana, dando lugar a células alargadas y a la deslocalización del anillo Z en subestructuras anómalas (Figura 4B). Por lo tanto, en este trabajo hemos puesto a punto el primer ensayo de unión competitiva dirigido al sitio de unión alostérico de FtsZ, que nos ha permitido identificar a (*R*)-**41** como el inhibidor alostérico más prometedor de la serie, con buena afinidad y actividad antibacteriana [MIC(*B. subtilis*) = 2.5 µM].[11]

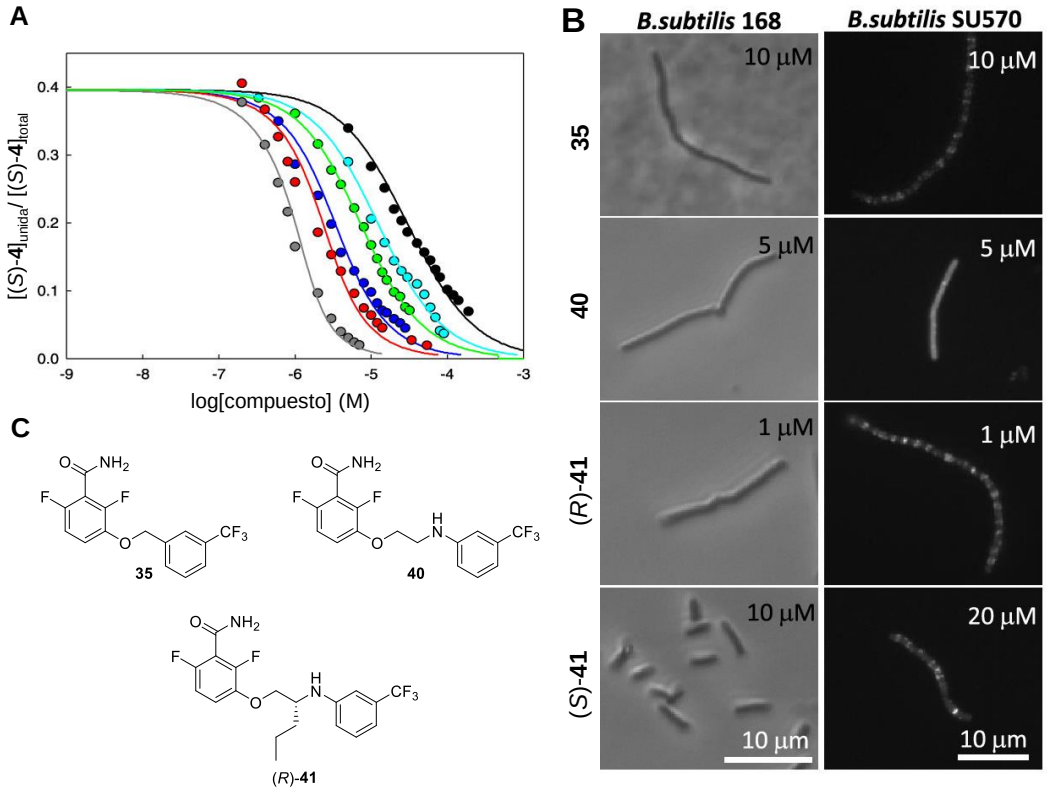

Figura 4. Inhibidores de FtsZ con afinidad y fenotipo mejorados. (A) Curvas de desplazamiento de la sonda (*R*)-**4** por los derivados **24** (negro), **35** (azul), **40** (verde), (*R*)-**41** (rojo), (*S*)-**41** (cian), y por PC190723 (gris). (B) Efectos celulares de los compuestos **35**, **40** y, (*R*)- y (*S*)-**41** en células de *B. subtilis*. Barras, 10 µm. (C) Estructuras de los inhibidores de alta afinidad **35**, **40** y (*R*)-**41**.

REFERENCIAS

1. Cook, M. A.; Wright, G. D. The past, present, and future of antibiotics. *Sci. Transl. Med.* **2022**, *14*, eabo7793.

2. Kusuma, K. D.; Payne, M.; Ung, A. T.; Bottomley, A. L.; Harry, E. J. FtsZ as an antibacterial target: status and guidelines for progressing this avenue. *ACS Infect. Dis.* **2019**, *5*, 1279-1294.

3 Bisson-Filho, A. W.; Hsu, Y. P.; Squyres, G. R.; Kuru, E.; Wu, F.; Jukes, C.; Sun, Y.; Dekker, C.; Holden, S.; VanNieuwenhze, M. S.; *et al*. Treadmilling by FtsZ filaments drives peptidoglycan synthesis and bacterial cell division. *Science* **2017**, *355*, 739-743.

4. Squyres, G. R.; Holmes, M. J.; Barger, S. R.; Pennycook, B. R.; Ryan, J.; Yan, V. T.; Garner, E. C. Single-molecule imaging reveals that Z-ring condensation is essential for cell division in *Bacillus subtilis*. *Nat. Microbiol.* **2021**, *6*, 553-562.

5. Andreu, J. M.; Huecas, S.; Araújo-Bazán, L.; Vázquez-Villa, H.; Martín-Fontecha, M. The search for antibacterial inhibitors targeting cell division protein FtsZ at its nucleotide and allosteric binding sites. *Biomedicines* **2022**, *10*, 1825.

6. Silber, N.; Matos de Opitz, C. L.; Mayer, C.; Sass, P. Cell division protein FtsZ: from structure and mechanism to antibiotic target. *Future Microbiol.* **2020**, *15*, 801-831.

7. Pradhan, P.; Margolin, W.; Beuria, T. K. Targeting the Achilles heel of FtsZ: the interdomain cleft. *Front. Microbiol.* **2021**, *12*, 732796.

8. Andreu, J. M.; Schaffner-Barbero, C.; Huecas, S.; Alonso, D.; Lopez-Rodriguez, M. L.; Ruiz-Avila, L. B.; Núñez-Ramírez, R.; Llorca, O.; Martín-Galiano, A. J. The antibacterial cell division inhibitor PC190723 is an FtsZ polymer-stabilizing agent that induces filament assembly and condensation. *J. Biol. Chem.* **2010**, *285*, 14239-14246.

9. Haydon, D. J.; Stokes, N. R.; Ure, R.; Galbraith, G.; Bennett, J. M.; Brown, D. R.; Baker, P. J.; Barynin, V. V.; Rice, D. W.; Sedelnikova, S. E.; *et al*. An inhibitor of FtsZ with potent and selective anti-staphylococcal activity. *Science* **2008**, *321*, 1673-1675

10. Artola, M.; Ruíz-Avila, L. B.; Ramírez-Aportela, E.; Martínez, R. F.; Araujo-Bazán, L.; Vázquez-Villa, H.; Martín-Fontecha, M.; Oliva, M. A.; Martín-Galiano, A. J.; Chacón, P.; *et al*. The structural assembly switch of cell division protein FtsZ probed with fluorescent allosteric inhibitors. *Chem. Sci.* **2017**, *8*, 1525-1534.

11. Huecas, S.; Araujo-Bazan, L.; Ruiz, F. M.; Ruiz-Avila, L. B.; Martinez, R. F.; Escobar-Pena, A.; Artola, M.; Vazquez-Villa, H.; Martin-Fontecha, M.; Fernandez-Tornero, C.; *et al*. Targeting the FtsZ allosteric binding site with a novel fluorescence polarization screen, cytological and structural approaches for antibacterial discovery. *J. Med. Chem.* **2021**, *64*, 5730-5745.

SUMMARY

SUMMARY

NEW PHARMACOLOGICAL STRATEGIES FOR THE TREATMENT OF BACTERIAL INFECTIONS: FtsZ PROTEIN AND ANTIBODY-DRUG CONJUGATES

The discovery and development of antibiotics was the greatest medical breakthrough of the 20th century. However, the antibacterial resistance represents a big threat for the health system in the 21st century and novel approaches to fight against resistant infections are urgently needed.[1]

In this context, the global aim of the present work is the development of new pharmacological strategies for the treatment of resistant bacterial infections based on the inhibition of the bacterial cell protein FtsZ (Chapter 1) and the development of antibody-drug conjugates for the treatment of high incidence infections, such as tuberculosis (Chapter 2).

CHAPTER 1: INHIBITION OF THE BACTERIAL CELL PROTEIN FtsZ

FtsZ protein has been proposed as an attractive new therapeutic target for the development of antibiotics since it is the central protein organizing cell division in most bacteria.[2-4] Hence, molecules able to inhibit its activity will eventually disrupt bacteria viability. To date, the main druggable pockets experimentally identified of FtsZ are the nucleotide-binding site, and the interdomain cleft located between H7 and the C-terminal domain, where the allosteric benzamide inhibitors, such as PC190723, bind (Figure 1).[5-7]

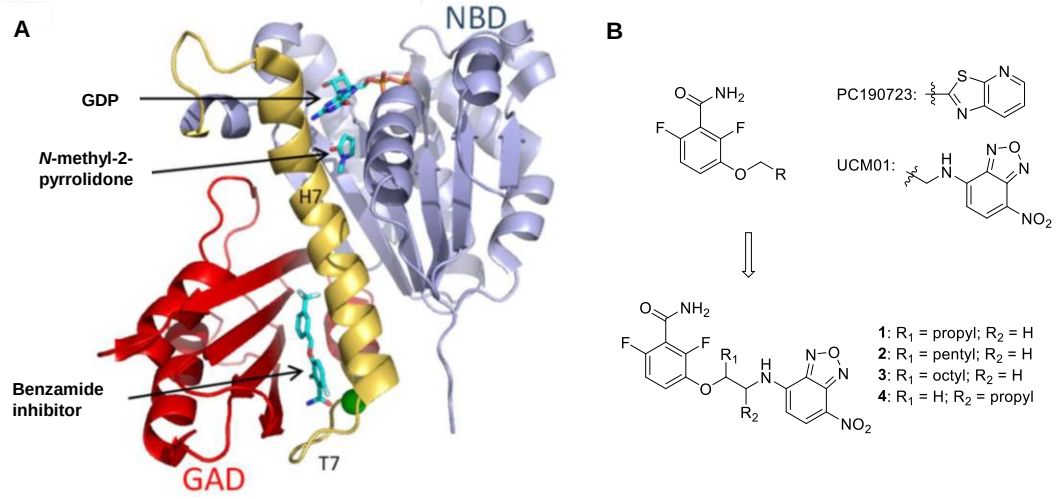

Figure 1. Design of fluorescence probes with high affinity for the FtsZ allosteric binding site. (A) Structure of *Staphylococcus aureus* FtsZ. The N-terminal nucleotide-binding domain (NBD) is colored blue, the central helix H7 and its flanking loops yellow, and the C-terminal GTPase activation domain (GAD) red. The bound GDP nucleotide, a co-solvent molecule of *N*-methyl-2-pyrrolidone and one benzamide allosteric inhibitor are shown (PDB 6YD6). (B) Chemical structures of fluorescent derivatives **1**-**4**.

Binding of small molecules to FtsZ by an allosteric mechanism impair its function and eventually inhibit bacterial division.[8] Indeed, the promising results obtained by PC190723 in protecting mice from lethal dose of *S. aureus* in a model of infection, validated FtsZ as a target for antibacterial intervention.[9] However, its unsuitable pharmacological properties and high frequency of resistance mutation have impeded its clinical development. Moreover, the lack of a binding assay against this pocket has hampered the discovery of new ligands with affinity for this site. In this context, the main objective of this work is the development of a competitive binding assay based on fluorescent probes, based on the most studied inhibitor PC190723, for the identification of new allosteric inhibitors of FtsZ.

Thus, the fluorescent probe previously developed in our research group, UCM01[10] was taken as starting point to design new probes with higher FtsZ affinity, and derivatives **1**-**4** bearing alkyl chains of different lengths in the spacer between the benzamide and the fluorophore were synthesized (Figure 1B). The potential of the synthesized fluorescent derivatives **1**-**4** as chemical tools to develop a binding assay against the FtsZ PC-binding site of *Bacillus subtilis* (*B. subtilis*) was evaluated by the assessment of their fluorescent properties. Among them, (*S*)-**1** and (*R*)-**4** stand up as the fluorescent probes that exhibited the highest variation of fluorescence anisotropy (*r*) in the presence of FtsZ polymers with respect to the free probe (*r* = 0.172 and 0.227, respectively, Figure 2A) and this parameter recovered the initial anisotropy values after the addition of an excess of competing PC190723 (*r* = 0.065 and 0.052, respectively). In addition, derivatives (*S*)-**1** and (*R*)-**4** showed high affinity for FtsZ (K_D = 8 and 1.9 µM, respectively, Figure 2B) and

antibacterial activity in *B. subtilis* with minimal division inhibitory concentration (MDC) of 25 and 100 µM, respectively (Figure 2C).[11]

A

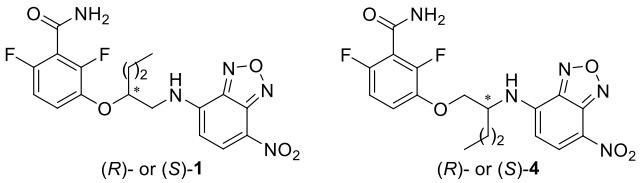

	Anisotropy values (*r*)					
Conditions	**1**	**(*R*)-1**	**(*S*)-1**	**4**	**(*R*)-4**	**(*S*)-4**
Free probe (10 µM)	0.037	0.037	0.037	0.031	0.029	0.030
+ Bs-FtsZ (10 µM)	0.039	0.046	0.041	0.034	0.041	0.042
+ GMPCPP (0.1 mM)	0.046	0.050	0.044	0.036	0.040	0.041
+ $MgCl_2$ (10 mM)	0.157	0.081	0.172	0.203	0.227	0.096
+ PC190723 (10 µM)	0.053	0.051	0.065	0.055	0.052	0.038

B

Compd	K_D (µM) BsFtsZ	MDC (µM) *B. Subtilis*	MIC (µM) *B. Subtilis*
(*S*)-**1**	8 ± 1	100	250
(*R*)-**1**	N.D.	>100	>250
(*S*)-**4**	15 ± 2	>50	250
(*R*)-**4**	1.9 ± 0.6	25	25

C

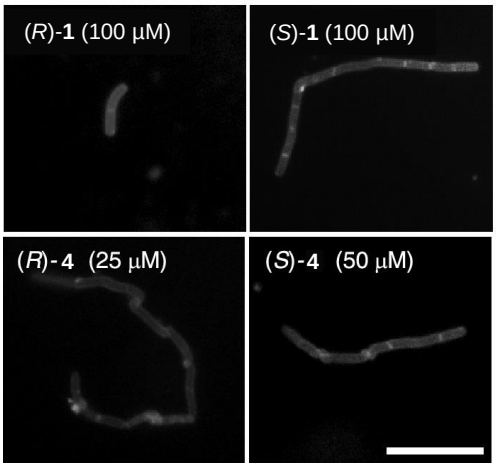

Figure 2. Characterization of both enantiomers of probes **1** and **4**. (A) Fluorescence anisotropy values of new NBD-derivatives **1** and **4** (10 µM). (B) Binding affinity and activity values of the fluorescent probes **1** and **4** on *B. subtilis*. (C) Fluorescence microscopy images of *B. subtilis* cells treated with both enantiomers of **1** and **4**. Bars, 10 µm.

The affinity binding assay was developed with these two probes and validated with FtsZ inhibitors previously identified, such as PC190723 and DFMBA. Once the new methodology was validated, it was employed to identify new FtsZ allosteric inhibitors, in a series of new benzamide derivatives **19**-**28** and **33**-**41** synthesized in this thesis (Figure 3). Among them, derivatives **35**, **40** and **41** exerted high binding affinities [K_D(**35**) = 0.7 µM, K_D(**40**) = 1.9 µM and K_D(**41**) = 1.1 µM], whereas the evaluation of the enantiomers of

41 revealed that compound (*R*)-**41** displayed the highest binding affinity of the series with K_D = 0.2 µM.

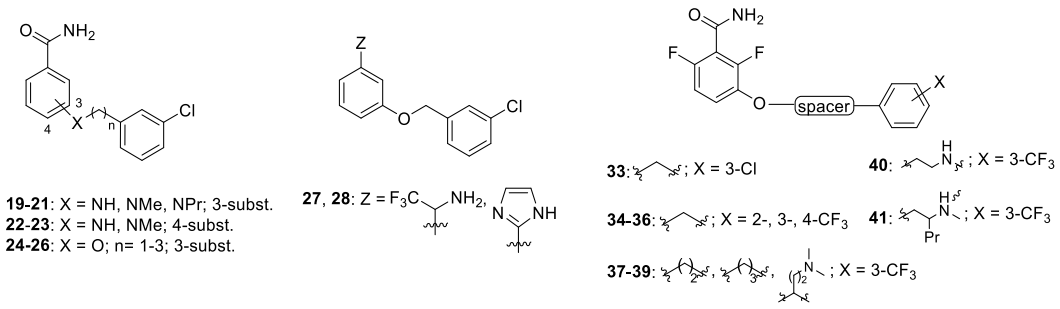

Figure 3. Chemical structures of benzamide derivatives **19**-**28** and **33**-**41** synthesized and evaluated as FtsZ inhibitors.

Cytological profiling of the high-affinity compound (*R*)-**41** showed that bacteria exposed to this derivative (1 µM) exhibited the characteristic filamentous phenotype due to the cell division inhibition. Moreover, (*R*)-**41** impaired the normal assembly of FtsZ-GFP into the midcell Z-ring prior to division of *B. subtilis* SU570, supporting FtsZ targeting (Figure 4). Therefore, we have successfully set up the first competitive binding assay targeting the interdomain cleft of FtsZ, which has allowed us to identify derivative (*R*)-**41** as the most promising allosteric inhibitor, with good binding affinity and antibacterial activity [MIC(*B. subtilis*) = 2.5 µM].[11]

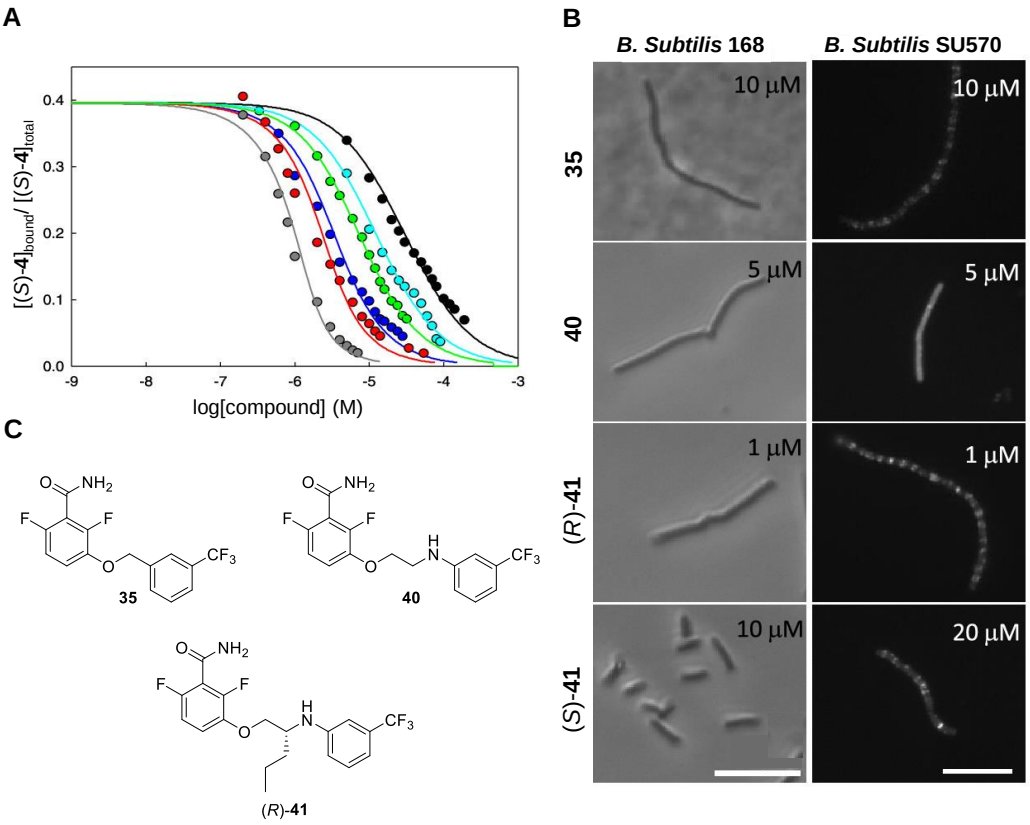

Figure 4. FtsZ inhibitors with enhanced affinity and phenotype. (A) Displacement curves of probe (*R*)-**4** by synthetic derivatives **24** (black), **35** (blue), **40** (green), (*R*)-**41** (red), (*S*)-**41** (cyan), and by PC190723 (gray). (B) Cellular effects of compounds **35**, **40** and, (*R*)- and (*S*)-**41** on *B. subtilis* cells. Bars, 10 µm. (C) Structures of the high-affinity inhibitors **35**, **40** and (*R*)-**41**.

REFERENCES

1. Cook, M. A.; Wright, G. D. The past, present, and future of antibiotics. *Sci. Transl. Med.* **2022**, *14*, eabo7793.

2. Kusuma, K. D.; Payne, M.; Ung, A. T.; Bottomley, A. L.; Harry, E. J. FtsZ as an antibacterial target: status and guidelines for progressing this avenue. *ACS Infect. Dis.* **2019**, *5*, 1279-1294.

3 Bisson-Filho, A. W.; Hsu, Y. P.; Squyres, G. R.; Kuru, E.; Wu, F.; Jukes, C.; Sun, Y.; Dekker, C.; Holden, S.; VanNieuwenhze, M. S.; *et al*. Treadmilling by FtsZ filaments drives peptidoglycan synthesis and bacterial cell division. *Science* **2017**, *355*, 739-743.

4. Squyres, G. R.; Holmes, M. J.; Barger, S. R.; Pennycook, B. R.; Ryan, J.; Yan, V. T.; Garner, E. C. Single-molecule imaging reveals that Z-ring condensation is essential for cell division in *Bacillus subtilis*. *Nat. Microbiol.* **2021**, *6*, 553-562.

5. Andreu, J. M.; Huecas, S.; Araújo-Bazán, L.; Vázquez-Villa, H.; Martín-Fontecha, M. The search for antibacterial inhibitors targeting cell division protein FtsZ at its nucleotide and allosteric binding sites. *Biomedicines* **2022**, *10*, 1825.

6. Silber, N.; Matos de Opitz, C. L.; Mayer, C.; Sass, P. Cell division protein FtsZ: from structure and mechanism to antibiotic target. *Future Microbiol.* **2020**, *15*, 801-831.

7. Pradhan, P.; Margolin, W.; Beuria, T. K. Targeting the Achilles heel of FtsZ: the interdomain cleft. *Front. Microbiol.* **2021**, *12*, 732796.

8. Andreu, J. M.; Schaffner-Barbero, C.; Huecas, S.; Alonso, D.; Lopez-Rodriguez, M. L.; Ruiz-Avila, L. B.; Núñez-Ramírez, R.; Llorca, O.; Martín-Galiano, A. J. The antibacterial cell division inhibitor PC190723 is an FtsZ polymer-stabilizing agent that induces filament assembly and condensation. *J. Biol. Chem.* **2010**, *285*, 14239-14246.

9. Haydon, D. J.; Stokes, N. R.; Ure, R.; Galbraith, G.; Bennett, J. M.; Brown, D. R.; Baker, P. J.; Barynin, V. V.; Rice, D. W.; Sedelnikova, S. E.; *et al*. An inhibitor of FtsZ with potent and selective anti-staphylococcal activity. *Science* **2008**, *321*, 1673-1675

10. Artola, M.; Ruíz-Avila, L. B.; Ramírez-Aportela, E.; Martínez, R. F.; Araujo-Bazán, L.; Vázquez-Villa, H.; Martín-Fontecha, M.; Oliva, M. A.; Martín-Galiano, A. J.; Chacón, P.; *et al*. The structural assembly switch of cell division protein FtsZ probed with fluorescent allosteric inhibitors. *Chem. Sci.* **2017**, *8*, 1525-1534.

11. Huecas, S.; Araujo-Bazan, L.; Ruiz, F. M.; Ruiz-Avila, L. B.; Martinez, R. F.; Escobar-Pena, A.; Artola, M.; Vazquez-Villa, H.; Martin-Fontecha, M.; Fernandez-Tornero, C.; *et al*. Targeting the FtsZ allosteric binding site with a novel fluorescence polarization screen, cytological and structural approaches for antibacterial discovery. *J. Med. Chem.* **2021**, *64*, 5730-5745.

GENERAL INTRODUCTION

GENERAL INTRODUCTION. ANTIBIOTIC RESISTANCE

The discovery and development of antibiotics was the greatest medical breakthrough of the 20th century. Their introduction into the clinical use allowed rapid treatment of patients with previously fatal bacterial infections and, consequently, led to a significant increase in the life expectancy of the population. Moreover, these drugs made possible many medical procedures such as cancer treatments, organ transplantation, and complex surgeries.[1]

Most classes of antibiotics in current clinical use were discovered during a period of extensive research and development known as the "Golden Age" of antibiotic discovery from the 1940s to the 1960s. Thereafter, a gradual decline in the identification and development of antibiotics was occurred, with the lipopeptides being the last class of antibiotic discovered in 1987.[2] This scenario has been aggravated by the misuse of existing antibiotics, leading us to a critical situation in which many human pathogens have evolved to evade or tolerate the effects of the drugs designed to kill them through a phenomenon known as antimicrobial resistance, causing infectious diseases that we considered controlled to become difficult to treat and even lethal.[3]

Antimicrobial resistance has emerged as one of the leading public health threats of the 21st century, being particularly worrying the antibiotic resistance.[4] Antibacterial resistance occurs naturally when changes in bacteria cause the drugs used to treat infections to become less effective, either due to errors in DNA replication leading to mutations or the acquisition of resistance genes mobilized through plasmids or transposons (Figure 1).[1] However, factors such as high rates of antimicrobial prescriptions, antibiotic mismanagement, in the form of self-medication or interruption of therapy, and large-scale antibiotic use as growth promotors in livestock farming can accelerate the emergence of resistance.[3,4] The rapid increase in antibacterial resistance, particularly in low- and middle-income countries, is causing significant levels of mortality and morbidity.[5] Indeed, 1.2 million deaths were directly attributable to antibiotic resistance in 2019,[4] and a previous study estimates that unless action is taken soon, there will be 10 million deaths each year due to antibiotic resistance by 2050.[6]

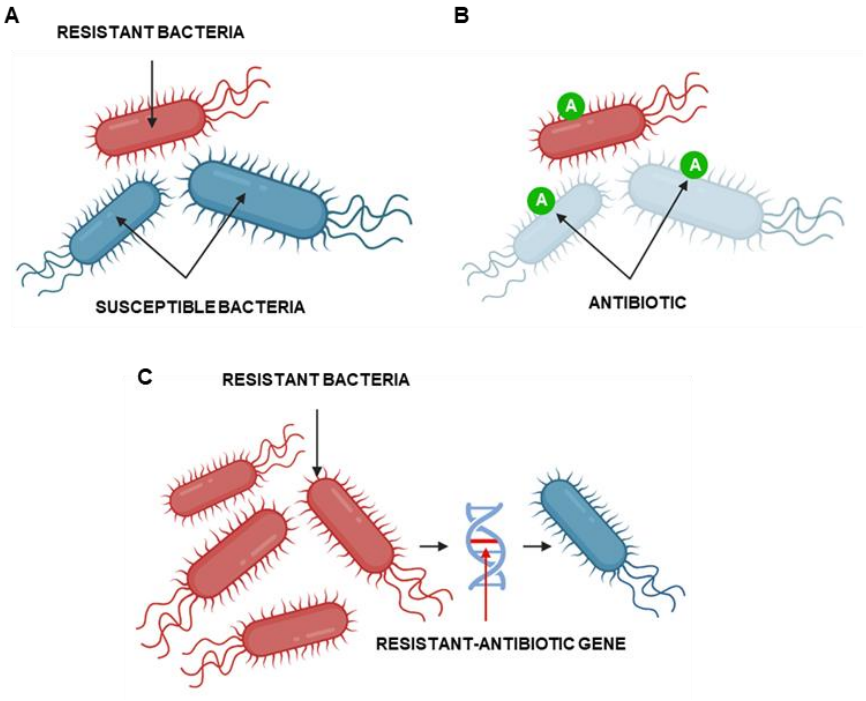

Figure 1. Antibiotic resistance. (A) Some bacteria develop mutations that make them resistant to antibiotic. (B) Antibiotics kill non-resistant bacteria. (C) Resistant bacteria proliferate and transmit their mutations to offspring. In addition, the bacteria can transfer the antibiotic-resistant gene to other bacteria via plasmid or transposon.

Global public health agencies such as the World Health Organization (WHO) and the Center for Disease, Control, and Prevention (CDC) have released reports warning of an impending crisis due to antibiotic resistance.[5,7] Among the urgent needs identified by these agencies to minimize the impact of this crisis is the development of new antibiotics with novel mechanisms of action (MoA), especially for the highly virulent and antibiotic resistant pathogens such as *Stahylococcus aureus* (*S. aureus*), *Kleibsella pneumoniae* (*K. pneumoniae*), *Pseudomona aeruginosa* (*P. aeruginosa*), *Mycobacterium tuberculosis* (*M. tuberculosis*), among others.[8] According to WHO annual analyses, the current clinical antibacterial pipeline contains 45 antibiotics, of which, approximately one-quarter are directed toward new targets or represent new chemical scaffolds. Moreover, 32 non-traditional antibacterial agents including bacteriophages, antimicrobial peptides, and antibodies, are in clinical trials.[9] Despite research and development on new antibacterial agents[9,10] is vital to fight against bacterial antimicrobial resistance, it is not enough on its own. To efficiently address the problem of bacterial resistance, it is necessary to develop better infection prevention and control programs, to make appropriate use of existing antibiotics in humans and animals, as well as the rational use of any new antibiotics developed in the future.[4]

In this context, we propose herein the development of two new pharmacological strategies to tackle the issue of antibacterial resistance based on the inhibition of the bacterial division protein filamenting temperature-sensitive mutant Z (FtsZ) protein, which is an unexplored bacterial target (Chapter 1), and the use of a drug delivery approach, for example antibody-drug conjugates (ADC), for the treatment of infectious diseases of great incidence, such as tuberculosis (TB) (Chapter 2).

1. REFERENCES

1. Cook, M. A.; Wright, G. D. The past, present, and future of antibiotics. *Sci. Transl. Med.* **2022**, *14*, eabo7793.

2. Durand, G. A.; Raoult, D.; Dubourg, G. Antibiotic discovery: history, methods and perspectives. *Int. J. Antimicrob. Agents* **2019**, *53*, 371-382.

3. *Antibiotic resistance*. World Health Organization, 2020. https://www.who.int/news-room/fact-sheets/detail/antibiotic-resistance (accessed Dec 2022).

4. Murray, C. J. L.; Ikuta, K. S.; Sharara, F.; Swetschinski, L.; Robles Aguilar, G.; Gray, A.; Han, C.; Bisignano, C.; Rao, P.; Wool, E.*; et al.* Global burden of bacterial antimicrobial resistance in 2019: a systematic analysis. *Lancet* **2022**, *399*, 629-655.

5. *Monitoring and evaluation of the global action plan on antimicrobial resistance*. World Health Organization, 2019. https://www.who.int/publications/i/item/monitoring-and-evaluation-of-the-global-action-plan-on-antimicrobial-resistance (accessed Dec 2022).

6. O'Neill, J. *Tackling drug-resistant infections globally: final report and recommendations*; Government of the United Kingdom, 2016.

7. *Antibiotic resistance threats in the United States, 2019*. Centers for Disease, Control Prevention, 2019. https://www.cdc.gov/drugresistance/pdf/threats-report/2019-ar-threats-report-508.pdf (accessed Dec 2022).

8. *WHO publishes list of bacteria for which new antibiotics are urgently needed*. World Health Organization, 2017. https://www.who.int/news/item/27-02-2017-who-publishes-list-of-bacteria-for-which-new-antibiotics-are-urgently-needed (accessed Dec 2022).

9. *2021 Antibacterial agents in clinical and preclinical development: an overview and analysis*. World Health Organization, 2022. https://www.who.int/publications/i/item/9789240047655 (accessed Dec 2022).

10. Theuretzbacher, U.; Piddock, L. J. V. Non-traditional Antibacterial Therapeutic Options and Challenges. *Cell Host Microbe* **2019**, *26*, 61-72.

CHAPTER 1

INHIBITION OF THE BACTERIAL CELL PROTEIN FtsZ

INTRODUCTION

1. INTRODUCTION AND OBJECTIVES

The growing threat of bacterial resistance is putting the health of the population at risk and highlights the urgent need for developing new antibiotics to treat common infectious diseases for which current drugs do not seem to be effective. In this regard, the inhibition of essential processes for bacterial reproduction and spreading, such as bacterial cell division, remain still clinically unexploited. In particular, the best characterized cell division protein FtsZ, has been identified as a potential new therapeutic target for the treatment of infectious diseases.

1.1. FtsZ and the divisome

Bacterial division is a complex process that involves several steps such as replication and segregation of chromosomal DNA, elongation of the cell wall and formation of a division septum at the midcell to generate the two identical daughter cells. All these cellular processes are coordinated by a macromolecular structure composed for more than 20 regulating proteins, known as the divisome.[1,2]

The divisome is initiated by the recruitment of the tubulin homologue protein FtsZ at the division site where this protein self-polymerizes into a discontinuous ring-like structure known as the Z-ring, which is a highly dynamic structure that functions as a scaffold for the assembly of the remaining division proteins.[3-5] FtsZ polymerization occurs in a guanosine 5'-triphosphate (GTP)-dependent manner, forming linear protofilaments in a head-to-tail arrangement that eventually form the Z-ring. On the other hand, these straight filaments acquire a curve conformation and disassemble upon hydrolysis of GTP to guanosine 5'-diphosphate (GDP).[6,7] FtsZ subunits within the Z-ring are in continuous exchange with monomers from the cytoplasmic pool, with a turnover half time of approximately 8 seconds in *Escherichia coli* (*E. coli*) and *Bacillus subtilis* (*B. subtilis*),[8] resulting in a directional movement around the site of septum formation called treadmilling, in which FtsZ monomers are added to one end of the filament while simultaneously being removed from the opposite end.[9-11]

Although the specific organization of the Z-ring is still unclear, it seems that this structure is affected by a lot of regulatory proteins to promote efficient assembly of the cell division machinery and ensure orderly progression through the cell cycle.[12-14] Among these regulatory factors, the nucleoid occlusion (NO) and the minicell (Min) systems, together with EzrA protein, stand out as negative regulators and are the responsible for placing the Z-ring at the midcell when the bacterium is big enough to divide. The NO system prevents FtsZ assembly over the unsegregated chromosomes, Min proteins impede the formation of Z-ring in the regions near the cell poles and ErzA inhibits aberrant FtsZ assembly through the longitudinal axis of the cell. On the other hand, membrane tether proteins FtsA and ZapA, along with ZipA and SepF are positive regulators that stabilize FtsZ assembly. Furthermore, modulators such as UgtP, SulA and MciZ control the bacterial division depending on the environment of the cell. For instance, under nutritional starvation, UgtP does not inhibit FtsZ assembly and the divisome is formed earlier with the consequent production of smaller daughter cells.[4] Table 1 summarizes some of the FtsZ polymerization regulatory proteins.

Table 1. FtsZ and the proteins that modulate its assembly (adapted from reference 12).

Protein	**Role**
Assembly of the Z-ring	
FtsZ	A structural subunit of the Z-ring that is required for initiation of cell division and serves as a scaffold for divisome assembly
FtsA	A principal membrane tether that is required for Z-ring assembly, organization of FtsZ polymers and recruitment of downstream proteins
ZipA	Promotes Z-ring assembly and is a secondary membrane anchor
Regulators of the Z-ring dynamics	
ZapA	A positive modulator of Z-ring assembly and stability
ZapB	Has a redundant role in ensuring proper Z-ring assembly
SepF	Has an overlapping role with FtsA in Z-ring assembly and is required for proper septal morphology
EzrA	A negative regulator of Z-ring assembly throughout the cell membrane that contributes to midcell Z-ring dynamics and has a role in coordinating cell elongation with division
Cell cycle-responsive regulators	
UgtP	A growth rate-dependent inhibitor of cell division
SulA	A cell division inhibitor of the SOS response that prevents the assembly of new Z-rings and facilitates the disassembly of existing Z-rings
MciZ	Contributes to the inhibition of Z ring assembly following the initiation of sporulation
Regulators of the Z-ring assembly	
Min system	A negative regulator of Z-ring assembly that prevents the formation of new Z-rings in the regions near the cell poles
NO system	A negative regulator of Z-ring assembly that prevents premature division events over unsegregated nucleoids

1.2. FtsZ as an antibacterial target

FtsZ is the central protein organizing cell division in most bacteria. This GTPase is almost universally conserved throughout the bacteria and shows a remarkable similarity to the eukaryotic tubulin despite its only 20% sequence homology.[15-17] Unlike tubulin, which is a known target for many anticancer drugs, the discovery of new useful antibiotics targeting FtsZ remains a challenge. To date, the fact that only a few FtsZ-small molecule complex structures have been reported[18,19] in comparison to over a hundred tubulin-inhibitor complexes,[20] suggests a lower degree of druggability for FtsZ. Nevertheless, considerable knowledge has accumulated on the structure, assembly dynamics and function of FtsZ filaments and the Z-ring, the FtsZ partner proteins, and several small molecule chemotypes that specifically interact with FtsZ.

The crystal structure of FtsZ revealed that this protein contains two globular domains: an N-terminal nucleotide-binding domain (NBD) and a C-terminal GTPase activation domain (GAD), joined by the central core helix H7 (Figure 1).[15,21] The GTPase activity of this protein depends on FtsZ polymerization since its catalytic pocket is formed during the assembly of FtsZ monomers into filaments.[22] The C-terminal GTPase-activating domain of the upper subunit contacts the nucleotide site of the subunit below by insertion of the T7 loop into the nucleotide-binding site, which leads to the formation of the enzymatic pocket. In addition, the conformational changes that FtsZ undergoes in the transition from the monomeric to the polymeric state, open an interdomain cleft located between H7 and the C-terminal domain, where the allosteric benzamide inhibitors bind. This cleft is structurally distinct to tubulin and provides a different pocket for ligands binding.[23,24]

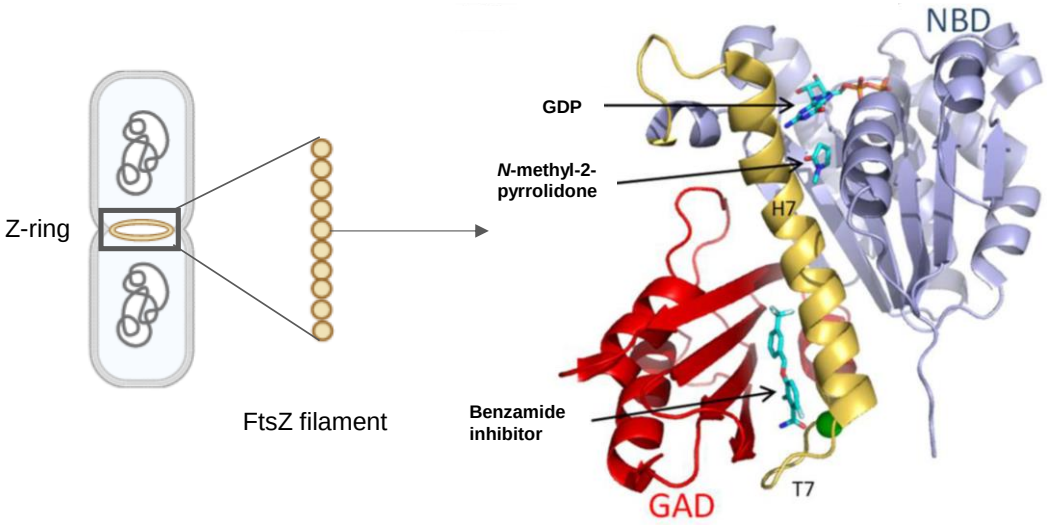

Figure 1. Structure of one *Staphylococcus aureus* FtsZ filament subunit. The N-terminal nucleotide-binding domain (NBD) is colored blue, the central helix H7 and its flanking loops yellow, and the C-terminal GTPase activation domain (GAD) red. The bound GDP nucleotide, a co-solvent molecule of *N*-methyl-2-pyrrolidone and one benzamide allosteric inhibitor are shown (PDB 6YD6).

Considering the key role of FtsZ in the bacterial division, this protein was soon deemed as an attractive target for the development of clinically efficacious antibiotics with an unexplored MoA. In fact, FtsZ was validated as a target for bacterial infections with the development of the benzamide inhibitor PC190723. However, FtsZ inhibitors have not reached the clinic yet although extensive screenings using phenotypic assays or *in silico* studies have allowed the identification of several small molecules with antibacterial activity capable of interfering with FtsZ functions.[12,25-28] The slow progress in this field can be explained by the scarce number of inhibitors that have been experimentally proven to specifically interact with the protein.[24] The limited number of reported compounds that effectively act on FtsZ either by disrupting its GTPase activity or the assembly/disassembly dynamics of the Z-ring, include both natural and synthetic products and have been identified by high throughput screening (HTS) or specifically developed to inhibit FtsZ.

Currently, the main druggable pockets experimentally identified of FtsZ are the nucleotide-binding site and the interdomain cleft (Figure 1), thus FtsZ inhibitors can be classified according to the binding site they bind to. Moreover, there are selective inhibitors with minimum inhibitory concentration (MIC) in the micromolar range such as zantrin Z3 and PC170942 whose binding sites are still unknown (Figure 2).[29,30]

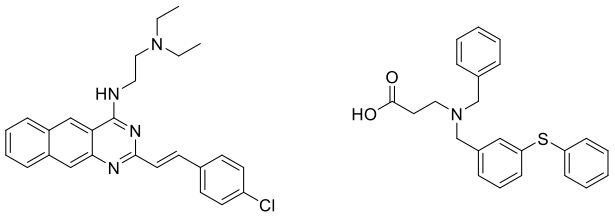

Zantrin Z3 — MIC(*B. subtilis*) = 2.5 μM

PC170942 — MIC(*B. subtilis*) = 42 μM

Figure 2. FtsZ unknown-binding site inhibitors.

1.2.1. Inhibitors targeting the nucleotide-binding site

The GTP-binding site of FtsZ is a highly conserved region among different bacterial species due to the fact that GTP recognition and its subsequent hydrolysis are essential for proper FtsZ functions.[25] This feature become to FtsZ in a suitable target for designing of broad-spectrum antibacterial agents. Some compounds that have been demonstrated to interact to FtsZ through its GTP-binding site are shown in Figure 3.

One of the main strategies to alter FtsZ polymerization is to perturb the GTPase activity of the protein. Therefore, an approach in the development of FtsZ inhibitors was the design of GTP analogues. Despite the structural similarity of FtsZ and tubulin nucleotide-binding pockets, C8-substituted GTP derivatives, such as 8-bromo-GTP and 8-methoxy-GTP, successfully inhibited FtsZ polymerization *in vitro* without affecting microtubule assembly, confirming that selective inhibition of the GTP-binding site of this bacterial protein is possible without unwanted side effects in eukaryotic cells.[18,31] Unfortunately, these GTP

analogues lack antibacterial activity probably due to their poor penetration through the bacterial cell wall.

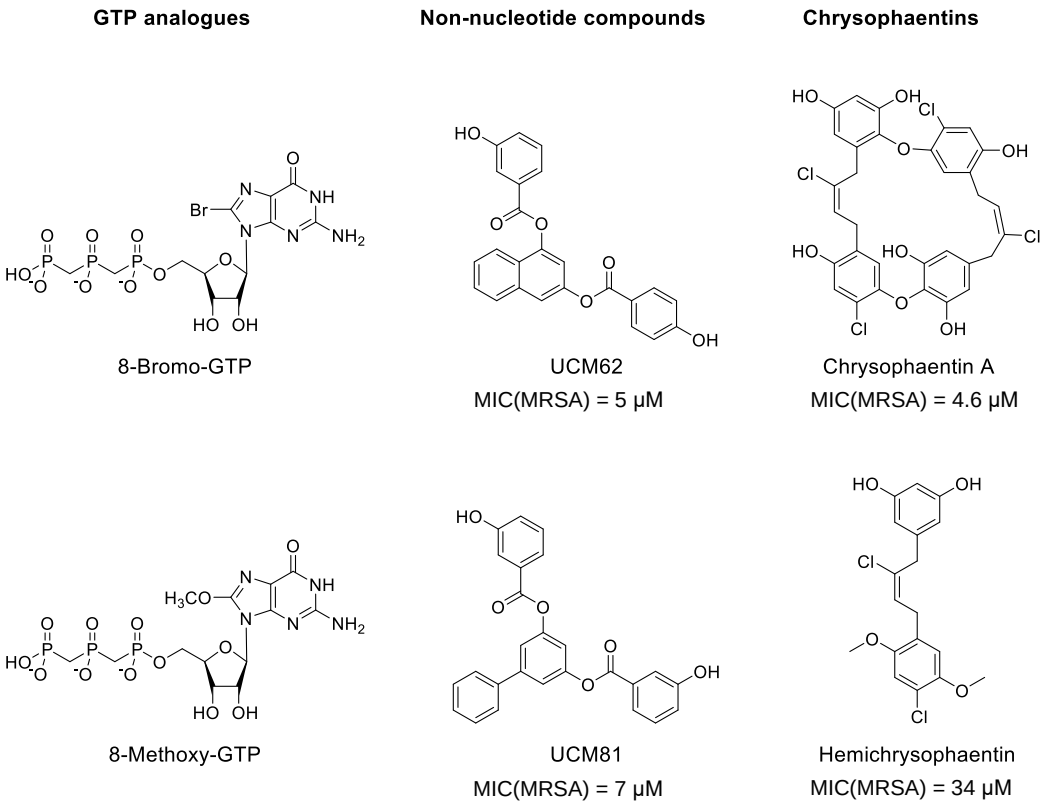

Figure 3. FtsZ inhibitors that bind to the GTP-binding site: GTP analogues, non-nucleotide compounds, and chrysophaentins. MRSA: methicillin-resistant *S. aureus*.

In the next years, site-directed approaches were outlined as a good alternative to HTS for identifying molecules able to inhibit FtsZ function. In particular, the development and validation of a competitive binding assay based on the fluorescence anisotropy changes of 2'/3'-*O*-(*N*-methylanthraniloyl)-GTP (*mant*-GTP) upon binding to nucleotide-free FtsZ,[32] allowed the identification of GTP-replacing ligands such as the polyhydroxy aromatic compounds UCM62 and UCM81, developed by the Medicinal Chemistry Laboratory at Universidad Complutense de Madrid (UCM). These ligands represent the first non-nucleotide synthetic molecules that effectively compete with GTP for binding to FtsZ with affinity constants (K_D) in the submicromolar range in FtsZ from *B. subtilis* [K_D(BsFtsZ) = 0.8 and 0.5 μM, respectively] and high antibacterial activity in methicillin-resistant *S. aureus* (MRSA) (MIC = 5 and 7 μM, respectively). In addition, these compounds act as FtsZ assembly modifiers and lead to filamentous undivided cells, with the consequent disruption of bacterial viability without affecting eukaryotic tubulin.[33,34]

Other examples of inhibitors of the nucleotide-binding site of FtsZ are the natural product isolated from the marine algae *Chrysophaeum taylorii*, chrysophaentin A, and its synthetic derivative hemichrysophaentin. These compounds were identified by the fluorescence *mant*-GTP competitive assay and display antibacterial activity against Gram-positive pathogens, such as MRSA and vancomycin-resistant *Enterococcus faecium* (VREF) by blocking the GTPase activity and polymerization of the protein.[35,36] Nuclear magnetic resonance studies have validated the GTP-binding site of FtsZ as the binding pocket of these two derivatives.

1.2.2. Interdomain cleft inhibitors

The interdomain cleft of FtsZ is not a highly conserved region across different bacterial species, hampering the design and development of broad-spectrum inhibitors with affinity for this binding site. The different amino acid composition, as well as the structural variability of this area, suggest that the interdomain cleft is a suitable pocket for the development of species-specific inhibitors.

Benzamide-based compounds are the main class of FtsZ inhibitors that are known to interact with this interdomain cleft. The discovery of the ability of 3-methoxybenzamide (3-MBA) to inhibit the proliferation of *B. subtilis* by targeting FtsZ sparked interest in this class of compounds and, although 3-MBA exhibited low antibacterial activity [MIC(*B. subtilis*) = 26.5 mM], this compound became an attractive starting point for the development of new FtsZ inhibitors,[37] leading to the potent FtsZ difluorobenzamide derivative PC190723 [MIC(*S. aureus*) = 2.8 µM] (Figure 4).[38-40] PC190723 acts as an FtsZ polymer-stabilizing agent that modulates the flexibility and assembly of the protein, inhibits the GTPase activity at 10 µM and is a selective bactericide.[41] However, the promising results obtained by this compound in protecting mice from lethal dose of *S. aureus* in a model of infection, which validated FtsZ as a target for antibacterial intervention,[42] were not translated into the clinic probably due to its unsuitable pharmacological properties and high frequency of resistance mutations.

To improve the pharmacological properties of PC190723, different derivatives and prodrugs have been developed (Figure 4). Among them, an oxazole-benzamide derivative and TXA707 showed higher antibacterial activity in *S. aureus* than PC190723 (MIC = 0.3 and 1.3 µM, respectively).[43] Moreover, compound TXA707 and its prodrug TXA709 exhibited *in vivo* efficacy against MRSA in a mouse model of infection.[44,45] Indeed, TXA709 was designated as a qualified infectious disease product by the US Food and Drug Administration (FDA) and has recently completed a phase I clinical trial.[46]

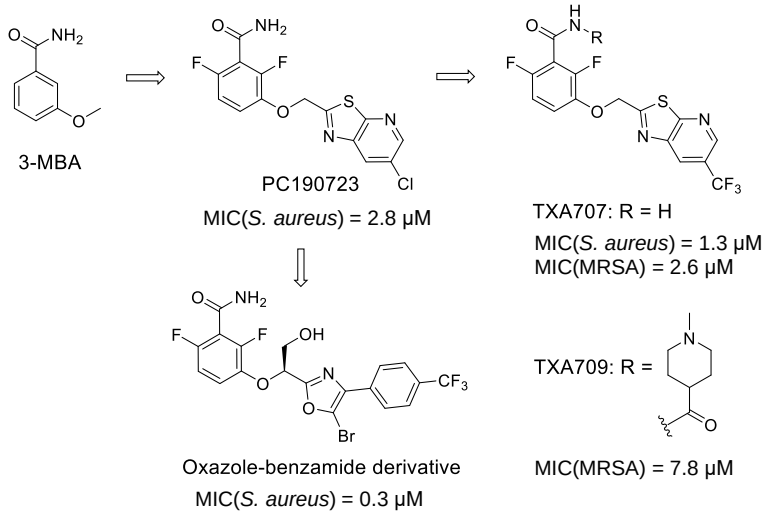

Figure 4. Interdomain cleft inhibitors: 3-methoxybenzamide derivatives.

X-ray structure of *S. aureus* FtsZ (SaFtsZ) in complex with PC190723 showed that this compound binds to a narrow pocket within the deep cleft formed by the H7 helix, the T7 loop, and the C-terminal (Figure 1).[47] In addition, the crystallographic structure revealed a new conformation of FtsZ, different from the ones obtained only in the presence of GTP or GDP.[48] In view of this breakthrough, it was proposed that the interaction of PC190723 in this allosteric cleft modulates the conformational switch that enables the assembly of the protein.[48] To confirm this hypothesis, the Medicinal Chemistry Laboratory developed more than 30 fluorescent probes based on the PC190723 structure, that specifically bind to FtsZ polymers (Figure 5A). Among them, probe UCM01, in which the clorothiazolopyridine tail of PC190723 was replaced by the 4-chloro-7-nitro-2,1,3-benzoxadiazol (NBD) fluorophore, displayed optimal fluorescence properties towards this aim (Figure 5B). Thus, although the fluorescence intensity of this NBD derivative does not change significantly under FtsZ polymerization conditions, the fluorescence anisotropy of UCM01 is modified upon binding and dissociating from FtsZ during the protein assembly-disassembly process, indicating that the interdomain cleft opens in assembled FtsZ subunits and closes in unassembled monomers, demonstrating the structural switch mechanism of FtsZ.[49]

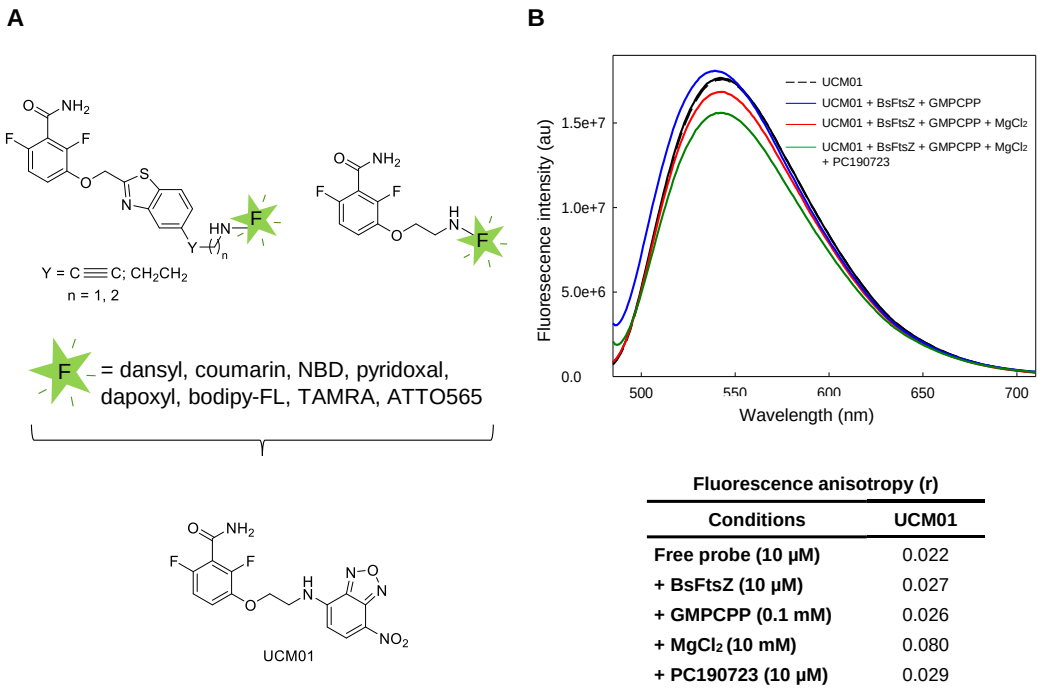

Fluorescence anisotropy (r)

Conditions	UCM01
Free probe (10 µM)	0.022
+ BsFtsZ (10 µM)	0.027
+ GMPCPP (0.1 mM)	0.026
+ $MgCl_2$ (10 mM)	0.080
+ PC190723 (10 µM)	0.029

Figure 5. Fluorescent probes with affinity for the FtsZ interdomain binding site. (A) Design of fluorescent analogues of PC190723. (B) Fluorescence properties of selected probe UCM01. Top: fluorescence spectra of the free and bound probe; bottom: fluorescence anisotropy values of the free and bound probe.

Hence, targeting the interdomain cleft to inhibit FtsZ filament dynamics, which is required for FtsZ function in cell division, could be a promising strategy for the identification of new FtsZ inhibitors. However, the lack of a binding assay against this pocket has hampered the discovery of ligands structurally different from PC190723 with affinity for this site. In this context, the main objective of this work is the development of a competitive binding assay based on fluorescent probes derived from PC190723 for the identification of new allosteric inhibitors of FtsZ in order to develop more effective antibacterial agents. This objective involves the following steps:

1) Design and synthesis of new fluorescent derivatives of PC190723.

2) Development and validation of a fluorescence-based competitive binding assay targeting the FtsZ interdomain cleft for the identification of new allosteric inhibitors.

3) Use of the developed methodology to identify allosteric inhibitors of FtsZ.

RESULTS AND DISCUSSION

2. RESULTS AND DISCUSSION

2.1. Design and synthesis of new fluorescent derivatives of PC190723

The generation of fluorescent probes that specifically target the FtsZ interdomain cleft is a key step in the development of an affinity assay for screening FtsZ allosteric ligands. A probe may be used for this purpose if its binding to FtsZ produces a significant modification in its fluorescent properties [emission intensity (I_{em}), wavelength (λ) or anisotropy value (*r*)], which returns to the values of the free probe by adding a competitive inhibitor, such as the reference ligand PC190723. For this kind of competitive assay is required that both, the probe and the competing ligand, have comparable affinities then, a given probe can only be used in a limited measurement range of competitor affinities.[50] Therefore, medium-affinity probes are required for the effective detection of molecules with low affinity for FtsZ, whereas compounds with high affinity will be identified by high-affinity probes.

Although UCM01 undergoes an increase in its fluorescence anisotropy value upon binding to the interdomain cleft of FtsZ (Figure 5B), this change is very small to stablish a competitive binding assay with enough sensitivity. Therefore, some structural modifications on UCM01 were performed in order to design new probes with higher FtsZ affinity and thereby achieve a greater change in the fluorescence anisotropy upon binding. Molecular dynamics simulations showed that PC190723 and UCM01 bind to FtsZ near an unfilled hydrophobic pocket, formed by helices H6 and H7 and the C-terminal subdomain (Figure 6), thus leaving room for chemical modifications.[49] Consequently, taking UCM01 as a starting point, alkyl chains of different lengths were introduced in the spacer between the benzamide and the fluorophore to gain hydrophobic interactions, affording derivatives **1**-**4**.

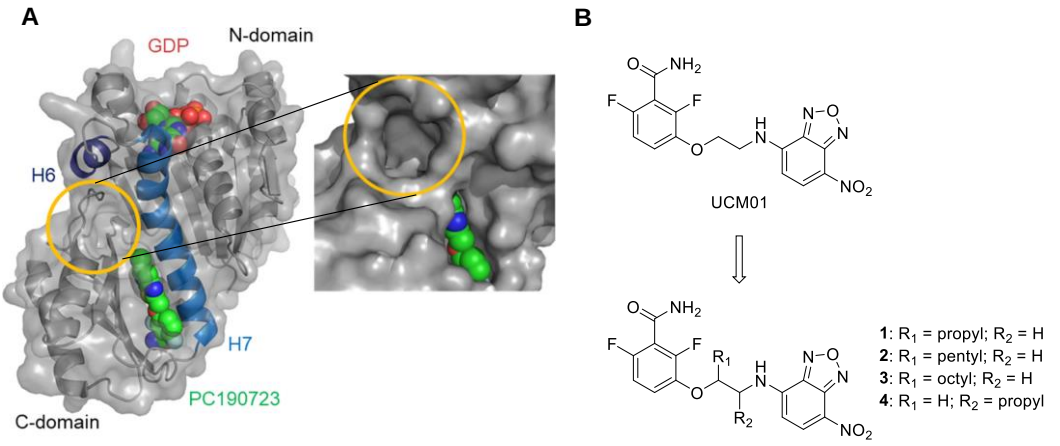

Figure 6. Design of fluorescence probes with high affinity for the FtsZ allosteric binding site. (A) Representation of the structure of SaFtsZ-PC190723 complex. The yellow circle marks a pocket above PC190723 potentially available for ligand binding. (B) Chemical structures of fluorescent derivatives **1**-**4**.

Fluorescent racemic derivatives **1**-**3** were synthesized starting from 2,6-difluoro-3-methoxybenzamide by deprotection of the methoxy group with boron tribromide at room temperature (rt), followed by Williamson alkylation of the resulting 3-hydroxybenzamide **5**[40] with *N*-Boc-2-bromoalkylamines **6**-**8**, using potassium carbonate as a base and catalytic sodium iodide in *N*,*N*-dimethylformamide (DMF), as depicted in Scheme 1. Further treatment of the obtained ethers **9**-**11** with trifluoroacetic acid (TFA) at rt to remove the Boc protecting group yielded primary amines **12**-**14**, which were treated with NBD chloride to afford the desired fluorescent compounds **1**-**3** by nucleophilic aromatic substitution. *N*-Boc-2-bromoalkylamines **6**-**8** were prepared by addition of *tert*-butyl-*N*,*N*-dibromocarbamate (BBC) to the corresponding terminal alkenes in an anti-Markovnikov fashion, followed by reduction of the obtained intermediates with aqueous sodium sulfite, according to the procedure described in the literature.[51]

O-alkylation of phenol **5** with *N*-Boc-aminoalcohol **15** via Mitsunobu reaction using diisopropyl azodicarboxylate (DIAD) and tributylphosphine as reagents under thermal conditions, followed by the removal of the Boc group and further nucleophilic substitution of the resulting amine **17** with NBD chloride allowed the obtention of NBD-derivative **4** (Scheme 1). Aminoalcohol **15**[52] was prepared by protection of 2-aminopentanol with *tert*-butyl dicarbonate in tetrahydrofuran (THF).

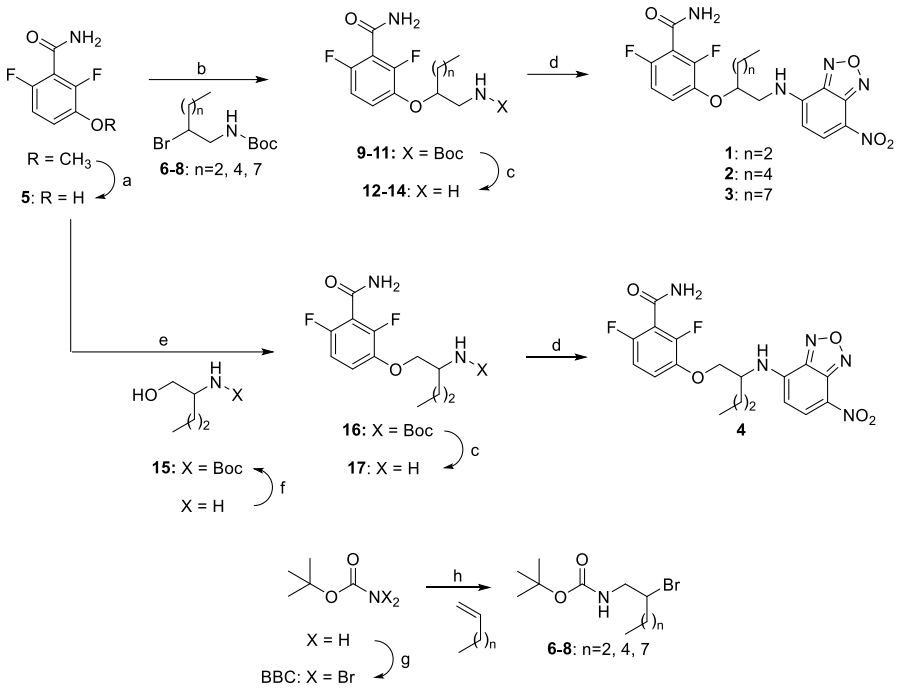

Scheme 1. Reagents and conditions: a) BBr_3, DCM, rt, 3 d, 95%; b) **6-8**, K_2CO_3, NaI, DMF, rt, 24 h, 14-23%; c) TFA, DCM, rt, 1 h, 80-90%; d) Cl-NBD, Cs_2CO_3, MeCN, 80 ºC, 1 h, 11-50%; e) **15**, DIAD, PBu_3, DMF, 80 ºC, 48 h, 18%; f) Boc_2O, pyridine, THF, 0 ºC to rt, on, 95%; g) Br_2, K_2CO_3, H_2O, rt, 2 h, 79%; h) i. DCM, reflux, 3 h, rt, 16 h; ii. 12% aq. Na_2SO_3, 5-10 ºC, 15 min, 55-58%.

Once fluorescent derivatives **1**-**4** were synthesized, we evaluated their potential as chemical tools to develop a binding assay against the FtsZ PC-binding site of *B*. *subtilis* by the assessment of their fluorescent properties. Therefore, fluorescence emission spectra and anisotropy values of compounds **1**-**4** were first registered employing an excitation wavelength corresponding to the maximum absorption of each compound in 4-(2-hydroxyethyl)-1-piperazineethanesulfonic acid (HEPES) buffer at pH 6.8 and 25 ºC at a concentration of 10 µM. Then, BsFtsZ (10 µM) in HEPES buffer, the slowly hydrolyzable GTP analogue GMPCPP (0.1 mM) and $MgCl_2$ (10 mM) were subsequently added to set up the polymerization conditions. Finally, PC190723 (10 µM) was added to displace the fluorescent probes and revert the possible changes.

In both, fluorescence emission spectra and anisotropy values, probes **1**-**4** showed significant changes under FtsZ polymerization conditions (Figure 7). However, fluorescence anisotropy was preferred due to its robustness compared to intensity measurements, which are more prone to interferences by light absorbing or fluorescent compounds.[41]

A

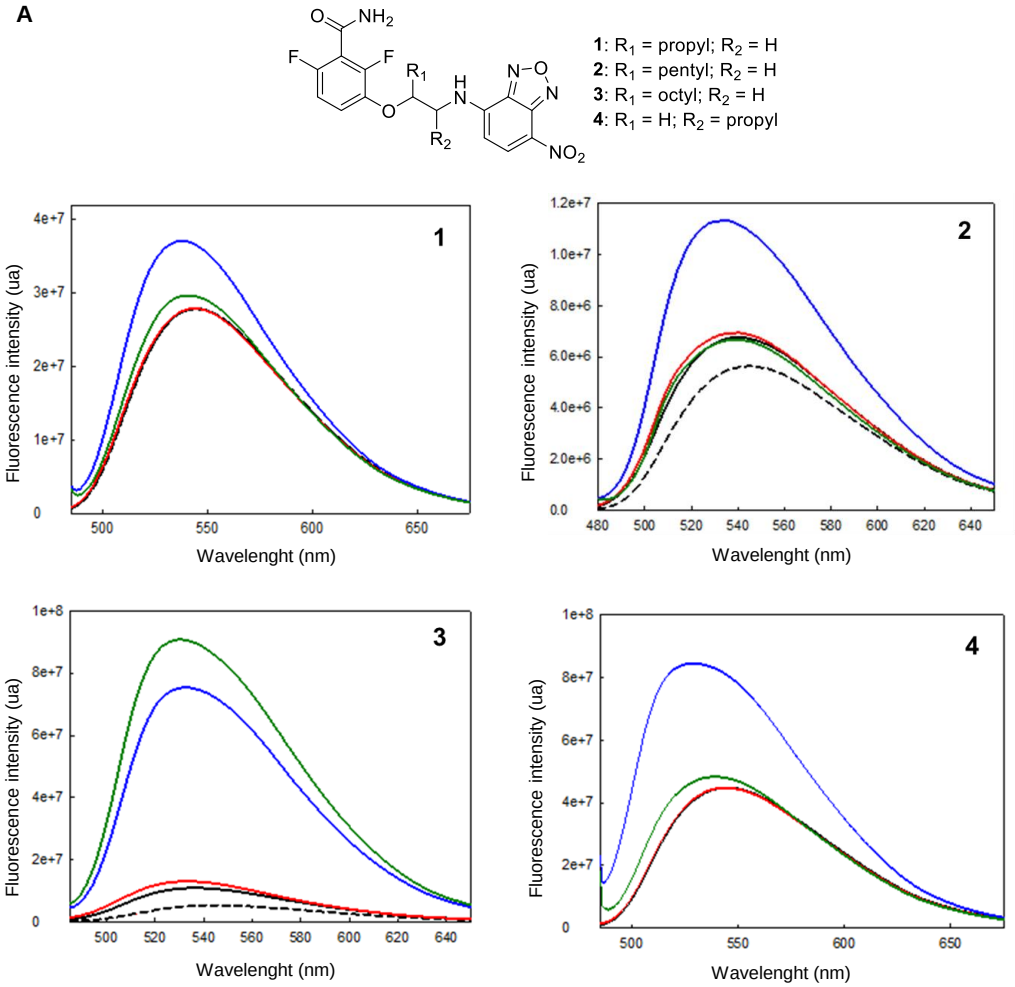

B

	Anisotropy values (*r*)				
Conditions	**UCM01**	**1**	**2**	**3**	**4**
Free probe (10 µM)	0.022	0.037	0.049	0.045	0.031
+ Bs-FtsZ (10 µM)	0.027	0.039	0.104	0.130	0.034
+ GMPCPP (0.1 mM)	0.026	0.046	0.115	0.186	0.036
+ $MgCl_2$ (10 mM)	0.080	0.157	0.261	0.317	0.203
+ PC190723 (10 µM)	0.029	0.053	0.135	0.324	0.055

Figure 7. Fluorescence properties of NBD-derivatives **1**-**4**. (A) Fluorescence emission spectra of each compound alone (10 µM, dashed line), and following consecutive additions of 10 µM BsFtsZ (black line), 0.1 mM GMPCPP (red line), 10 mM $MgCl_2$ (blue line) and 10 µM PC190723 (green line). (B) Fluorescence anisotropy of derivatives **1**-**4**.

The fluorescence anisotropy values of the four new compounds **1**-**4** underwent a larger increase in the presence of FtsZ polymers compared to the free probe, than the initial derivative UCM01. However, only fluorescent derivatives **1** and **4** recovered their initial anisotropy values after the addition of an excess of competing PC190723, which indicates that these derivatives bind to the protein at the same binding site that its parent compound. NBD-derivatives **2** and **3**, bearing a pentyl and octyl chain, respectively, exhibited an increase in background anisotropy with unassembled FtsZ in the absence of magnesium that was deemed nonspecific. Furthermore, the addition of PC190723 did not reduce the increase in their anisotropy values in the presence of FtsZ polymers.

In view of these results, we focused our attention on derivatives **1** and **4**, and both enantiomers of each compound were synthesized and evaluated. Regarding compounds (*R*)- and (*S*)-**1**, their synthesis was carried out following a synthetic route different from the one used for the racemic derivative, since the required enantiomers of *N*-Boc-bromoalkylamine **6** cannot be prepared from the addition of BBC to 1-pentene. Thus, compounds (*R*)- and (*S*)-**1** were synthesized by Mitsunobu reaction between phenol **5** and *N*-Boc-aminoalcohols (*R*)- and (*S*)-**18**, which were obtained in moderate yield from the aminolytic kinetic resolution of 1,2-epoxypentane catalyzed by chiral (salen)Co^{III} complexes using *tert*-butylcarbamate as nucleophile in *tert*-butylmethyl ether (TBME) at rt[53] (Scheme 2). Then, in an attempt to reduce the time of the Mitsunobu reaction, phenol **5** and aminoalcohols (*R*)- and (*S*)-**18** were treated with DIAD and tributylphosphine in DMF under microwave (MW) irradiation to successfully provide ethers (*R*)- and (*S*)-**9**. Next, the removal of the Boc group with TFA and subsequent reaction of the resulting amines (*R*)- and (*S*)-**12** with NBD chloride yielded desired fluorescent compounds (*R*)- and (*S*)-**1**.

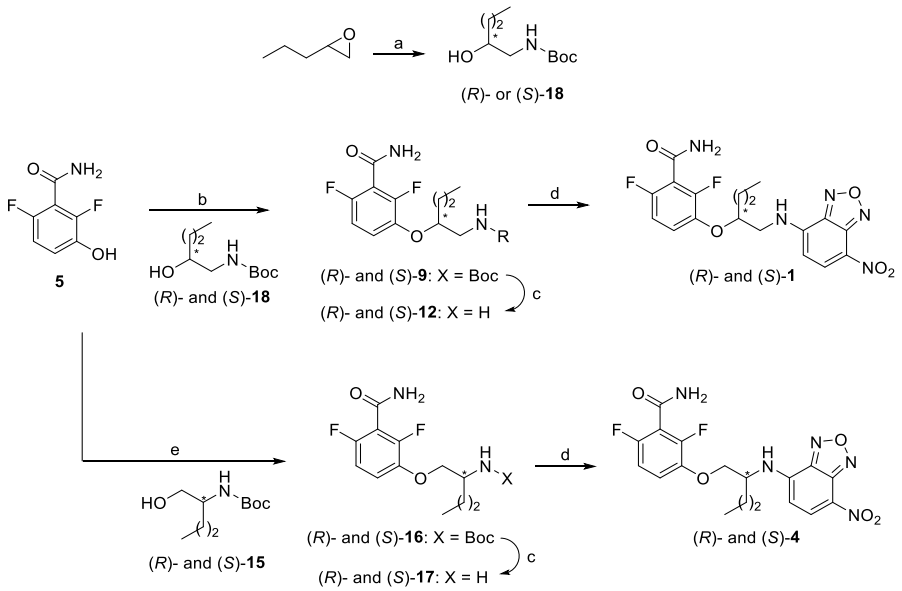

Scheme 2. Reagents and conditions: a) (*R,R*)- or (*S,S*)-(salen)-Co(II) complex, NH_2Boc, *p*-nitrobenzoic acid, TBME, rt, 24 h, 56-61%; b) DIAD, PBu_3, DMF, MW 150 ºC, 2 h, 28-31%; c) TFA, DCM, rt, 1 h, 70-83%; d) Cl-NBD, Cs_2CO_3, MeCN, 80 ºC, 1 h, 7-33%; e) DIAD, PBu_3, DMF, 80 ºC, 48 h, 18-19%.

Enantiomers (*R*)- and (*S*)-**4** were prepared following the same synthetic route described for the racemic derivative **4** but using the appropriate enantiomers of the *N*-Boc-aminoalcohol **15**. Hence, Mitsunobu reaction between benzamide **5** and aminoalcohols (*R*)- or (*S*)-**15**, followed by the removal of the Boc-protecting group and subsequent reaction of amines (*R*)- and (*S*)-**17** with NBD chloride afforded the enantiopure compounds (*R*)- and (*S*)-**4**. It is worthy to mention that in this case the Mitsunobu reaction was carried out under thermal conditions since all the attempts to perform the reaction under MW irradiation resulted in high levels of decomposition of the starting materials.

In order to evaluate the enantiomers of NBD-derivatives **1** and **4**, the anisotropy values of these compounds were registered under the previously described experimental conditions (Figure 8A). Fluorescence anisotropy changes of (*S*)-**1** were quite similar to those exhibited by its racemic analogue under polymerization conditions, whereas the *R* enantiomer showed only a small increase in its anisotropy in the presence of FtsZ polymers. In both cases the values were restored to the value of the free probe with the addition of PC190723. A comparable situation took place with the enantiomers of fluorescent derivative **4**, but in this case the compound that showed the highest anisotropy changes was (*R*)-**4**. Characterization of these new fluorescent derivatives was completed by assessment of their binding affinities to FtsZ and evaluating their effects in growing cells. Binding constants of the probes (dissociation equilibrium constant, K_D) were calculated from anisotropy measurements recorded throughout the titration of the probe (3 μM) with different concentrations of FtsZ polymers (0-40 μM) in HEPES buffer, giving K_D values of 8 and 1.9 μM for (*S*)-**1** and (*R*)-**4**, respectively (Figure 8B). Treating *B. subtilis* cells with the enantiomers of **1** and **4** at different concentrations (25−100 μM) induced the characteristic filamentous phenotype due to the inhibition of cell division, with the higher affinity probe (*R*)-**4** showing the best efficacy at a concentration of 25 μM, supporting FtsZ targeting (Figure 8C). Moreover, (*R*)-**4** and (*S*)-**1** displayed antibacterial activity in *B. subtilis* with minimal division inhibitory concentration (MDC) of 25 and 100 μM, respectively (Figure 8B). Therefore, changes in the anisotropy values in the presence of FtsZ polymers, correlate with binding affinity constants and phenotypic effects on bacterial cells. All these data supported the suitability of fluorescent probes (*S*)-**1** and (*R*)-**4** for the development of a competitive binding assay against the interdomain cleft of FtsZ.[54]

A

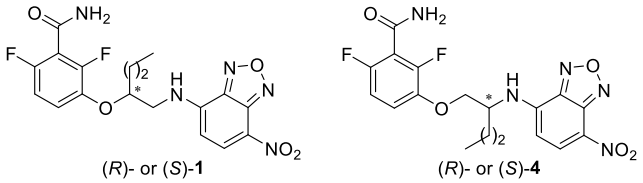

	Anisotropy values (*r*)					
Conditions	**1**	**(*R*)-1**	**(*S*)-1**	**4**	**(*R*)-4**	**(*S*)-4**
Free probe (10 µM)	0.037	0.037	0.037	0.031	0.029	0.030
+ Bs-FtsZ (10 µM)	0.039	0.046	0.041	0.034	0.041	0.042
+ GMPCPP (0.1 mM)	0.046	0.050	0.044	0.036	0.040	0.041
+ $MgCl_2$ (10 mM)	0.157	0.081	0.172	0.203	0.227	0.096
+ PC190723 (10 µM)	0.053	0.051	0.065	0.055	0.052	0.038

B

Compd	K_D (µM) BsFtsZ	MDC (µM) *B. Subtilis*	MIC (µM) *B. Subtilis*
(*S*)-**1**	8 ± 1	100	250
(*R*)-**1**	N.D.	>100	>250
(*S*)-**4**	15 ± 2	>50	250
(*R*)-**4**	1.9 ± 0.6	25	25

C

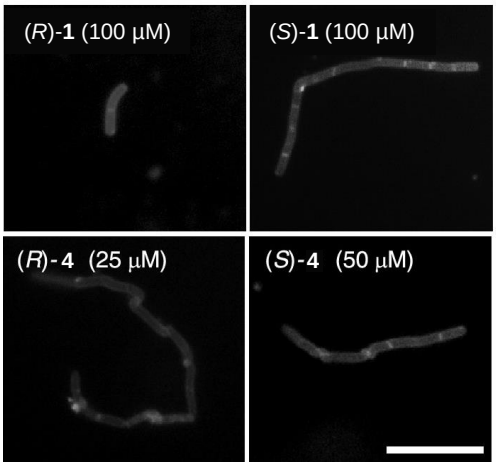

Figure 8. Characterization of both enantiomers of probes **1** and **4**. (A) Fluorescence anisotropy values of new NBD-derivatives **1** and **4** (10 µM). (B) Binding affinity and activity values of the fluorescent probes **1** and **4** on *B. subtilis*. (C) Fluorescence microscopy images of *B. subtilis* cells treated with both enantiomers of **1** and **4**. Bars, 10 µm.

2.2. Development and validation of a fluorescence-based competitive binding assay targeting the FtsZ interdomain cleft for the identification of new allosteric inhibitors

Based on the good results showed by probes (*S*)-**1** and (*R*)-**4**, we designed a competitive binding assay to identify compounds with affinity for the PC-binding site. For the development of this new method is necessary to form stable FtsZ polymers that do not disassemble upon GTP hydrolysis or by the addition of FtsZ polymerization inhibitors. Thus, FtsZ in HEPES buffer was subjected to polymerization conditions (10 mM $MgCl_2$ and 50 µM GMPCPP) and the assembled FtsZ-GMPCPP polymers were treated with a 0.15%

glutaraldehyde solution to produce stabilized *B. subtillis* FtsZ cross-linked polymers that were resistant to depolymerization by GDP addition. The binding assay was performed by treating stabilized FtsZ polymers with the probe [(*S*)-**1** or (*R*)-**4**] and measuring the decrease in anisotropy upon displacement of the fluorescent probe to determine binding at increasing concentrations of competing ligands.

A competition assay between probe (*S*)-**1** and PC190723 and its moieties, 2,6-difluoro-3-methoxybenzamide (DFMBA) and 6-(chloro[1,3]thiazolo[5,4-*b*]pyridin-2-yl)methanol (CTPM), was used to validate this methodology. Thus, the competition binding isotherms of the ligands showed that the high-affinity ligand PC190723 rapidly displaced the probe (*S*)-**1**, whereas higher concentrations of the weakly binding moieties DFMBA and CTPM were required to displace the probe (Figure 9). Noteworthy, the addition of the potent polymerization inhibitor GDP, used as a negative control, did not change the probe (*S*)-**1** anisotropy since this inhibitor exerts its activity by binding to the GTP-binding site. All these data confirm that our binding assay is able to identify compounds that specifically bind to the FtsZ PC-binding site, making it an extremely valuable tool for the identification of new allosteric ligands of FtsZ.

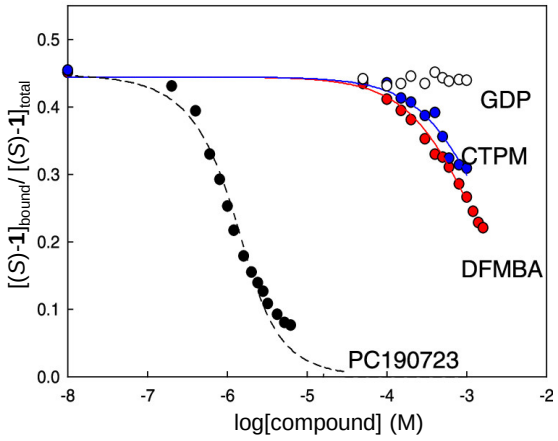

Figure 9. Displacement curves of (*S*)-**1** (3 μM) from stabilized FtsZ-GMPCPP polymers (8 μM binding sites) by PC190723 (black circles, K_D < 0.1 μM), and its moieties 2,6-difluoro-3-methoxybenzamide (DFMBA, K_D = 0.67 ± 0.05 mM) (red), and 6-(chloro[1,3]thiazolo[5,4-b]pyridin-2-yl)methanol (CTPM, K_D = 1.0 ± 0.1 mM) (blue). Addition of GDP (void circles) was used as a negative control.

2.3. Use of the developed methodology to identify allosteric inhibitors of FtsZ

Once the competitive binding assay was validated, we evaluated its potential to identify allosteric inhibitors of FtsZ. The screening was carried out by recording the fluorescence anisotropy values of the probe (*S*)-**1** upon the addition of the tested compound at two concentrations (20 and 200 μM). Compounds with high affinity for the PC-binding site should markedly decrease the anisotropy value of the probe at both concentrations (Figure 10). For those compounds that significantly decrease the anisotropy values,

complementary cytological profiling tests were performed to ascertain their ability to target FtsZ in bacterial cells. First, we screened for binding to the interdomain cleft compounds that had been previously identified as FtsZ inhibitors with unknown binding site such as zantrin Z3,[55] PC170942,[29] plumbagin,[56] resveratrol,[57] and tiplaxtinin.[58] PC190723 and the GTP-replacing inhibitor UCM44[33] were also included in the screening as positive and negative controls, respectively. Screen results revealed that PC170942, zantrin Z3 and tiplaxtinin did not modify the fluorescence anisotropy value of the probe (*S*)-**1**, evidencing that they do not interact with FtsZ through the interdomain cleft. Surprisingly, the promiscuous inhibitors plumbagin and resveratrol, and UCM044 produced a slightly variation in the anisotropy value of the probe, although these compounds seem to exhibit very low affinity for the PC-binding site. As expected, PC190723 totally displaced the probe from its binding site, drastically modifying the fluorescence anisotropy value of (*S*)-**1**.

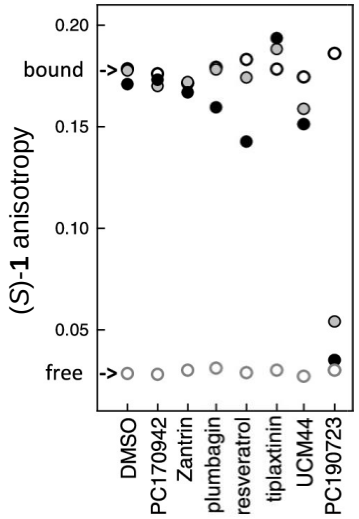

Figure 10. Affinity evaluation of FtsZ described inhibitors for the interdomain cleft employing the fluorescence anisotropy changes of probe (*S*)-**1** (3 µM) and stabilized FtsZ-GMPCPP polymers. The anisotropy values of the bound probe (void black circles), the free probe (void gray circles), and the values with two concentrations of each compound, 20 µM (gray circles) and 200 µM (black circles), are represented. Control values of dimethylsulfoxide vehicle (DMSO, 2% gray circle and 4% black circle) are also shown.

Next, in order to identify new FtsZ allosteric inhibitors, we developed a series of structurally simplified *N*- or *O*-(alkylphenyl)benzamides **19**-**26** and evaluated their binding affinities using our fluorescence screening (Figure 11). In this series the benzamide ring is linked to a 3-chlorophenyl moiety through nitrogen or oxygen atoms and we decided to perform some structural modifications to study the contribution of these moieties to the FtsZ affinity. Thus, we analyzed the effect of the relative position of the benzamide and 3-chlorophenyl ring, the influence of *N*-, *N*-substituted or *O*- as the linker between the two rings and the alkyl spacer length. Then, once the above parameters were optimized, we replaced the amide group of the benzamide by different bioisosteres (**27**, **28**).

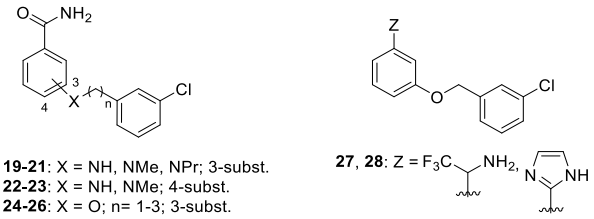

Figure 11. Chemical structures of benzamide derivatives **19**-**26** and bioisosteres **27**, **28**.

2.3.1. Synthesis and biological evaluation of compounds **19**-**28**

Secondary amines **19** and **22** were obtained by reductive amination of 3-chlorobenzaldehyde with 3- or 4-aminobenzamide under MW irradiation. Their *N*-alkylation with iodomethane provided compounds **20** and **23**. Propyl derivative **21** was synthesized by reductive amination of propionaldehyde with secondary amine **19** (Scheme 3).

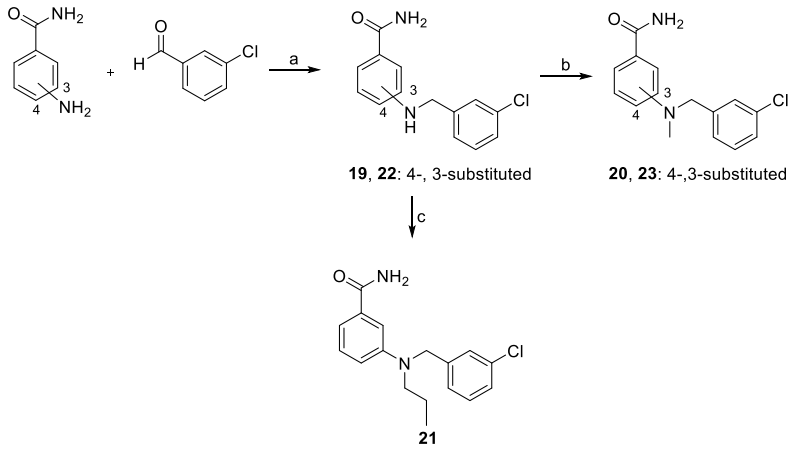

Scheme 3. Reagents and conditions: a) i. MW, 100 °C, 10 min; ii. H_2, Pd/C, MeOH, rt, 18 h, 32-74%; b) MeI, K_2CO_3, DMF, 60 °C, 18 h, 31-35%; c) i. CH_3CH_2CHO, MeOH, rt, 18 h; ii. $NaBH_3CN$, rt, 72 h, 52%.

Alkoxybenzamides **24** and **26** were prepared by alkylation reaction of 3-hydroxybenzamide with 3-chlorobenzyl bromide and 1-(3-bromopropyl)-3-chlorobenzene, respectively, under classical Williamson conditions (Scheme 4), whereas compound **25** was synthesized by Mitsunobu reaction between 3-hydroxybenzamide and 2-(3-chlorophenyl)ethanol using triphenylphosphine and diethyl azodicarboxylate (DEAD) in THF at rt.

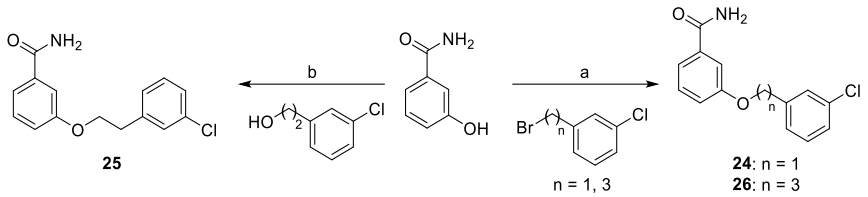

Scheme 4. Reagents and conditions: a) K_2CO_3, NaI, DMF, rt, 24 h, 47-54%; b) PPh_3, DEAD, Et_3N, THF, rt, 24 h, 46%.

The synthesized derivatives **19**-**26** were then tested in our competitive assay in order to determine their binding affinities for BsFtsZ. Results were represented as the variation of the fluorescence anisotropy of the probe (*S*)-**1** to easily distinguish weak inhibitors from high-affinity compounds (Figure 12A). Amino derivatives **19**-**23** produced a small modification of the anisotropy of the probe (*S*)-**1**, indicating that they are weak FtsZ inhibitors. Among them, compound **20** showed the highest variation in the anisotropy values of these first derivatives, revealing that relative *meta*- position of the benzamide was favored over *para*- position for FtsZ binding to the interdomain cleft. Then, to confirm the FtsZ targeting, we examined the effects of derivative **20** on the cell division of wild type *B. subtilis* 168 and on the FtsZ subcellular localization in *B. subtilis* SU570, a strain that has FtsZ fused to a green fluorescent protein (FtsZ-GFP) as the only FtsZ protein. We observed that *B. subtilis* cells treated with compound **20** showed the classic filamentous phenotype due to the cell division inhibition at 0.75 mM. Moreover, **20** induced GFP-FtsZ delocalization into punctate *foci* at 0.2 mM, supporting FtsZ targeting (Figure 12B). Therefore, our fluorescence binding screen method combined with phenotypic tests can effectively detect relatively weak FtsZ-targeting ligands.

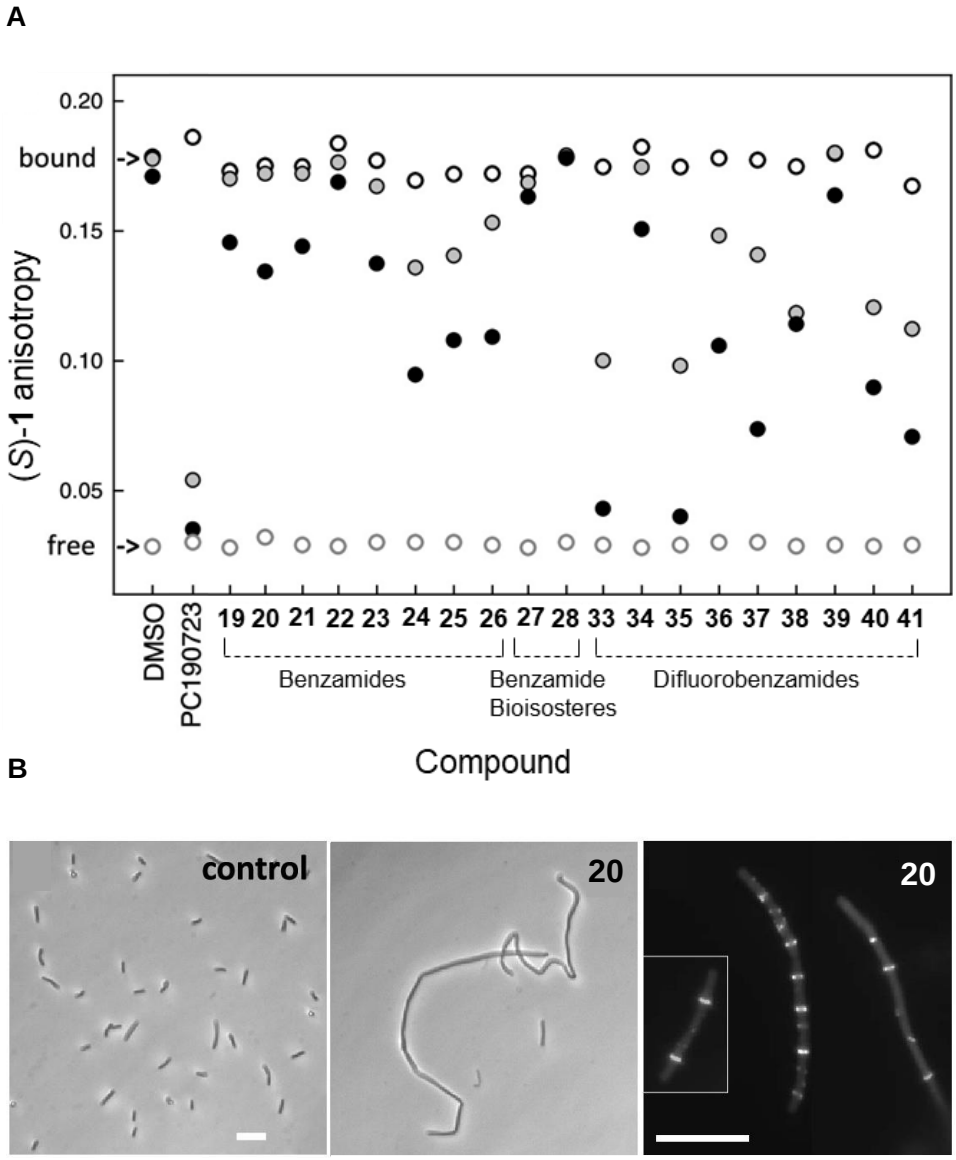

Figure 12. Fluorescence anisotropy screen for FtsZ allosteric inhibitor combined with cell-based methods. (A) Anisotropy changes of probe (*S*)-**1** produced by benzamide derivatives. The anisotropy values of the bound probe (void black circles), the free probe (void gray circles), and the values with two concentrations of each compound, 20 μM (gray circles) and 200 μM (black circles) and dimethylsulfoxide vehicle (DMSO, 2% gray circle and 4% black circle) are shown. (B) Cellular effects of compound **20** on *B. subtilis* cells. Bars, 10 μm.

Regarding the affinity of alkoxybenzamides **24**-**26**, the replacement of the nitrogen by an oxygen atom produced higher fluorescence anisotropy modification of the probe (*S*)-**1** than the amino derivatives **19**-**23**, with compound **24** showing the biggest anisotropy change at both concentrations (20 and 200 μM), as shown in Figure 12A. These data suggest that oxygen is a more suitable linker than nitrogen for this kind of inhibitors and the

optimal length of the spacer is one methylene subunit. Next, in order to endow the series with structural novelty we prepared compounds **27** and **28** in which the amide group of the benzamide **24** was replaced by bioisosteres.

Thus, *O*-alkylation of 3-hydroxybenzaldehyde with 3-chlorobenzyl bromide, followed by treatment of the corresponding intermediate with trimethyl(trifluoromethyl)silane ($TMSCF_3$) in DMF at rt afforded trifluoromethyl alcohol **29,** which was oxidized with Dess-Martin reagent to obtain the corresponding ketone **30** in quantitative yield. Finally, the desired compound **27** was obtained by reductive amination of ketone **30** with *tert*-butanesulfinamide, as an ammonia equivalent, in ethyl ether (Scheme 5).

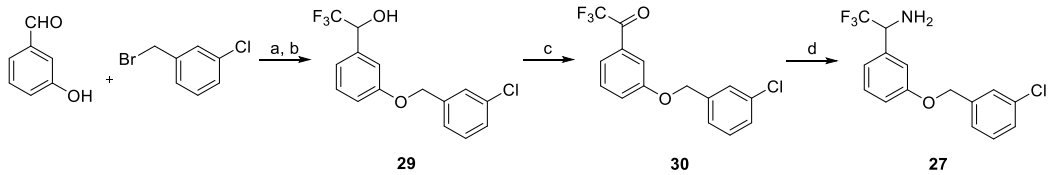

Scheme 5. Reagents and conditions: a) K_2CO_3, NaI, DMF, rt, 24 h, 99%. b) i. $TMSCF_3$, K_2CO_3, DMF, rt, 48 h; ii. 2 M HCl, rt, 4 h, 87%; c) Dess-Martin periodinane, DCM, rt, 18 h, 99%; d) i. $(CH_3)_3CSONH_2$, $Ti(OiPr)_4$, Et_2O, reflux, 24 h; ii. $NaBH_4$, Et_2O, rt, 24 h; iii. 4 M HCl, 1,4-dioxane, rt, 1 h, 24%.

Compound **28** was prepared by the Pd- and Cu-mediated cross-coupling reaction of imidazole and 3-iodoanisole under MW irradiation, followed by deprotection of the methoxy derivative **31** with boron tribromide, and subsequent *O*-alkylation of phenol **32** with 3-chlorobenzyl bromide under classical Williamson conditions (Scheme 6).

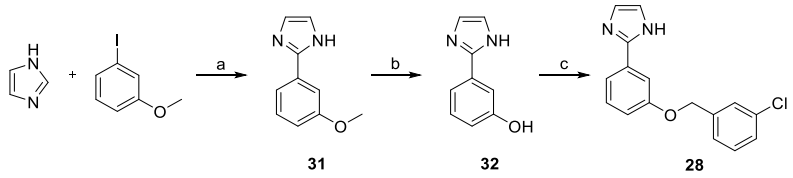

Scheme 6. Reagents and conditions: a) $Pd(OAc)_2$, CuI, DMF, MW, 200 °C, 40 min, 53%; b) BBr_3, DCM, 0 ºC to rt, 24 h, 95%; c) 3-chlorobenzyl bromide, K_2CO_3, NaI, DMF, rt, 24 h, 72%.

Unfortunately, biososteres **27** and **28** did not produce any change in the fluorescence anisotropy value of (*S*)-**1**, thus indicating that they do not bind to FtsZ. Hence, 3-benzyloxybenzamide **24** remained the compound that most significantly modified the anisotropy value of the probe (*S*)-**1**, showing the highest affinity for FtsZ among the synthesized derivatives so far.

2.3.2. Synthesis and biological evaluation of compounds **33**-**41**

In order to enhance the affinity of the ligands for the interdomain cleft of FtsZ, we explored additional structural modifications around the three structural moieties of benzamide inhibitor **24** (Figure 13): (i) difluorination of the benzamide core (**33**), (ii) replacement of the 3-chloro substituent by a trifluoromethyl group located at *ortho*-, *meta*- and *para*- position of the phenyl ring (**34**-**36**); and (iii) introduction of linear or branched linkers of different lengths as spacers (**37**-**41**).

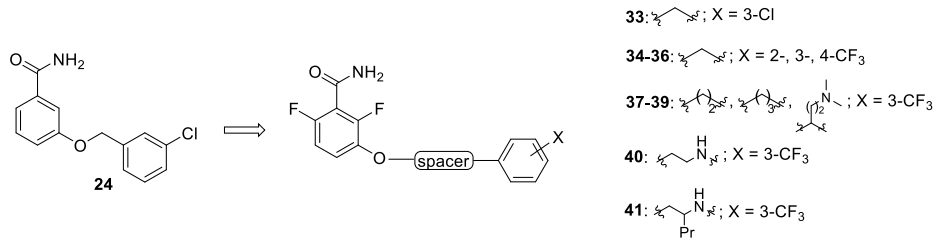

Figure 13. Structural modifications to enhance the affinity of the benzamide inhibitors for FtsZ.

Starting with the synthesis of derivatives **33**-**36**, these compounds were prepared by *O*-alkylation of benzamide **5** with the corresponding benzyl bromide under Williamson conditions in high yields (Scheme 8).

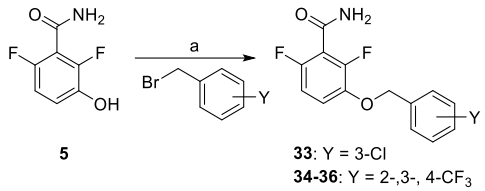

Scheme 8. Reagents and conditions: a) K_2CO_3, NaI, DMF, rt, 24 h, 81-98%.

Compounds **37**-**39** were obtained by Mitsunobu reaction of benzamide **5** with the commercially available corresponding primary alcohols or the secondary alcohol **42,** using tributylphosphine and DIAD as reagents under MW irradiation. Alcohol **42** was synthesized by Mannich reaction of paraformaldehyde (PFA) with dimethylamine and 1-(3-(trifluoromethyl)phenyl)ethenone, followed by reduction of the obtained β-aminoketone **43** in the presence of lithium aluminium hydride (Scheme 9).

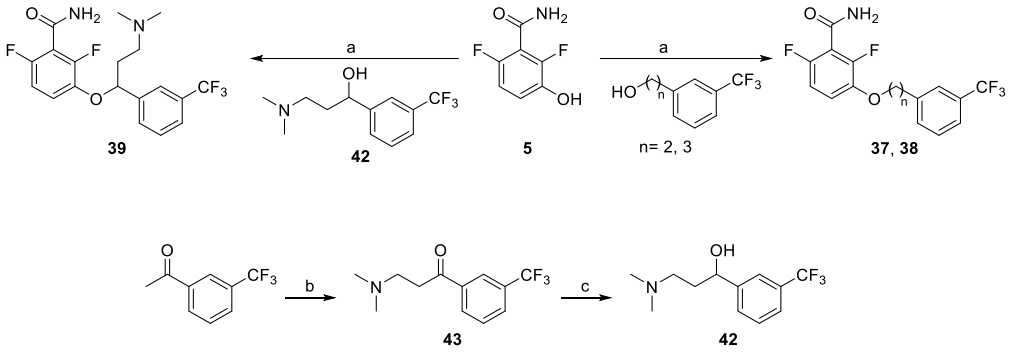

Scheme 9. Reagents and conditions: a) PBu_3, DIAD, DMF, MW, 150 ºC, 1.5 h, 45-50%; b) $(CH_3)_2NH$, PFA, HCl, ethanol, reflux, 2 d, 27%; c) $LiAlH_4$, THF, rt, 2 h, 76%.

Compounds **40** and **41**, bearing an aminoethoxy linker between the two aromatic subunits, were prepared via Mitsunobu reaction of benzamide **5** with the appropriate alcohol **44** and **45**. Primary alcohols **44** and **45** were obtained by the Ullman-type reaction between 1-iodo-3-(trifluoromethyl)benzene and 2-aminoethanol or 2-aminopentanol, respectively. Both enantiomers of compound **41** were also synthesized following the same synthetic route but starting from the corresponding enantiopure alcohol (*R*)- or (*S*)-**45** (Scheme 10).

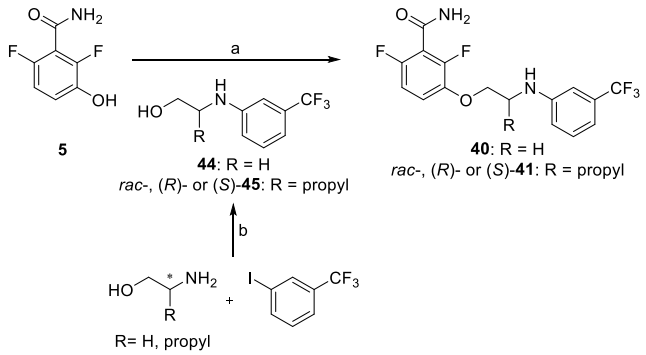

Scheme 10. Reagents and conditions: a) PBu_3, DIAD, DMF, MW, 150 ºC, 1.5 h, 36-49%; b) K_3PO_4, CuI, $(CH_2OH)_2$, *i*-PrOH, MW, 150 ºC, 105 min, 46-56%.

Biological evaluation of 2,6-difluorobenzamides **33**-**41** in the competitive binding assay showed that most of these derivatives are stronger competitors and bind to the FtsZ interdomain cleft with higher affinities than their defluorinated counterparts. For all these derivatives the affinity constants were also determined using the high-affinity probe (*R*)-**4** and the results are summarized in Table 2.

As expected, the incorporation of the fluorine atoms effectively increased the binding affinity of the derivative **33** compared to compound **24** [K_D(**33**) = 1.3 and K_D(**24**) = 9.3 μM].

On the other hand, the replacement of the chlorine atom of **33** by a trifluoromethyl group provided compound **35** with submicromolar affinity for FtsZ (K_D = 0.7 μM), and the position of this substituent plays a key role in the affinity for the protein, since derivatives with the trifluoromethyl group at 2- or 4-position (**34** and **36**) displayed lower binding affinities than compound **35** [K_D(**34**) = 71 μM and K_D(**36**) = 6.7 μM].

Increasing the spacer length between the two aromatic rings to 2 or 3 methylene subunits in compounds **37** and **38** did not improve the affinity for FtsZ [K_D(**37**) = 5.9 μM and K_D(**38**) = 1.5 μM], and the hydrochloride salt of derivative **39** containing a branched spacer with a positive charge, eliminated both the binding affinity and inhibitory activity for FtsZ.

Table 2. Binding affinity (K_D) and antibacterial activity of the synthesized compounds.

Compd	K_D (μM) Bs-FtsZ	MDC (μM) *B. Subtilis*	MIC (μM) *B. Subtilis*	MDC (μM) *S. aureus* Mu50	MIC (μM) *S. aureus* Mu50
24	9.3 ± 0.5	50	50	ND	>100
33	1.3 ± 0.1	10	25	50	100
34	71 ± 6	>100	>100	ND	>100
35	0.7 ± 0.2	10	25	50	50
36	6.7 ± 0.4	25	50	ND	100
37	5.9 ± 0.4	15	50	100	200
38	1.5 ± 0.1	5	10	25	50
39	145 ± 10	>50	>100	>100	>100
40	1.9 ± 0.2	5	10	50	100
41	1.1 ± 0.1	2.5	5	25	50
(*R*)-**41**	0.2 ± 0.1	1	2.5	10	25
(*S*)-**41**	3.8 ± 0.2	>10	50	100	100
PC190723	<0.1	2.5	5	1	5

Finally, aminoethoxy derivatives **40** and **41** exerted high binding affinities comparable with derivative **35** [K_D(**40**) = 1.9 μM and K_D(**41**) = 1.1 μM], whereas the evaluation of the enantiomers of **41** revealed that compound (*R*)-**41** displayed the highest binding affinity of the series with K_D = 0.2 μM. Figure 14A shows the binding isotherms of the higher affinity ligands **24**, **35**, **40**, (*S*)-**41** and (*R*)-**41** obtained in the competitive binding assay with probe (*R*)-**4**.

Cytological profiling of high-affinity compounds **35**, **40** and (*R*)-**41** showed that *B. subtilis* cells exposed to each of these compounds exhibited the characteristic filamentous phenotype due to the cell division inhibition. Moreover, these compounds impaired the normal assembly of FtsZ-GFP into the midcell Z-ring prior to division of *B. subtilis* SU570 at concentrations near their MIC values, further supporting FtsZ targeting (Figure 14B).

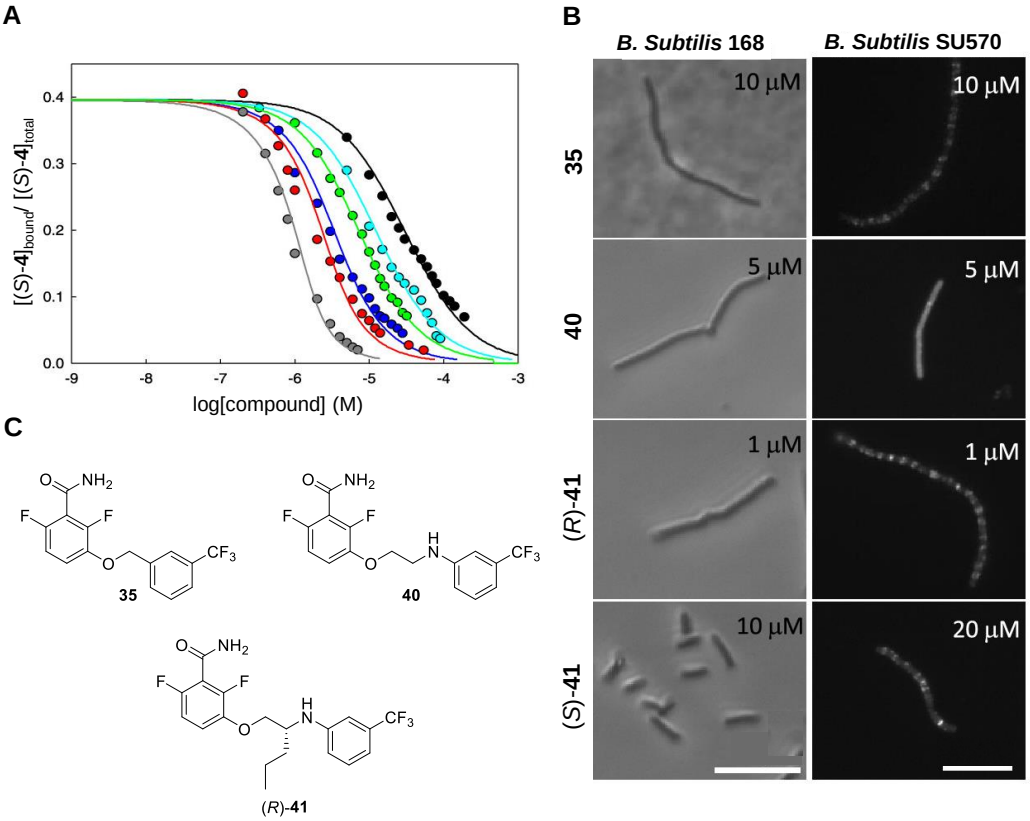

Figure 14. FtsZ inhibitors with enhanced affinity and phenotype. (A) Displacement curves of probe (*R*)-**4** by synthetic derivatives **24** (black), **35** (blue), **40** (green), (*R*)-**41** (red), (*S*)-**41** (cyan), and by PC190723 (gray). (B) Cellular effects of compounds **35**, **40** and, (*R*)- and (*S*)-**41** on *B. subtilis* cells. Bars, 10 µm. (C) Structures of the high-affinity inhibitors **35**, **40** and (*R*)-**41**.

The antibacterial activity of compounds **24** and **33**-**41** against *B. subtilis* and *S. aureus* Mu50 was also assessed (Table 2). In general, MDC and MIC values in *B. subtilis* follow the same trend as the FtsZ affinity (K_D) along the compound series, reaching values similar to PC190723 for derivative (*R*)-**41** (affinities order **33** < **35** ≤ **40** < (*R*)-**41**). Regarding the activity in *S. aureus*, the affinity improvement from **35** to (*R*)-**41** was not reflected in the antistaphylococcal activity as MIC values decreased marginally compared to a 10-fold decrease in *B. subtilis*. Furthermore, the MDC values of **35** on *S. aureus* Mu50 and *B. subtilis* differ with the trend shown by PC190723. This fact suggests that the 3-trifluoromethylphenyl tail confers somewhat less activity against this strain than the chloro-thiazolopyridine tail.

In summary, the use of the new competitive binding assay targeting the interdomain cleft of FtsZ has allowed us to identify ligands **33**, **35**, **40** and (*R*)-**41**, with moderate to high affinity for the protein, within our series of simplified benzamide derivatives. Evaluation of cellular effects of these compounds on *B. subtilis* cells showed that all of them were able to inhibit bacterial cell division leading to filamentous undivided cells and delocalization of FtsZ. Among them, derivative (*R*)-**41** stood out as the most effective bacterial cell division inhibitor and also displayed good antibacterial activity.[54]

2.3.3. Structural insights into the inhibitor binding site of *S. aureus* FtsZ

Due to the comparatively high MDC and MIC values in *S. aureus* shown by compounds **33**, **35**, **40** and (*R*)-**41**, the spontaneous mutants of *S. aureus* Mu50 resistant to these compounds were analyzed. Most mutations mapped to the *ftsZ* gene, at positions corresponding to amino acids P115, V151, A182, G196, V214, A237, L249, L261, M262, N263, A285, V297, T309 and T358. These residues cluster predominantly around the interdomain cleft and are concentrated at the PC190723 binding site. Thus, these results supported that the inhibitors identified target *S. aureus* FtsZ at the interdomain cleft. But to confirm the proposal interactions of the ligands, crystal structures of SaFtsZ folded core in complex with inhibitors **33** and **35** were determined. Crystallographic structures proved that these molecules bind into the interdomain cleft as PC190723.

By studying the interactions of the protein with the different parts of the molecules we found out that the interactions of the benzamide ring are conserved in compounds **33**, **35** and PC190723. However, these interactions are not sufficient for strong binding, as suggested by the 66% occupancy of DMFBA compatible with its low affinity. Regarding halogenated phenyl moieties of compounds **33** and **35**, their benzene rings interact with residues T309 and I311. The T309 residue acts as gate presenting two different conformations, closed and open. In the closed conformation, the hydroxyl group of the T309 side chain points to the solvent, while the methyl group lies next to G196, thus closing the central region of the binding site. By contrast, in the open conformation the hydroxyl group points toward N263 and allows access to the central region of binding pocket. This open conformation is observed with **33**, **35** and PC190723. Finally, the chlorine atom of **33** is placed at 4 Å from both the O atom of G193 and the α-carbon of G196, while the trifluoromethyl group of **35** interacts with the backbone carbonyl oxygens of Q192, G193, G227, and V310 (Figure 15).

Taking into account all these crystallographic analyses, we can confirm that the benzamide inhibitors identified in our fluorescence screening, bind into the interdomain cleft of SaFtsZ, validating again the use of the methodology for the identification of new allosteric inhibitors of FtsZ.

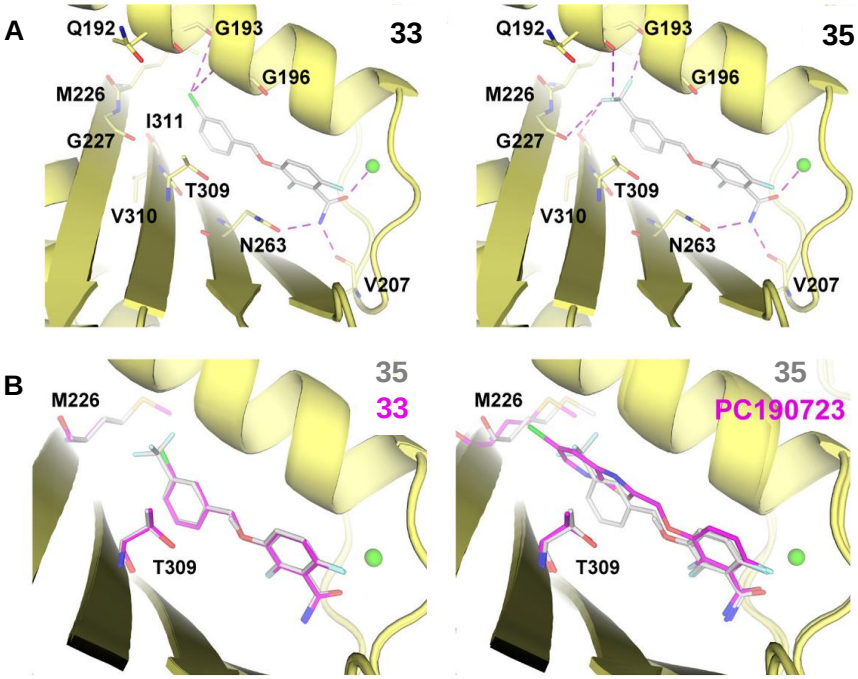

Figure 15. Crystal structures of FtsZ-inhibitors complexes. (A) Ligand−protein interactions in the binding site of compounds **33** and **35**, indicated by dashed magenta lines (the green sphere represents a coordinated metal ion). (B) Structural comparison between the SaFtsZ-**35** (gray) complex with SaFtsZ-**33** and PC190723 (PDB: 4DXD) complexes (pink carbon atoms).

CONCLUSIONS

3. CONCLUSIONS

In this work, we have successfully set up the first competitive binding assay to identify FtsZ allosteric ligands employing specific medium to high-affinity fluorescent probes (*S*)-**1** and (*R*)-**4**. This methodology, together with phenotypic profiling and X-ray crystallographic, has allowed to identify unequivocally compounds **33**, **35**, **40** and (*R*)-**41** as bacterial cell division inhibitors targeting the interdomain cleft of FtsZ in *B. subtilis* and *S. aureus*. Among them, derivative (*R*)-**41** stands out as the most promising allosteric inhibitor of FtsZ with good binding affinity (K_D = 0.2 µM) and antibacterial activity similar to PC190723 in *B. subtilis* [MIC values 2.5 and 5 µM for (*R*)-**41** and PC190723, respectively].

The use of this methodology in combination with cytological profiling and structural insights will facilitate the identification and characterization of ligands with affinity for the allosteric binding site of FtsZ, which could be the starting point for the development of more effective antibacterial agents.

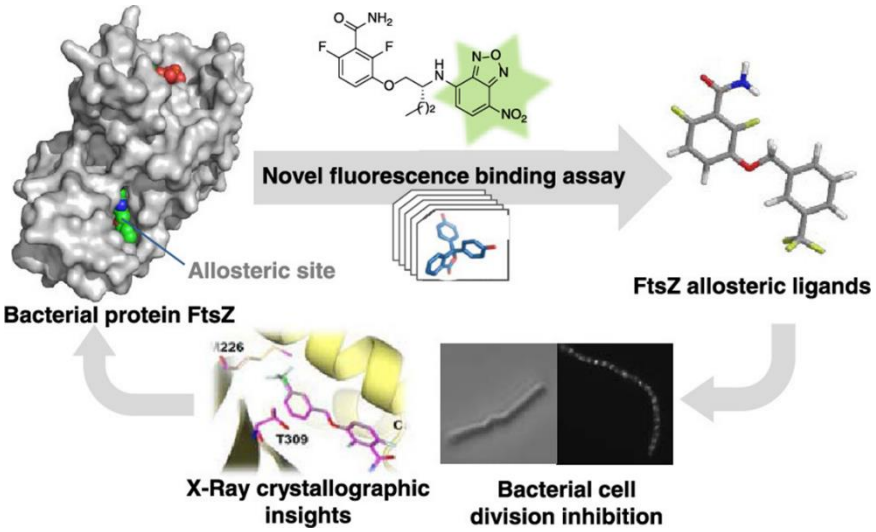

EXPERIMENTAL SECTION

4. EXPERIMENTAL SECTION

4.1. Synthesis and characterization

Unless stated otherwise, starting materials, reagents and solvents were purchased as high-grade commercial products from Abcr, Acros, Scharlab, Alfa Aesar, Bachem, Sigma-Aldrich, or Thermo Fisher Scientific, and were used without further purification. All non-aqueous reactions were performed under an argon atmosphere in oven-dried glassware. Tetrahydrofuran (THF), diethyl ether, and dichloromethane (DCM) were dried using a Pure Solv™ Micro 100 Liter solvent purification system. Reactions under MW irradiation were performed in a Biotage Initiator 2.5 reactor using a compressed air system for cooling.

Analytical thin-layer chromatography (TLC) was run on Merck silica gel plates (Kieselgel 60 F-254) with detection by UV light (λ = 254 nm), 5% ninhydrin solution in ethanol, 10% phosphomolybdic acid solution in ethanol or potassium permanganate. Unless otherwise stated, products were purified by flash chromatography on glass columns using silica gel (60 Å pore size, 230-400 mesh particle size from Supelco) or using a VARIAN 971-FP system with cartridges of silica gel (Varian, particle size 50 μm).

Melting points (m.p., uncorrected) were determined on a Stuart Scientific electrothermal apparatus. Infrared (IR) spectra were measured on a Bruker Tensor 27 instrument equipped with a Specac ATR accessory of 5200-650 cm^{-1} transmission range; frequencies (v) are expressed in cm^{-1}. Nuclear Magnetic Resonance (NMR) spectra were recorded on a Bruker Avance III 700 MHz (^{1}H, 700 MHz; ^{13}C, 175 MHz), Bruker Avance 500 MHz (^{1}H, 500 MHz; ^{13}C, 125 MHz), or Bruker DPX 300 MHz (^{1}H, 300 MHz; ^{13}C, 75 MHz) instruments at the Universidad Complutense de Madrid's NMR core facilities. Chemical shifts (δ) are expressed in parts per million relative to the residual solvent peak for ^{1}H and ^{13}C nucleus ($CDCl_3$: δ_H = 7.26, δ_C = 77.2; MeOH-*d*$_4$: δ_H = 3.31, δ_C = 49.0; DMSO-*d*$_6$: δ_H = 2.50, δ_C = 39.5; acetone-*d*$_6$: δ_H = 2.05, δ_C = 29.8, 206.3), and coupling constants (*J*) are in hertz (Hz). The following abbreviations are used to describe peak patterns when appropriate: s (singlet), d (doublet), t (triplet), q (quadruplet), qt (quintuplet), sext (sextuplet), m (multiplet), app (apparent), and br (broad). 2D NMR experiments –homonuclear correlation spectroscopy (H,H-COSY), heteronuclear multiple quantum correlation (HMQC) and heteronuclear multiple bond correlation (HMBC)– of representative compounds were acquired to assign protons and carbons of new structures. High resolution mass

spectrometry (HRMS) was carried out on a FTMS Buker APEX-Q-IV spectrometer in electrospray ionization (ESI) or matrix-assisted laser desorption ionization (MALDI) mode at UCM's mass spectrometry core facility.

Spectroscopic data of all described compounds were consistent with the proposed structures. Satisfactory HPLC-MS chromatograms were obtained for all tested compounds, which confirmed a purity of at least 95%. HPLC-MS analysis was performed using an Agilent 1200LC-MSD VL instrument. LC separation was achieved with a Zorbax Eclipse XDB-C18 column (5 µm, 4.6 mm x 150 mm) together with a guard column (5 µm, 4.6 mm x 12.5 mm). The gradient mobile phases consisted of A (water) and B (acetonitrile) with 0.1% formic acid as the solvent modifier. Gradients are indicated in Table 3. MS analysis was performed with an ESI source. The capillary voltage was set to 3.0 kV and the fragmentor voltage was set at 72 eV. The drying gas temperature was 350 ºC, the drying gas flow was 10 L/min, and the nebulizer pressure was 20 psi. Spectra were acquired in positive or negative ionization mode from 100 to 1200 *m/z* and in UV-mode at four different wavelengths (210, 230, 254, and 280 nm).

Table 3. HPLC gradient.

t (min)	%B
0	0
2	0
8	60
20	100
25	100
35	0

Optical rotation [α] was measured on an Anton Paar MCP 100 modular circular polarimeter using a sodium lamp (λ = 589 nm) with a 1 dm path length; concentrations (c) are given as g/100 mL. The enantiomeric excess (*ee*) was determined by HPLC using a chiral column (Chiralpak® IA, 5 µm, 4.6 mm x 150 mm) and hexane:isopropanol:triethylamine:TFA (70/30/0.3/0.1) as mobile phase (1 mL/min). HPLC traces were compared to racemic samples obtained by mixing equal amounts of the enantiopure compounds independently obtained.

4.1.1. General synthetic procedures

4.1.1.1. Williamson alkylation (**9**-**11**, **24**, **26**, and **33**-**36**)

To a solution of the corresponding benzamide (**5**, 3- or 4-hydroxybenzamide, 1.0-1.5 equiv), K_2CO_3 (1.-5-3.0 equiv) and NaI (0.2 equiv) in anhydrous DMF (6-10 mL/mmol), a solution of the proper bromo derivative (1.0-1.5 equiv; 1 mL/mmol) in anhydrous DMF was added dropwise. The reaction mixture was stirred at rt for 24 h. Then, the reaction was concentrated under reduced pressure and the residue was dissolved in ethyl acetate (EtOAc) and washed with brine (x3). The organic layer was dried over Na_2SO_4, filtered and the solvent was evaporated under reduced pressure. The crude was purified by flash chromatography.

4.1.1.2. Mitsunobu reaction [(*R*)-, (*S*)-**9**, **37**-**41**, *rac*-, (*R*)- and (*S*)-**16**]

Method A: To a solution of benzamide **5** (1.0 equiv) in anhydrous DMF (10 mL/mmol), the corresponding alcohol (1.0 equiv), tributylphosphine (1.0 equiv), and DIAD (1.0 equiv) were added, and the reaction mixture was stirred under MW irradiation at 150 ºC for 1.5-2 h. Then, the mixture was diluted with EtOAc and the organic layer was washed with brine (x3), dried over Na_2SO_4, filtered, and concentrated under reduced pressure. The residue was purified by flash chromatography. **Method B**: To a solution of benzamide **5** (1.0 equiv) in anhydrous DMF (5 mL/mmol), alcohol *rac*-, (*R*)-, or (*S*)-**15** (1.0 equiv), tributylphosphine (1.0 equiv), and DIAD (1.0 equiv) were added, and the reaction mixture was stirred at 80 ºC for 48 h. Then, the mixture was diluted with EtOAc and the organic layers were washed with brine (x3), dried over Na_2SO_4, filtered, and concentrated under reduced pressure. The residue was purified by flash chromatography.

4.1.1.3. Synthesis of *N*-Boc-2-bromoalkylamines (**6**-**8**)

To a solution of the corresponding terminal alkene (1.0 equiv) in refluxing anhydrous DCM (10 mL), a solution of BBC in anhydrous DCM (1.0 equiv; 1.6 mL/mmol) was added dropwise, and the reaction was refluxed for 3 h and then stirred at rt overnight. Afterward, the reaction was cooled to 5-10 ºC and a 12% aqueous solution of Na_2SO_3 (1.1 mL/mmol) was slowly added and the mixture was stirred for 15 min. After this time, the mixture was extracted with DCM and the organic phase was washed with water, dried over Na_2SO_4, filtered, and concentrated under reduced pressure. The crude was purified by flash chromatography.

4.1.1.4. Boc protection of amines [*rac*-, (*R*)-, and (*S*)-**15**]

To a solution of *rac*-, (*R*)-, or (*S*)-2-aminopentanol (1.0 equiv) and pyridine (1.1 equiv) in anhydrous THF at 0 ºC, di-*tert*-butyldicarbonate was added, and the mixture was allowed to warm to rt and stirred overnight. Then, the mixture was poured into aqueous 2 M HCl

and was extracted with EtOAc (x2). Organic layer was dried over Na_2SO_4, filtered, and concentrated under reduced pressure to afford the corresponding *N*-Boc-2-aminoalcohol.

4.1.1.5. Synthesis of *N*-Boc-aminoalcohols [(*R*)- and (*S*)-**18**]

To an open-air solution of the (*R,R*)- or (*S,S*)-(salen)-Co(II) complex [(*R,R*)- or (*S,S*)-(*N*,*N'*-bis(3,5-di-*tert*-butylsalicylidene)-1,2-cyclohexanediaminocobalt(II)] (4.4 mol%) in methyl *tert*-butyl ether (TBME, 0.3 mL/mmol) in a vial, *p*-nitrobenzoic acid (8.8 mol%) was added. The vial was closed with a rubber stopper and the mixture was stirred at rt till the red color turned to dark brown. Next, *tert*-butyl carbamate (1 equiv) and TBME (0.1 mL/mmol) were added. After 5 min stirring, 1,2-epoxypentane (2.2 equiv) was added dropwise and stirring was continued at rt for 24 h. Then, the mixture was flushed through a plug of silica gel and the solvent was removed under reduced pressure. The residue was purified by flash chromatography.

4.1.1.6. Removal of the Boc protecting group [**12**-**14**, and **17**]

To a solution of Boc derivatives **9**-**11**, **16** (1.0 equiv) in anhydrous DCM (10 mL/mmol), TFA (20 equiv) was added dropwise, and the reaction mixture was stirred at rt for 1 h. Then, the mixture was concentrated under reduced pressure and the residue was dissolved in DCM and neutralized with a saturated aqueous solution of $NaHCO_3$. The aqueous phase was then extracted with DCM and the organic layer was dried over Na_2SO_4, filtered, and concentrated under reduced pressure. The residue was purified by flash chromatography.

4.1.1.7. Nucleophilic substitution of Cl-NBD with amines (**1**-**4**)

To a solution of amine **12-14** or **17** (1 equiv), and Cs_2CO_3 (3 equiv) in anhydrous acetonitrile (50 mL/mmol), a solution of Cl-NBD (1-1.2 equiv) in anhydrous acetonitrile (1 mL/mmol) was added and the reaction was stirred at 80 ºC for 1 h. Then, the solvent was evaporated under reduced pressure and the crude was purified by flash chromatography.

4.1.1.8. Reductive amination (**19** and **22**)

A mixture of 3-chlorobenzaldehyde (1.0 equiv) and 3- or 4-aminobenzamide (1.2 equiv) was stirred at 100 °C under MW irradiation for 10 min. The crude was purified by chromatography with neutralized silica to afford the pure imine intermediate. Next, the imine was dissolved in methanol (25 mL/mmol) and the solution was pumped through an H-Cube® hydrogenation reactor at a flow-rate of 1 mL/min at 40 °C under full-H_2 mode, using a 10% Pd/C CatCart® cartridge. Then, the solvent was removed under reduced pressure and the residue was purified by flash chromatography.

4.1.1.9. *N*-methylation (**20** and **23**)

To a solution of the corresponding secondary amine **19, 22** (1 equiv) in anhydrous DMF (11 mL/mmol), methyl iodide (3 equiv) and potassium carbonate (4 equiv) were added, and the reaction was stirred at 60 °C for 24 h. Afterward, the mixture was diluted with EtOAc and washed with brine (x3). The organic layer was dried over Na_2SO_4, filtered, and concentrated under reduced pressure. The residue was purified by flash chromatography.

4.1.1.10. Cross coupling of aryliodides with amines [**44**, *rac*-, (*R*)-, (*S*)-**45**]

A mixture of 1-iodo-3-(trifluoromethyl)benzene (1 equiv), tripotassium phosphate (2 equiv), copper (I) iodide (0.04 equiv), the corresponding aminoalcohol (2-aminoethanol or 2-aminopentan-1-ol, 1.0 equiv), ethylene glycol (2.0 equiv) in 2-propanol (13 mL/mmol) was stirred under MW irradiation at 150 °C for 105 min. Then, the reaction was diluted with EtOAc (30 mL) and poured into water. The organic layer was separated, and the aqueous phase was extracted with EtOAc (x2). The combined organic phases were washed with brine, dried over Na_2SO_4, filtered, and concentrated under reduced pressure. The residue was purified by flash chromatography.

4.1.2. Synthesis of fluorescent NBD-derivatives **1**-**4** (and both enantiomers of compounds **1** and-**4**)

2,6-Difluoro-3-hydroxybenzamide, 5. To a suspension of 2,6-difluoro-3-methoxybenzamide (5.0 g, 27 mmol) in anhydrous DCM (50 mL), a 1 M solution of BBr_3 in DCM (53 mL, 53 mmol) was added dropwise at 0 ºC, and the reaction was stirred at rt for 3 days. Then, the mixture was quenched with a saturated aqueous solution of $NaHCO_3$, followed by addition of a 10% aqueous solution of NaOH (70 mL). The organic phase was separated, the aqueous layer was acidified with 2 M HCl and extracted with EtOAc (4 x 70 mL). The combined organic phases were dried over Na_2SO_4, filtered, and concentrated under reduced pressure. The residue was filtered through a pad of silica to afford benzamide **5** as a white solid (4.40 g, 95%).

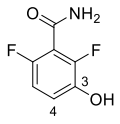

5

M.p.: 123-124 ºC. Rf: 0.50 (hexane/EtOAc, 2:8). IR (ATR): ν 3193 (NH), 1666 (C=O), 1596, 1493, 1396 (Ar). ^{1}H NMR (300 MHz, acetone-d_6) δ 6.87 (td, J = 8.8, 1.8, 1H, H_5), 7.01 (td, J = 9.2, 5.4, 1H, H_4), 7.17 (br s, 1H, ½NH_2), 7.41 (br s, 1H, ½NH_2), 8.79 (s, 1H, OH). The spectroscopic data are in agreement with those previously described.[40]

***tert*-Butyl *N,N*-dibromocarbamate (BBC).** To a solution of *t*-butyl carbamate (1.3 g, 11 mmol) and K_2CO_3 (1.5 g 22 mmol) in water (20 mL), bromine (1.2 mL, 22 mmol) was added dropwise, and the reaction was stirred at rt for 2 h. Afterward, DCM (100 mL) was added and stirring was continued for 15 min. Then, the organic layer was separated, and the aqueous phase was extracted with DCM (3 x 10 mL). The combined organic phases were washed with water (40 mL), dried over Na_2SO_4 and concentrated under reduced pressure to afford BBC as an orange solid (2.40 g, 79%), which was used without further purification.

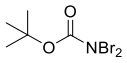

BBC

^{1}H NMR (300 MHz, $CDCl_3$) δ 1.49 (s, 9H, $3CH_3$). The spectroscopic data are in agreement with those previously described.[51]

***tert*-Butyl (2-bromopentyl)carbamate, 6.** Following general procedure 4.1.1.3, compound **6** was obtained from 1-pentene (500 mg, 7.1 mmol) and BBC (1.96 g, 7.1 mmol) as an oil (1.04 g, 55%). The spectroscopic data are in agreement with those previously described.[51]

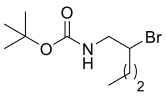

6

***tert*-Butyl (2-bromoheptyl)carbamate, 7.** Following general procedure 4.1.1.3, compound **7** was obtained from 1-heptene (640 mg, 6.5 mmol) and BBC (1.79 g, 6.5 mmol) as an oil (1.11 g, 58%). The spectroscopic data are in agreement with those previously described.[51]

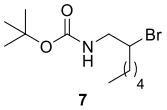

7

***tert*-Butyl (2-bromodecyl)carbamate, 8.** Following general procedure 4.1.1.3, compound **8** was obtained from 1-decene (860 mg, 6.1 mmol) and BBC (1.68 g, 6.1 mmol) as an oil (1.15 g, 56%).

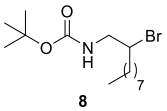

8

Rf: 0.38 (hexane/EtOAc, 1:1). IR (ATR) ν 3360 (NH), 1703 (C=O). ^{1}H NMR (300 MHz, $CDCl_3$) δ 0.87 (t, J = 6.6, 3H, CH_3), 1.26 (br s, 10H, $5CH_2$), 1.44-1.48 (m, 11H, CH_2,

$(CH_3)_3C$), 1.75-1.83 (m, 2H, C<u>H</u>$_2$CHBr), 3.29-3.36 (m, 1H, ½C<u>H</u>$_2$NH), 3.60-3.62 (m, 1H, ½C<u>H</u>$_2$NH), 4.08 (br s, 1H, CH), 4.98 (br s, 1H, NH). ^{13}C NMR (75 MHz, $CDCl_3$) δ 14.2 (CH_3), 22.8, 27.5 (CH_2), 28.5 (($\underline{C}H_3)_3C$), 29.1, 29.3, 29.5, 32.0 (CH_2), 36.3 ($\underline{C}H_2$CHBr), 47.7 (CH_2NH), 57.8 (CHBr), 79.9 (($CH_3)_3\underline{C}$), 155.9 (CO).

***tert*-Butyl (1-hydroxypentan-2-yl)carbamate, 15.** Following general procedure 4.1.1.4, compound **15** was obtained from 2-aminopentanol (600 mg, 5.8 mmol) as an oil (1.12 g, 95%).

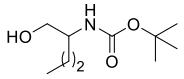

15

^{1}H NMR (300 MHz, $CDCl_3$) δ 0.93 (t, *J* = 7.1, 3H, CH_3), 1.33-1.50 (m, 13H, $2CH_2$, $(CH_3)_3C$), 2.10 (br s, 1H, OH), 3.47-3.58 (m, 1H, CH), 3.59-3.70 (m, 2H, C<u>H</u>$_2$OH), 4.59 (br s, 1H, NH). The spectroscopic data are in agreement with those previously described.[52]

(*R*)-15. Following general procedure 4.1.1.4, compound (*R*)-**15** was obtained from (*R*)-2-aminopentanol (700 mg, 6.8 mmol) as an oil (1.28 g, 93%). The spectroscopic data were in agreement with those described for *rac*-**15**.

(*S*)-15. Following general procedure 4.1.1.4, compound (*S*)-**15** was obtained from (*S*)-2-aminopentanol (600 mg, 5.8 mmol) as an oil (1.13 g, 96%). The spectroscopic data were in agreement with those described for *rac*-**15**.

(*R*)-*tert*-Butyl (2-hydroxypentyl)carbamate, (*R*)-18. Following general procedure 4.1.1.5, compound **(*R*)-18** was obtained from *tert*-butyl carbamate (308 mg, 2.6 mmol), (*S,S*)-(salen)-Co(II) complex (70 mg, 0.12 mmol), and 1,2-epoxypentane (493 mg, 5.7 mmol) as an oil (325 mg, 61%).

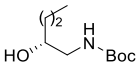

(*R*)-**18**

^{1}H NMR (300 MHz, $CDCl_3$) 0.94 (t, *J* = 6.9, 3H, CH_3), 1.33-156 (m, 13H, $(CH_3)_3C$, $2CH_2$), 3.00 (dd, *J* = 14.1, 7.7, 1H, ½CH_2N), 3.30 (d, *J* = 14.1, 1H, ½CH_2N), 3.66-3.74 (q, *J* = 2.8, 1H, CH), 4.90 (s, 1H, OH). The spectroscopic data were in agreement with those previously reported.[12] $[\alpha]_D^{24}$ = – 11.5 (c = 0.24, $CHCl_3$) [lit.[12]: $[\alpha]_D^{24}$ = – 13.2 (c = 0.98, $CHCl_3$, for *ee* ≥ 96%].

(*S*)-*tert*-Butyl (2-hydroxypentyl)carbamate, (*S*)-18. Following general procedure 4.1.1.5, compound **(*S*)-18** was obtained from *tert*-butyl carbamate (308 mg, 2.6 mmol), (*R,R*)-(salen)-Co(II) complex (70 mg, 0.12 mmol), and 1,2-epoxypentane (493 mg, 5.7 mmol) as an oil (300 mg, 56%). The spectroscopic data were in agreement with those described for enantiomer *R*. $[\alpha]_D^{24}$ = + 12.0 (c = 0.24, $CHCl_3$).

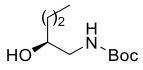

(*S*)-**18**

3-[(1-*N*-Boc-Aminopentan-2-yl)oxy]-2,6-difluorobenzamide, 9. Following general procedure 4.1.1.1, compound **9** was obtained from **5** (162 mg, 0.94 mmol) and bromo derivative **6** (249 mg, 0.94 mmol) as an oil (48 mg, 15%).

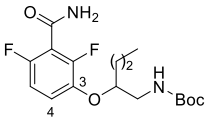

9

Rf: 0.50 (hexane/EtOAc, 2:1). IR (ATR): ν 3376 (NH), 1683 (C=O), 1612, 1509, 1490 (Ar). ^{1}H NMR (700 MHz, $CDCl_3$) δ 0.93 (t, *J* = 7.5, 3H, CH_3), 1.43 (s, 11H, $(CH_3)_3C$, CH_2), 1.55-1.60 (m, 1H, ½CH_2), 1.64-1.70 (m, 1H, ½CH_2), 3.25-3.29 (m, 1H, ½CH_2N), 3.42-3.44 (m, 1H, ½CH_2N), 4.29 (m, 1H, CH), 4.89 (br s, 1H, NH), 6.02 (br s, 2H, NH_2), 6.86-6.89 (m, 1H, H_5), 7.07-7.11 (m, 1H, H_4). ^{13}C NMR (175 MHz, $CDCl_3$) δ 14.2 (CH_3), 18.6 (CH_2), 28.5 ($(\underline{C}H_3)_3C$), 34.1 (CH_2), 43.9 (CH_2N), 79.8 ($(CH_3)_3\underline{C}$), 80.6 (CHO), 111.5 (dd, $J_{C\text{-}F}$ = 23.1, 4.0, C_5), 114.1 (dd, $J_{C\text{-}F}$ = 14.0, 9.0, C_1), 120.3 (dd, $J_{C\text{-}F}$ = 9.9, 2.3, C_4), 143.3 (dd, $J_{C\text{-}F}$ = 10.9, 3.2, C_3), 151.2 (dd, $J_{C\text{-}F}$ = 254.0, 7.7, CF), 154.0 (dd, $J_{C\text{-}F}$ = 247.5, 5.0, CF), 156.2 (NHCO), 162.1 ($CONH_2$). MS (ESI, m/z): 259.2 $[(M\text{-Boc})+H]^+$.

(*R*)-9. Following general procedure 4.1.1.2 Method A, compound (*R*)-**9** was obtained from **5** (244 mg, 1.4 mmol) and (*S*)-**18** (287 mg, 1.4 mmol) as an oil (140 mg, 28%). The spectroscopic data were in agreement with those described for *rac*-**9**.

(*S*)-9. Following general procedure 4.1.1.2 Method A, compound (*S*)-**9** was obtained from **5** (298 mg, 1.7 mmol) and (*R*)-**18** (350 mg, 1.7 mmol) as an oil (190 mg, 31%). The spectroscopic data were in agreement with those described for *rac*-**9**.

3-[(1-*N*-Boc-Aminoheptan-2-yl)oxy]-2,6-difluorobenzamide, 10. Following general procedure 4.1.1.1, compound **10** was obtained from **5** (176 mg, 1.0 mmol) and bromo derivative **7** (294 mg, 1.0 mmol) as an oil (56 mg, 14%).

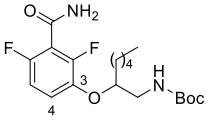

10

Rf: 0.69 (hexane/EtOAc, 2:1). IR (ATR): ν 3380 (NH), 1684 (C=O), 1519, 1489 (Ar). ^{1}H NMR (700 MHz, $CDCl_3$) δ 0.86-0.90 (m, 3H, CH_3), 1.28-1.31 (m, 4H, $2CH_2$), 1.42 (s, 11H, $(CH_3)_3C$, CH_2), 1.56-1.61 (m, 1H, ½CH_2), 1.64-1.70 (m, 1H, ½CH_2), 3.24-3.28 (m, 1H, ½CH_2N), 3.42-3.44 (m, 1H, ½CH_2N), 4.26 (m, 1H, CH), 4.91 (br s, 1H, NH), 6.06 (br s, 1H,

½NH_2), 6.22 (br s, 1H, ½NH_2), 6.87 (app t, J = 9.0, 1H, H_5), 7.06-7.09 (m, 1H, H_4). ^{13}C NMR (175 MHz, $CDCl_3$) δ 14.1 (CH_3), 22.6 (CH_2), 24.9 (CH_2), 28.5 (($\underline{C}H_3)_3C$), 31.6 (CH_2), 31.9 (CH_2), 43.9 (CH_2N), 79.7 (($CH_3)_3\underline{C}$), 80.8 (CHO), 111.5 (dd, $J_{C\text{-}F}$ = 23.5, 3.4, C_5), 114.2 (t, $J_{C\text{-}F}$ = 18.7, C_1), 120.3 (d, $J_{C\text{-}F}$ = 8.8, C_4), 143.2 (dd, $J_{C\text{-}F}$ = 11.1, 3.4, C_3), 151.1 (dd, $J_{C\text{-}F}$ = 254.0, 7.0, CF), 154.0 (d, $J_{C\text{-}F}$ = 247.4, 4.6, CF), 156.2 (NHCO), 162.2 ($CONH_2$). MS (ESI, m/z): 287.2 $[(M\text{-Boc})+H]^+$.

3-[(1-*N*-Boc-Aminodecan-2-yl)oxy]-2,6-difluorobenzamide, 11. Following general procedure 4.1.1.1, compound **11** was obtained from **5** (300 mg, 1.7 mmol) and bromo derivative **8** (403 mg, 1.2 mmol) as an oil (115 mg, 23%).

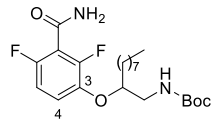

11

Rf: 0.53 (hexane/EtOAc, 6:4). IR (ATR): ν 3356 (NH), 1681 (C=O), 1489, 1367 (Ar). ^{1}H NMR (300 MHz, $CDCl_3$) δ 0.85 (t, J = 6.7, 3H, CH_3), 1.24 (br s, 10H, 5CH_2), 1.41-1.42 (m, 11H, CH_2, $(CH_3)_3C$), 1.54-1.69 (m, 2H, CH_2), 3.22-3.29 (m, 1H, ½CH_2N), 3.39-3.43 (m, 1H, ½CH_2N), 4.25 (br s, 1H, CH), 4.96 (br s, 1H, NH), 6.16 (br s, 1H, ½NH_2), 6.58 (br s, 1H, ½NH_2), 6.84 (td, J = 9.1, 1.8, 1H, H_5), 7.38 (td, J = 8.9, 5.3 1H, H_4). ^{13}C NMR (75 MHz, $CDCl_3$) δ 14.5 (CH_3), 23.0, 25.5 (CH_2), 28.7 (($\underline{C}H_3)_3C$), 29.6, 29.8, 30.0 (CH_2), 32.2 (CH_2), 44.1 (CH_2N), 80.0 (($CH_3)_3\underline{C}$), 81.1 (CHO), 111.7 (dd, $J_{C\text{-}F}$ = 23.3, 4.3, C_5), 114.6 (dd, $J_{C\text{-}F}$ = 20.5, 16.8, C_1), 120.5 (dd, $J_{C\text{-}F}$ = 9.9, 2.3, C_4), 143.3 (dd, $J_{C\text{-}F}$ = 11.2, 3.3, C_3), 151.3 (dd, $J_{C\text{-}F}$ = 253.9, 6.9, CF), 154.7 (dd, $J_{C\text{-}F}$ = 256.6, 7.1, CF), 156.5 (NHCO), 162.8 ($CONH_2$). MS (ESI, m/z): 328.2 $[M+H]^+$.

3-[(2-*N*-Boc-Aminopentyl)oxy]-2,6-difluorobenzamide, 16. Following general procedure 4.1.1.2 Method B, compound **16** was obtained from **5** (400 mg, 2.3 mmol) and racemic alcohol **15** (466 mg, 2.3 mmol) as an oil (147 mg, 18%).

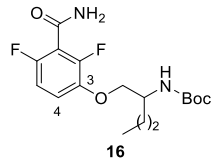

16

Rf: 0.58 (hexane/EtOAc, 6:4). IR (ATR): ν 3317, 3192 (NH), 1676 (C=O), 1627, 1492, 1461 (Ar). ^{1}H NMR (700 MHz, $CDCl_3$) δ 0.94 (t, J = 7.5, 3H, CH_3), 1.34-1.41 (m, 2H, CH_2), 1.44 (s, 9H, $(CH_3)_3C$), 1.54-1.59 (m, 1H, ½CH_2), 1.63-1.66 (m, 1H, ½CH_2), 3.90 (m, 1H, CH), 4.00 (m, 2H, CH_2O), 4.75 (d, J = 8.5, 1H, NH), 6.06 (br s, 1H, ½NH_2), 6.20 (br s, 1H, ½NH_2), 6.87 (td, J = 9.1, 1.5, 1H, H_5), 7.01-7.04 (m, 1H, H_4). ^{13}C NMR (175 MHz, $CDCl_3$) δ 14.0 (CH_3), 19.4 (CH_2), 28.5 (($\underline{C}H_3)_3C$), 33.9 (CH_2), 49.9 (CHN), 72.1 (CH_2O), 79.7 (($CH_3)_3\underline{C}$), 111.3 (dd, $J_{C\text{-}F}$ = 23.5, 4.0, C_5), 114.1 (dd, $J_{C\text{-}F}$ = 20.5, 16.5, C_1), 117.3 (d, $J_{C\text{-}F}$ =

8.5, C_4), 144.0 (dd, J_{C-F} = 11.1, 3.0, C_3), 150.2 (dd, J_{C-F} = 255.0, 6.5, CF), 153.7 (dd, J_{C-F} = 246.5, 3.0, CF), 155.7 (NHCO), 162.2 ($CONH_2$). MS (ESI, m/z): 259.2 $[(M\text{-}Boc)+H]^+$.

(*R*)-16. Following general procedure 4.1.1.2 Method B, compound (*R*)-**16** was obtained from **5** (675 mg, 3.9 mmol) and (*R*)-**15** (793 mg, 3.9 mmol) as an oil (250 mg, 18%). The spectroscopic data were in agreement with those described for *rac*-**16.**

(*S*)-16. Following general procedure 4.1.1.2 Method B, compound (*S*)-**16** was obtained from **5** (395 mg, 2.3 mmol) and (*S*)-**15** (464 mg, 2.3 mmol) as an oil (150 mg, 19%). The spectroscopic data were in agreement with those described for *rac*-**16**.

3-[(1-Aminopentan-2-yl)oxy]-2,6-difluorobenzamide, 12. Following general procedure 4.1.1.6, compound **12** was obtained from **9** (40 mg, 0.11 mmol) as an oil (24 mg, 83%). MS (ESI, m/z): 258.1 $[M+H]^+$.

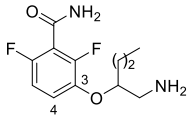

12

(*R*)-12. Following general procedure 4.1.1.6, compound (*R*)-**12** was obtained from (*R*)-**9** (120 mg, 0.33 mmol) as an oil (69 mg, 81%).

(*S*)-12. Following general procedure 4.1.1.6, compound (*S*)-**12** was obtained from (*S*)-**9** (128 mg, 0.36 mmol) as an oil (77 mg, 83%).

3-[(1-Aminoheptan-2-yl)oxy]-2,6-difluorobenzamide, **13.** Following general procedure 4.1.1.6, compound **13** was obtained from **10** (24 mg, 0.06 mmol) as an oil (27 mg, 85%). MS (ESI, m/z): 289.2 $[M+H]^+$.

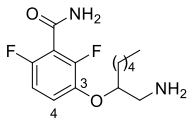

13

3-[(1-(Aminodecan-2-yl)oxy]-2,6-difluorobenzamide, 14. Following general procedure 4.1.1.6, compound **14** was obtained from **11** (110 mg, 0.26 mmol) as an oil (68 mg, 80%). MS (ESI, m/z): 329.2 $[M+H]^+$.

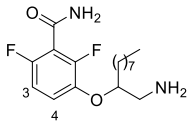

14

3-[(2-Aminopentyl)oxy]-2,6-difluorobenzamide, 17. Following general procedure 4.1.1.6, compound **17** was obtained from **16** (110 mg, 0.26 mmol) as an oil (60 mg, 90%). MS (ESI, m/z): 258.1 $[M+H]^+$.

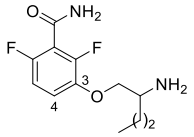

17

(*R*)-17. Following general procedure 4.1.1.6, compound (*R*)-**17** was obtained from (*R*)-**16** (266 mg, 0.74 mmol) as an oil (135 mg, 70%).

(*S*)-17. Following general procedure 4.1.1.6, compound (*S*)-**17** was obtained from (*S*)-**16** (225 mg, 0.63 mmol) as an oil (121 mg, 75%).

2,6-Difluoro-3-[(1-{[(7-nitro-2,1,3-benzoxadiazol-4-yl)amino]methyl}butyl)oxy] benzamide, 1. Following general procedure 4.1.1.7, compound *rac*-**1** was obtained from amine *rac*-**35** (28 mg, 0.11 mmol), Cl-NBD (22 mg, 0.11 mmol) and Cs_2CO_3 (108 mg, 0.33 mmol) as an oil (23 mg, 50%).

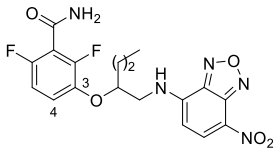

1

Rf: 0.52 (hexane/EtOAc, 1:2). IR (ATR): ν 3351 (NH), 1683 (C=O), 1623, 1507, 1489 (Ar). ^{1}H NMR (700 MHz, $CDCl_3$) δ 0.99 (t, *J* = 7.5, 3H, CH_3), 1.46-1.54 (m, 2H, CH_2), 1.68-1.77 (m, 1H, ½CH_2), 1.81-1.89 (m, 1H, ½CH_2), 3.67-3.82 (m, 2H, CH_2N), 4.44-4.52 (m, 1H, CH), 6.00 (br s, 2H, NH_2), 6.25 (d, *J* = 8.5, 1H, CH_{NBD}), 6.59 (br s, 1H, NH), 6.88 (td, *J* = 9.0, 1.5, 1H, H_5), 7.07 (td, *J* = 9.0, 5.0, 1H, H_4), 8.49 (d, *J* = 8.5, 1H, CH_{NBD}). ^{13}C NMR (175 MHz, $CDCl_3$) δ 14.2 (CH_3), 18.6, 34.1 (CH_2), 46.9 (CH_2N), 80.3 (CHO), 99.3 (br s, CH_{NBD}), 111.9 (dd, $J_{C\text{-}F}$ = 23.5, 4.0, C_5), 114.6 (dd, $J_{C\text{-}F}$ = 20.9, 16.8, C_1), 122.0 (dd, $J_{C\text{-}F}$ = 9.8, 2.3, C_4), 124.6 (C_{NBD}), 136.4 (CH_{NBD}), 142.1 (dd, $J_{C\text{-}F}$ = 11.0, 3.0, C_3), 144.0 ($2C_{NBD}$), 144.4, (C_{NBD}), 151.6 (dd, $J_{C\text{-}F}$ = 254.0, 7.0, CF), 154.7 (dd, $J_{C\text{-}F}$ = 249.0, 5.5, CF), 161.8 ($CONH_2$). ESI-HRMS (calcd., found for $C_{18}H_{21}F_2N_6O_5$ $[M+NH_4]^+$): 439.1536, 439.1548.

(*R*)-1. Following general procedure 4.1.1.7, compound (*R*)-**1** was obtained from amine (*R*)-**12** (60 mg, 0.23 mmol), Cl-NBD (56 mg, 0.28 mmol) and Cs_2CO_3 (151 mg, 0.46 mmol) as an oil (30 mg, 31%). The spectroscopic data were in agreement with those described for *rac*-**1**. $[\alpha]_D^{24}$ = + 35.0 (c = 0.16, $CHCl_3$). Chiral HPLC (t_R, min): 7.99, *ee* = 98%.

(*S*)-1. Following general procedure 4.1.1.7, compound (*S*)-**1** was obtained from amine (*S*)-**12** (65 mg, 0.25 mmol), Cl-NBD (60 mg, 0.30 mmol) and Cs_2CO_3 (164 mg, 0.50 mmol) as an oil (35 mg, 33%). The spectroscopic data were in agreement with those described for *rac*-**1**. $[\alpha]_D^{24}$ = – 41.0 (c = 0.16, $CHCl_3$). Chiral HPLC (t_R, min): 6.82, *ee* = 99%.

2,6-Difluoro-3-[(1-{[(7-nitro-2,1,3-benzoxadiazol-4-yl)amino]methyl}hexyl)oxy] benzamide, 2. Following general procedure 4.1.1.7, compound **2** was obtained from amine **13** (17 mg, 0.06 mmol), Cl-NBD (12 mg, 0.06 mmol) and Cs_2CO_3 (59 mg, 0.18 mmol) as an oil (8 mg, 30%).

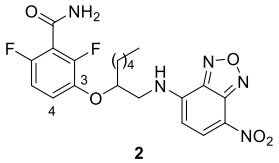

2

Rf: 0.42 (hexane/EtOAc, 1:2). IR (ATR): ν 3314 (NH), 1675 (C=O), 1626, 1582, 1487 (Ar). ^{1}H NMR (700 MHz, $CDCl_3$) δ 0.90 (t, *J* = 7.0, 3H, CH_3), 1.30-1.34 (m, 4H, $2CH_2$), 1.44-1.49 (m, 2H, CH_2), 1.70-1.76 (m, 1H, ½CH_2), 1.83-1.88 (m, 1H, ½CH_2), 3.69-3.76 (m, 1H, ½CH_2N), 3.79-3.85 (m, 1H, ½CH_2N), 4.43-4.50 (m, 1H, CH), 5.96-5.99 (m, 2H, NH_2), 6.25 (d, *J* = 8.6, 1H, CH_{NBD}), 6.58 (t, *J* = 5.7, 1H, NH), 6.89 (td, *J* = 9.0, 1.9, 1H, H_5), 7.07 (td, *J* = 9.0, 5.2, 1H, H_4), 8.49 (d, *J* = 8.6, 1H, CH_{NBD}). ^{13}C NMR (175 MHz, $CDCl_3$) δ 14.1 (CH_3), 22.6, 24.9, 31.8, 32.0 (CH_2), 46.8 (CH_2N), 80.6 (CHO), 99.2 (br s, CH_{NBD}), 111.9 (dd, J_{C-F} = 23.5, 3.5, C_5), 114.6 (dd, J_{C-F} = 20.9, 17.3, C_1), 122.3 (dd, J_{C-F} = 9.8, 2.2, C_4), 124.9 (C_{NBD}), 136.3 (CH_{NBD}), 142.0 (dd, J_{C-F} = 11.5, 2.5, C_3), 143.8, 144.0, 144.5 (C_{NBD}), 151.8 (dd, J_{C-F} = 254.0, 7.0, CF), 154.9 (dd, J_{C-F} = 249.0, 5.0, CF), 161.4 ($CONH_2$). ESI-HRMS (calcd., found for $C_{20}H_{20}F_2N_5O_5$ $[M-H]^-$): 448.1438, 448.1419.

2,6-Difluoro-3-[(1-{[(7-nitro-2,1,3-benzoxadiazol-4-yl)amino]methyl}nonyl)-oxy] benzamide, 3. Following general procedure 4.1.1.7, compound **3** was obtained from amine **14** (110 mg, 0.26 mmol), Cl-NBD (62 mg, 0.26 mmol) and Cs_2CO_3 (254 mg, 0.78 mmol) as an oil (14 mg, 11%).

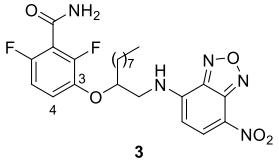

3

Rf: 0.42 (hexane/EtOAc, 1:1). IR (ATR): ν 3426 (NH), 1700 (C=O), 1378, 1364 (Ar). ^{1}H NMR (700 MHz, acetone-d_6) δ 0.86 (t, *J* = 7.1, 3H, CH_3), 1.25-1.36 (m, 10H, $5CH_2$), 1.50-1.59 (m, 2H, CH_2), 1.85-1.88 (m, 2H, CH_2), 4.01 (m, 2H, CH_2N), 4.82 (qt, *J* = 5.7, 2H, CH), 6.61 (d, *J* = 8.8, 1H, CH_{NBD}), 6.90 (td, *J* = 9.0, 1.8, 1H, H_5), 7.15 (br s, 1H, ½NH_2), 7.26 (td, *J* = 9.2, 5.2, 1H, H_4), 7.37 (br s, 1H, ½NH_2), 8.31 (br s, 1H, NH), 8.53 (d, *J* = 8.7, 1H, CH_{NBD}). ^{13}C NMR (175 MHz, acetone-d_6) δ 14.3 (CH_3), 23.3, 25.6, 30.2 (CH_2), 30.3 ($2CH_2$), 32.6, 32.8 (CH_2), 47.8 (br s, CH_2N), 80.1 (CHO), 100.2 (br s, CH_{NBD}), 111.7 (dd, J_{C-F} = 23.4, 3.9, C_5), 117.6 (dd, J_{C-F} = 24.3, 20.4, C_1), 119.3 (dd, J_{C-F} = 9.0, 1.7, C_4), 123.9 (C_{NBD}), 137.7 (br s, CH_{NBD}), 143.4 (dd, J_{C-F} = 11.1, 3.2, C_3), 145.1 (C_{NBD}), 145.6 ($2C_{NBD}$), 150.7 (dd, J_{C-F} = 249.7, 8.6, CF), 153.9 (dd, J_{C-F} = 243.2, 6.5, CF), 162.0 ($CONH_2$). ESI-HRMS (calcd., found for $C_{23}H_{26}F_2N_5O_5$ $[M-H]^-$): 490.1902, 490.1891.

2,6-Difluoro-3-{2-[(4-nitro-2,1,3-benzoxadiazol-7-yl)amino]pentoxy}benzamide, 4. Following general procedure 4.1.1.7, compound *rac*-**4** was obtained from amine *rac*-**17** (15 mg, 0.06 mmol), Cl-NBD (11 mg, 0.06 mmol) and Cs_2CO_3 (55 mg, 0.18 mmol) as an oil (3 mg, 13%).

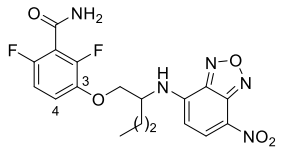

4

Rf: 0.32 (hexane/EtOAc, 1:2). IR (ATR): ν 3390 (NH), 1726 (C=O), 1634, 1485 (Ar). ^{1}H NMR (700 MHz, CD_3OD) δ 1.01 (t, *J* = 7.5, 3H, CH_3), 1.46-1.60 (m, 2H, CH_2), 1.81-1.91 (m, 2H, CH_2), 4.19-4.21 (m, 1H, ½CH_2O), 4.30 (dd, *J* = 10.0, 4.0, 1H, ½CH_2O), 4.37 (br s, 1H, CH), 6.54 (d, *J* = 9.0, 1H, CH_{NBD}), 6.93 (td, *J* = 9.0, 2.0, 1H, H_5), 7.18 (td, *J* = 9.0, 5.0, 1H, H_4), 8.52 (d, *J* = 8.5, 1H, CH_{NBD}). ^{13}C NMR (175 MHz, CD_3OD) δ 14.2 (CH_3), 20.3, 34.0 (CH_2), 54.8 (CHN), 73.3 (CH_2O), 100.4 (CH_{NBD}), 111.9 (dd, J_{C-F} = 23.0, 4.0, C_5), 116.8 (dd, J_{C-F} = 24.0, 20.0, C_1), 117.9 (d, J_{C-F} = 10.0, C_4), 123.3 (C_{NBD}), 138.5 (CH_{NBD}), 144.7 (dd, J_{C-F} = 11.0, 3.0, C_3), 145.6 ($2C_{NBD}$), 145.9 (C_{NBD}), 150.4 (dd, J_{C-F} = 251.5, 8.0, CF), 154.3 (dd, J_{C-F} = 244.0, 6.0, CF), 165.2 ($CONH_2$). HPLC (t_R, min): 14.41. MS (ESI, m/z): 422.1 $[M+H]^+$. ESI-HRMS (calcd., found for $C_{18}H_{16}F_2N_5O_5$ $[M-H]^-$): 420.1125, 420.1124.

(*R*)-4. Following general procedure 4.1.1.7, compound (*R*)-**4** was obtained from amine (*R*)-**17** (40 mg, 0.15 mmol), Cl-NBD (31 mg, 0.16 mmol) and Cs_2CO_3 (100 mg, 0.30 mmol) as an oil (19 mg, 30%). The spectroscopic data were in agreement with those described for *rac*-**4**.

(*S*)-4. Following general procedure 4.1.1.7, compound (*S*)-**4** was obtained from amine (*S*)-**17** (141 mg, 0.55 mmol), Cl-NBD (110 mg, 0.55 mmol) and Cs_2CO_3 (538 mg, 1.7 mmol) as an oil (19 mg, 7%). The spectroscopic data were in agreement with those described for *rac*-**4**.

4.1.3. Synthesis of compounds **19**-**26**

3-[(3-Chlorobenzyl)amino]benzamide, 19. Following general procedure 4.1.1.8, compound **19** was obtained from 3-aminobenzamide (270 mg, 2.0 mmol) and 3-chlorobenzaldehyde (0.19 mL, 1.7 mmol) as a white solid (137 mg, 32%).

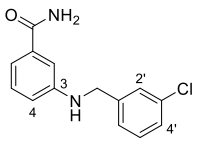

19

Rf: 0.24 (EtOAc). IR (ATR): ν 3346, 3199 (NH), 1655 (C=O), 1604, 1582, 1513, 1489 (Ar). ^{1}H NMR (300 MHz, acetone-d_6) δ 4.43 (s, 2H, CH_2), 5.80 (br s, 1H, NH), 6.45 (br s, 1H, ½NH_2) 6.77-6.80 (m, 1H, H_4), 7.13-7.15 (m, 2H, H_5, H_6), 7.24-7.27 (m, 2H, H_2, $H_{6'}$),

7.31-7.36 (m, 2H, $H_{4'}$, $H_{5'}$) 7.44 (s, 1H, $H_{2'}$). ^{13}C NMR (75 MHz, acetone-d_6) δ 47.3 (CH_2), 112.6 (C_2), 116.3 (C_4), 116.5 (C_6), 126.6 ($C_{4'}$), 127.7 ($C_{6'}$), 127.9 ($C_{2'}$), 129.7 (C_5), 130.9 ($C_{5'}$), 134.6 ($C_{3'}$), 136.4 (C_1), 143.8 ($C_{1'}$), 149.5 (C_3), 169.4 ($CONH_2$). HPLC (t_R, min): 24.38. MS (ESI, m/z): 261.1 ([M(^{35}Cl)+H]$^+$, 100%), 263.1 ([M(^{37}Cl)+H]$^+$, 35%). ESI-HRMS (calcd., found for $C_{14}H_{14}ClN_2O$ [M(^{35}Cl)+H]$^+$): 261.0744, 261.0741; (calcd., found for $C_{14}H_{14}ClN_2O$ [M(^{37}Cl)+H]$^+$): 263.0771, 263.0775.

4-[(3-Chlorobenzyl)amino]benzamide, 22. Following general procedure 4.1.1.8, compound **22** was obtained from 4-aminobenzamide (209 mg, 1.5 mmol) and 3-chlorobenzaldehyde (0.14 mL, 1.3 mmol) as a white solid (244 mg, 74%).

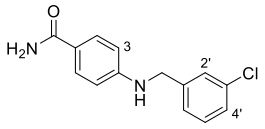

22

Rf: 0.23 (EtOAc). IR (ATR): ν 3338, 3203 (NH), 1647 (C=O), 1603, 1569, 1528, 1489 (Ar). ^{1}H NMR (300 MHz, DMSO-d_6) δ 4.34 (s, 2H, CH_2), 6.55 (d, J = 9.0, 2H, H_3, H_5), 6.83 (d, J = 8.5, 1H, ½NH_2), 6.91 (br s, 1H, NH), 7.26-7.35 (m, 3H, $H_{4'}$ - $H_{6'}$), 7.39 (s, 1H, $H_{2'}$), 7.61 (d, J = 9.0, 2H, H_2, H_6), 7.71 (d, J = 8.5, 1H, ½NH_2). ^{13}C NMR (75 MHz, DMSO-d_6) δ 45.3 (CH_2), 111.1 (C_3, C_5), 121.5 (C_1), 125.8 ($C_{4'}$), 126.7 ($C_{6'}$), 126.9 ($C_{2'}$), 129.0 (C_2, C_6), 130.2 ($C_{5'}$), 133.1 ($C_{3'}$), 142.6 ($C_{1'}$), 150.8 (C_4), 167.9 ($CONH_2$). HPLC (t_R, min): 19.43. MS (ESI, m/z): 260.9 ([M(^{35}Cl)+H]$^+$, 100%), 262.9 ([M(^{37}Cl)+H]$^+$, 35%). ESI-HRMS (calcd., found for $C_{14}H_{14}ClN_2O$ [M(^{35}Cl)+H]$^+$): 261.0744, 261.0741; (calcd., found for $C_{14}H_{14}ClN_2O$ [M(^{37}Cl)+H]$^+$): 263.0771; 263.0775.

3-[(3-Chlorobenzyl)(methyl)amino]benzamide, 20. Following general procedure 4.1.1.9, compound **20** was obtained from **19** (80 mg, 0.31 mmol) as a white solid (29 mg, 35%).

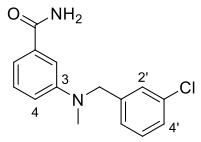

20

M.p.: 126-127 ºC. Rf: 0.24 (EtOAc). IR (ATR): ν 3380, 3188 (NH), 1645 (C=O), 1599, 1574 (Ar). ^{1}H NMR (300 MHz, acetone-d_6) δ 3.10 (s, 3H, CH_3), 4.66 (s, 2H, CH_2), 6.52 (br s, 1H, ½NH_2), 6.87-6.92 (m, 1H, H_4), 7.20-7.34 (m, 6H, H_2, H_5, H_6, $H_{3'}$-$H_{5'}$), 7.37 (s, 1H, $H_{2'}$). ^{13}C NMR (75 MHz, acetone-d_6) δ 39.0 (CH_3), 56.3 (CH_2), 112.3 (C_2), 115.9 (C_4), 116.4 (C_6), 126.1 ($C_{4'}$), 127.5 ($C_{6'}$), 127.7 (C_5), 129.8 ($C_{2'}$), 131.1 ($C_{5'}$), 134.8 ($C_{3'}$), 136.3 (C_1), 142.8 ($C_{1'}$), 150.3 (C_3), 169.5 ($CONH_2$). HPLC (t_R, min): 16.64. MS (ESI, m/z): 275.1 ([M(^{35}Cl)+H]$^+$, 100%), 277.1 ([M(^{37}Cl)+H]$^+$, 35%). ESI-HRMS (calcd., found for $C_{15}H_{16}ClN_2O$ [M(^{35}Cl)+H]$^+$): 275.0946, 275.0946; (calcd., found for $C_{15}H_{16}ClN_2O$ [M(^{37}Cl)+H]$^+$): 277.0916, 277.0917.

4-[(3-Chlorobenzyl)(methyl)amino]benzamide, 23. Following general procedure 4.1.1.9, compound **23** was obtained from **22** (73 mg, 0.28 mmol) as a yellow solid (24 mg, 31%).

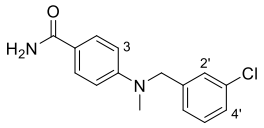

23

M.p.: 104-106 ºC. Rf: 0.40 (hexane/EtOAc, 1:2). IR (ATR): ν 3345 (NH), 1647 (CO), 1602, 1527, 1477 (Ar). ^{1}H NMR (300 MHz, DMSO-d_6) δ 3.08 (s, 3H, CH_3), 4.66 (s, 2H, CH_2), 6.69 (d, J = 9.0, 2H, H_3, H_5), 6.93 (br s, 1H, ½NH_2), 7.14 (d, J = 7.5, 1H, $H_{6'}$), 7.22 (s, 1H, $H_{2'}$), 7.27-7.38 (m, 2H, $H_{4'}$, $H_{5'}$), 7.61 (br s, 1H, ½NH_2), 7.70 (d, J = 9.0, 2H, H_2, H_6). ^{13}C NMR (75 MHz, DMSO-d_6) δ 38.7 (CH_3), 54.4 (CH_2), 110.7 (C_3, C_5), 121.3 (C_1), 125.3 ($C_{6'}$), 126.4 ($C_{2'}$), 126.8 ($C_{4'}$), 129.0 (C_2, C_6), 130.4 ($C_{5'}$), 133.2 ($C_{3'}$), 141.4 ($C_{1'}$), 150.8 (C_4), 167.8 ($CONH_2$). HPLC (t_R, min): 22.64. MS (ESI, m/z): 275.0 ([M(^{35}Cl)+H]$^+$, 100%), 277.0 ([M(^{37}Cl)+H]$^+$, 35%). ESI-HRMS (calcd., found for $C_{15}H_{16}ClN_2O$ [M(^{35}Cl)+H]$^+$): 275.0946, 275.0944; (calcd., found for $C_{15}H_{16}ClN_2O$ [M(^{37}Cl)+H]$^+$): 277.0916, 277.0916.

3-[(3-Chlorobenzyl)(propyl)amino]benzamide, 21. To a solution of amine **19** (30 mg, 0.12 mmol) in methanol (3 mL), propionaldehyde (20 mg, 0.35 mmol) and sodium cyanoborohydride (22 mg, 0.35 mmol) were added, and the reaction was stirred at rt for 72 h. Then, the solvent was evaporated under reduced pressure and the residue was purified by flash chromatography to afford compound **21** as an oil (18 mg, 52%).

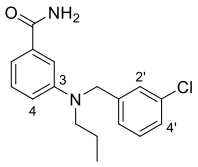

21

Rf: 0.62 (EtOAc). IR (ATR): ν 3404, 3199 (NH), 1650 (C=O), 1615, 1598, 1573 (Ar). ^{1}H NMR (300 MHz, acetone-d_6) δ 0.95 (t, J = 7.5, 3H, CH_3), 1.70 (sext, J = 7.5, 2H, CH_2), 3.48 (t, J = 7.5, 2H, CH_2N), 4.67 (s, 2H, C$\underline{H}_2$Ar), 6.55 (br s, 1H, ½NH_2), 6.82 (dt, J = 7.1, 2.6, 1H, H_4), 7.15-7.27 (m, 5H, H_5, H_6, $H_{2'}$, $H_{4'}$, $H_{6'}$), 7.33-7.36 (m, 2H, H_2, $H_{5'}$). ^{13}C NMR (75 MHz, acetone-d_6) δ 11.5 (CH_3), 21.0 (CH_2), 53.8 (CH_2N), 54.4 ($\underline{C}H_2$Ar), 112.1 (C_2), 115.7 (C_4), 115.9 (C_6), 126.0 ($C_{4'}$), 127.3 ($C_{6'}$), 127.6 ($C_{2'}$), 129.8 (C_5), 131.0 ($C_{5'}$), 134.8 ($C_{3'}$), 136.3 (C_1), 143.0 ($C_{1'}$), 149.2 (C_3), 169.5 ($CONH_2$). HPLC (t_R, min): 22.33. MS (ESI, m/z): 303.1 ([M(^{35}Cl)+H]$^+$, 100%), 305.1 ([M(^{37}Cl)+H]$^+$, 35%). ESI-HRMS (calcd., found for $C_{17}H_{19}ClN_2NaO$ [M(^{35}Cl)+Na]$^+$): 325.1078, 325.1078; (calcd., found for $C_{17}H_{19}ClN_2NaO$ [M(^{37}Cl)+Na]$^+$): 327.1050, 327.1049.

3-[(3-Chlorobenzyl)oxy]benzamide, 24.[59] Following general procedure 4.1.1.1, compound **24** was obtained from 3-hydroxybenzamide (225 mg, 1.6 mmol) and 3-chlorobenzylbromide (0.32 mL, 2.5 mmol) as a white solid (203 mg, 47%).

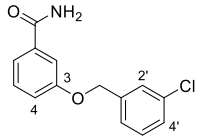

24

M.p.: 113-115 ºC (lit.[59] m.p. 106-108 °C). Rf: 0.48 (hexane/EtOAc, 2:8). IR (ATR): ν 3333, 3156 (NH), 1662 (C=O), 1630, 1581, 1477, 1446 (Ar), 1251 (C=O). ^{1}H NMR (300 MHz, acetone-*d*$_6$) δ 5.20 (s, 2H, CH_2), 6.73 (br s, 1H, ½NH_2), 7.19 (ddd, *J* = 8.2, 2.6, 1.0, 1H, H_4), 7.35-7.48 (m, 5H, $H_{2'}$, $H_{4'}$-$H_{6'}$, ½NH_2), 7.53-7.56 (m, 2H, H_5, H_6), 7.61 (dd, *J* = 2.5, 1.6, 1H, H_2). ^{13}C NMR (75 MHz, acetone-*d*$_6$) δ 69.6 (CH_2), 114.6 (C_2), 118.8 (C_4), 120.9 (C_6), 126.7 ($C_{2'}$), 128.2 (C_5), 128.6 ($C_{5'}$), 130.3 ($C_{6'}$), 131.0 ($C_{4'}$), 134.7 ($C_{3'}$), 136.9 (C_1), 140.7 ($C_{1'}$), 159.5 (C_3), 168.6 ($CONH_2$). HPLC (t_R, min): 19.43. MS (ESI, m/z): 261.9 ([M(^{35}Cl)+H]$^+$, 100%), 263.9 ([M(^{37}Cl)+H]$^+$, 35%). ESI-HRMS (cald., found for $C_{14}H_{12}ClNNaO_2$ [M(^{35}Cl)+Na]$^+$): 284.0449, 284.0448; (cald., found for $C_{14}H_{12}ClNNaO_2$ [M(^{37}Cl)+Na]$^+$): 286.0419, 286.0421.

3-[3-(3-Chlorophenyl)propoxy]benzamide, 26. Following general procedure 4.1.1.1, compound **26** was obtained from 3-hydroxybenzamide (129 mg, 0.94 mmol) and 1-(3-bromopropyl)-3-chlorobenzene (147 mg, 0.63 mmol) as a white solid (98 mg, 54%).

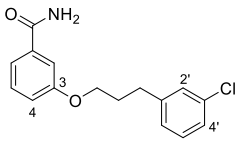

26

M.p.: 108-111 ºC. Rf: 0.36 (hexane/EtOAc, 3:7). IR (ATR): ν 3363, 3185 (NH), 1655 (C=O), 1587, 1449 (Ar). ^{1}H NMR (300 MHz, acetone-*d*$_6$) δ 2.09-2.16 (m, 2H, CH_2), 2.84 (t, *J* = 7.5, 2H, C$\underline{H}_2$Ar), 4.06 (t, *J* = 6.0, 2H, CH_2O), 6.69 (br s, 1H, ½NH_2), 7.09 (ddd, *J* = 8.2, 2.5, 1.1, 1H, H_4), 7.20-7.23 (m, 2H, $H_{2'}$, $H_{4'}$), 7.28-7.33 (m, 2H, $H_{5'}$, $H_{6'}$), 7.35 (t, *J* = 8.0, 1H, H_5), 7.46 (br s, 1H, ½NH_2), 7.50-7.52 (m, 2H, H_2, H_6). ^{13}C NMR (75 MHz, acetone-*d*$_6$) δ 31.4 (CH_2), 32.4 (C$\underline{H}_2$Ar), 67.7 (CH_2O), 114.2 (C_2), 118.5 (C_4), 120.5 (C_6), 126.8 ($C_{4'}$), 127.9 ($C_{6'}$), 129.3 ($C_{2'}$), 130.2 (C_5), 130.9 ($C_{5'}$), 134.5 ($C_{3'}$), 136.8 (C_1), 145.2 ($C_{1'}$), 160.0 (C_3), 168.7 ($CONH_2$). HPLC (t_R, min): 17.10. MS (ESI, m/z): 290.0 ([M(^{35}Cl)+H]$^+$, 100%), 292.0 ([M(^{37}Cl)+H]$^+$, 35%). ESI-HRMS (cald., found for $C_{16}H_{16}ClNNaO_2$ [M(^{35}Cl)+Na]$^+$): 312.0762, 312.0769; (cald., found for $C_{16}H_{16}ClNNaO_2$ [M(^{37}Cl)+Na]$^+$): 314.0732, 314.0742.

3-[2-(3-Chlorophenyl)ethoxy]benzamide, 25. To a solution of 3-hydroxybenzamide (122 mg, 0.89 mmol) in anhydrous THF (5 mL), 2-(3-chlorophenyl)ethanol (0.12 mL, 0.89 mmol), triphenylphosphine (350 mg, 1.3 mmol), trimethylamine (0.25 mL, 1.8 mmol) and DEAD (0.21 mL, 1.3 mmol) were added, and the reaction was stirred at rt overnight. Then, the mixture was diluted with EtOAc (20 mL) and washed with brine (2 x 20 mL). The organic layer was dried over Na_2SO_4, filtered, and concentrated under reduced pressure. The residue was purified by flash chromatography to afford **25** as a white solid (111 mg, 46%).

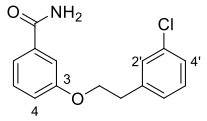

25

Rf: 0.36 (hexane/EtOAc, 3:7). IR (ATR): ν 3354, 3196 (NH), 1660 (C=O), 1583, 1448 (Ar). ^{1}H NMR (700 MHz, acetone-d_6) δ 3.13 (t, J = 6.5, 2H, C$\underline{H}_2$Ar), 4.29 (t, J = 6.5, 2H, CH_2O), 6.61 (br s, 1H, ½NH_2), 7.09 (ddd, J = 8.3, 2.5, 0.9, 1H, H_4), 7.26-7.27 (m, 1H, $H_{4'}$), 7.33-7.36 (m, 3H, H_5, $H_{5'}$, $H_{6'}$), 7.42 (s, 1H, $H_{2'}$), 7.44 (br s, 1H, ½NH_2), 7.49-7.51 (m, 2H, H_2, H_6). ^{13}C NMR (175 MHz, acetone-d_6) δ 35.8 (C$\underline{H}_2$Ar), 69.0 (CH_2O), 114.1 (C_2), 118.5 (C_4), 120.7 (C_6), 127.3 ($C_{4'}$), 128.5 ($C_{6'}$), 129.9 ($C_{2'}$), 130.2 (C_5), 130.8 ($C_{5'}$), 134.5 ($C_{3'}$), 136.8 (C_1), 142.1 ($C_{1'}$), 159.7 (C_3), 168.6 ($CONH_2$). HPLC (t_R, min): 15.74. MS (ESI, m/z): 276.1 ([M(^{35}Cl)+H]$^+$, 100%), 278.1 ([M(^{37}Cl)+H]$^+$, 35%). ESI-HRMS (calcd., found for $C_{15}H_{14}ClNNaO_2$ [M(^{35}Cl)+Na]$^+$): 298.0605, 298.0614; (calcd., found for $C_{15}H_{14}ClNNaO_2$ [M(^{37}Cl)+Na]$^+$): 300.0576, 300.0586.

4.1.4. Synthesis of compounds **27** and **28**

1-{3-[(3-Chlorobenzyl)oxy]phenyl}-2,2,2-trifluoroethanol, 29. Following general procedure 4.1.1.1, the intermediate compound 3-[(3-chlorobenzyl)oxy]benzaldehyde was obtained from 3-hydroxybenzaldehyde (500 mg, 4.1 mmol) and 3-chlorobenzyl bromide (0.6 mL, 4.5 mmol) as a white solid in quantitative yield (1.01 g), which was used in the next step without further purification.

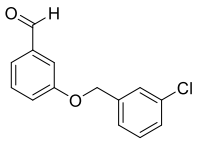

^{1}H NMR (300 MHz, $CDCl_3$) δ 5.10 (s, 2H, CH_2), 7.23-7.28 (m, 2H, $2CH_{Ar}$), 7.31-7.33 (m, 3H, $3CH_{Ar}$), 7.44-7.50 (m, 4H, $4CH_{Ar}$), 9.98 (s, 1H, CHO).

To a solution of 3-[(3-chlorobenzyl)oxy]benzaldehyde (1.0 g, 4.1 mmol) in anhydrous DMF (10 mL), trimethyl(trifluoromethyl)silane (0.73 mL, 4.9 mmol) and potassium carbonate (6 mg, 0.04 mmol) were added, and the reaction was stirred at rt for 24 h. After this time, one more equivalent of trimethyl(trifluoromethyl)silane was added (0.6 mL, 4.1 mmol) and the reaction was stirred at rt for additional 24 h. Then, 2 M HCl (2.0 mL, 4.1 mmol) was added and the mixture was stirred at rt for 4 h. The reaction was diluted with

EtOAc (20 mL) and washed with brine (3 x 20 mL). The organic phase was dried over Na_2SO_4, filtered, and concentrated under reduced pressure. The residue was purified by flash chromatography to afford compound **29** as an oil (1.13 g, 87%).

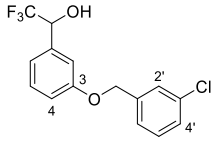

29

Rf: 0.30 (hexane/EtOAc, 5:1). IR (ATR): ν 3452 (OH), 1596, 1488, 1453 (Ar). ^{1}H NMR (300 MHz, $CDCl_3$) δ 2.62 (d, *J* = 4.5, 1H, OH), 4.96-5.02 (m, 1H, CHO), 5.05 (s, 2H, CH_2), 7.00 (ddd, *J* = 8.3, 2.6, 0.8, 1H, H_4), 7.08 (d, *J* = 7.6, 1H, H_6), 7.12 (br s, 1H, H_2), 7.30-7.36 (m, 4H, H_5, $H_{4'}$- $H_{6'}$), 7.45 (s, 1H, $H_{2'}$). ^{13}C NMR (75 MHz, $CDCl_3$) δ 69.3 (CH_2), 72.8 (q, J_{C-F} = 32.0, CH), 114.1 (C_2), 116.0 (C_4), 120.4 (C_6), 124.3 (q, J_{C-F} = 282.0, CF_3), 125.6 ($C_{4'}$), 127.6 ($C_{2'}$), 128.4, ($C_{6'}$), 129.9, 130.0 (C_5, $C_{5'}$), 134.7 ($C_{3'}$), 135.6 (C_1), 138.8 ($C_{1'}$), 158.8 (C_3).

1-{3-[(3-Chlorobenzyl)oxy]phenyl}-2,2,2-trifluoroethanone, 30. To a solution of compound **29** (600 mg, 1.9 mmol) in anhydrous DCM (10 mL), Dess-Martin periodinane (1.2 g, 2.8 mmol) was added, and the reaction was stirred at rt for 24 h. The mixture was diluted with DCM (10 mL) and washed with a saturated aqueous solution of sodium bicarbonate/sodium thiosulfate (2 x 20 mL). The organic phase was dried over Na_2SO_4, filtered, and concentrated under reduced pressure to give ketone **30** as an oil in quantitative yield (596 mg), which was used in the next step without further purification.

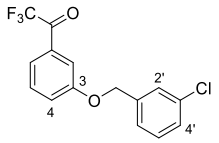

30

Rf: 0.30 (hexane/EtOAc, 5:1). IR (ATR): ν 1717 (C=O), 1597, 1581, 1489 (Ar). ^{1}H NMR (700 MHz, $CDCl_3$) δ 5.11 (s, 2H, CH_2), 7.31-7.35 (m, 4H, H_4, $H_{4'}$- $H_{6'}$), 7.46 (s, 1H, $H_{2'}$), 7.48 (t, *J* = 8.0, 1H, H_5), 7.64 (s, 1H, H_2), 7.69 (d, *J* = 7.5, 1H, H_6). ^{13}C NMR (175 MHz, $CDCl_3$) δ 69.6 (CH_2), 115.2 (C_2), 116.7 (q, J_{C-F} = 291.0, CF_3), 123.1 (C_4), 123.4 (C_6), 125.6 ($C_{6'}$), 127.7 ($C_{2'}$), 128.6, 130.1 ($C_{4'}$, $C_{5'}$), 130.4 (C_5), 131.3 (C_1), 134.8 ($C_{3'}$), 138.2 ($C_{1'}$), 158.9 (C_3), 180.4 (q, J_{C-F} = 35.0, $COCF_3$).

1-{3-[(3-Chlorobenzyl)oxy]phenyl}-2,2,2-trifluoroethanamine, 27. To a solution of compound **30** (244 mg, 0.78 mmol) in anhydrous diethyl ether (10 mL), 2-methyl-2-propanesulfinamide (117 mg, 0.97 mmol) and titanium(IV) isopropoxide (0.57 mL, 2.0 mmol) were added and the reaction was refluxed for 24 h. Then, sodium borohydride (88 mg, 2.3 mmol) was added, and the reaction was stirred at rt for 24 h. The reducing agent

was quenched with water and the mixture was filtered through celite and washed with EtOAc. The aqueous phase was extracted with EtOAc (3 x 20 mL) and the combined organic phases were dried over Na_2SO_4, filtered, and concentrated under reduced pressure to obtain the corresponding α–trifluoromethyl sulfinamide. Next, the resulting sulfinamide (325 mg, 0.77 mmol) was dissolved in methanol (10 mL) and 4 M HCl (0.97 mL, 3.9 mmol) was added. The reaction was stirred at rt for 1 h. Then, a saturated aqueous solution of $NaHCO_3$ was added to neutralize the acid and the mixture was concentrated under reduced pressure. The residue was purified by flash chromatography to afford compound **27** as a solid (60 mg, 24%).

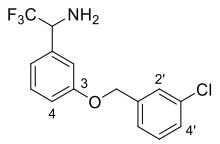

27

M.p.: 59-60 ºC. Rf: 0.12 (hexane/EtOAc, 5:1). IR (ATR): ν 3407, 3337 (NH), 1600, 1587 (Ar). ^{1}H NMR (700 MHz, $CDCl_3$) δ 4.37 (q, *J* = 7.4, 1H, CH), 5.05 (s, 2H, CH_2), 6.97 (dd, *J* = 8.2, 2.0, 1H, H_4), 7.04 (d, *J* = 7.7, 1H, H_6), 7.07 (s, 1H, H_2), 7.30-7.33 (m, 4H, H_5, $H_{4'}$-$H_{6'}$), 7.45 (s, 1H, $H_{2'}$). ^{13}C NMR (175 MHz, $CDCl_3$) δ 58.0 (q, $J_{C\text{-}F}$ = 29.7, CH), 69.3 (CH_2), 114.7 (C_2), 115.2 (C_4), 120.8 (C_6), 125.5 ($C_{6'}$), 125.7 (q, $J_{C\text{-}F}$ = 281.4, CF_3), 127.6 ($C_{2'}$), 128.3, 129.9, 130.0 ($3CH_{Ar}$), 134.7 ($C_{3'}$), 137.2 (C_1), 138.9 ($C_{1'}$), 158.8 (C_3). HPLC (t_R, min): 19.03. MS (ESI, m/z): 316.0 ([M+H]$^+$. MALDI-HRMS (calcd., found for $C_{15}H_{13}ClF_3NO$ [M(^{35}Cl)]$^+$): 315.0638, 315.0632; (calcd., found for $C_{15}H_{13}ClF_3NO$ [M(^{37}Cl)]$^+$): 317.0608, 317.0631.

2-(3-Methoxyphenyl)-1*H*-imidazole, 31.[60] A mixture of 3-iodoanisole (0.22 mL, 1.8 mmol), imidazole (252 mg, 3.7 mmol), palladium acetate (21 mg, 0.09 mmol), and copper(I) iodide (704 mg, 3.7 mmol) in anhydrous DMF (10 mL) was stirred under MW irradiation at 200 °C for 40 min. Then, the reaction was diluted in EtOAc (30 mL), poured into a saturated aqueous solution of NH_4Cl and stirred for 30 min. Afterwards, the mixture was extracted with EtOAc (3 x 40 mL) and the combined organic phases were washed with brine (2 x 50 mL), dried over Na_2SO_4, filtered, and concentrated under reduced pressure. The residue was purified by flash chromatography to afford compound **31** as an oil (171 mg, 53%).

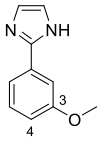

31

^{1}H NMR (300 MHz, acetone-d_6) δ 3.81 (s, 3H, CH_3), 6.94 (ddd, *J* = 8.0, 2.5, 1.0, 1H, H_4) 7.32 (s, 2H, $2H_{imidazole}$), 7.34 (t, *J* = 8.0, 1H, H_5), 7.57-7.62 (m, 2H, H_2, H_6), 8.63 (br s, 1H, NH). The spectroscopic data were in agreement with those previously reported.[60]

2-(3-Hydroxyphenyl)-1*H*-imidazole, 32. To a solution of compound **31** (142 mg, 0.82 mmol) in anhydrous DCM (20 mL) at 0 °C, a 1 M solution of BBr_3 in DCM (1.6 mL, 1.6 mmol) was added and the reaction was stirred at low temperature for 30 min and then at rt for 24 h. Then, the mixture was diluted with EtOAc (20 mL) and neutralized with a saturated aqueous solution of $NaHCO_3$. The aqueous phase was extracted with EtOAc (3 x 50 mL) and the organic phases were dried over Na_2SO_4, filtered, and concentrated under reduced pressure to give **32** as a white solid (124 mg, 95%), which was used for the next step without further purification.

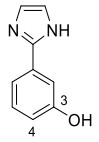

32

Rf: 0.29 (DCM/methanol, 9:1). ^{1}H NMR (300 MHz, CD_3OD) δ 6.82 (ddd, *J* = 8.0, 2.3, 1.6, 1H, H_4), 7.12 (s, 2H, $2H_{imidazole}$), 7.23-7.32 (m, 2H, H_2, H_5, H_6). ^{13}C NMR (75 MHz, CD_3OD) δ 113.4 (C_2), 116.9, 117.6 (C_4, C_6), 123.7 ($2CH_{imidazole}$), 131.0 (C_5), 132.4 (C_1), 148.1 ($C_{imidazole}$), 159.2 (C_3). MS (ESI, m/z): 161.1 $[M+H]^+$.

2-{3[(3-Chlorobenzyl)oxy]phenyl}-1*H*-imidazole, 28. Following general procedure 4.1.1.1, compound **28** was obtained from compound **32** (50 mg, 0.32 mmol) and 3-chlorobenzyl bromide (28 µL, 0.21 mmol) as a white solid (43 mg, 72%).

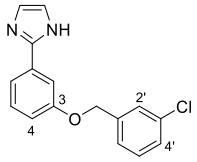

28

M.p.: 170-171 ºC. Rf: 0.43 (hexane/EtOAc, 2:8). IR (ATR): ν 1742 (C=N), 1591, 1465 (Ar). ^{1}H NMR (500 MHz, CD_3OD) δ 5.15 (s, 2H, CH_2), 7.02 (ddd, *J* = 8.2, 2.6, 0.9, 1H, H_4), 7.13 (s, 2H, $2CH_{imidazole}$), 7.32 (dt, *J* = 7.7, 1.8, 1H, $H_{4'}$) 7.35-7.41 (m, 3H, $H_{6'}$, H_5, $H_{5'}$), 7.46 (d, *J* = 7.8, 1H, H_6), 7.50 (br s, 1H, $H_{2'}$), 7.55 (br t, *J* = 2.1, 1H, H_2). ^{13}C NMR (125 MHz, CD_3OD) δ 70.1 (CH_2), 112.8 (C_2), 116.4 (C_4), 119.1 (C_6), 124.0 ($2CH_{imidazole}$), 126.8 ($C_{6'}$), 128.4 ($C_{2'}$), 128.9 ($C_{4'}$), 131.1, 131.2 (C_5, $C_{5'}$), 132.8 (C_1), 135.4 ($C_{3'}$), 141.0 ($C_{1'}$), 147.8 ($C_{imidazole}$), 160.5 (C_3). HPLC (t_R, min): 12.43. MS (ESI, m/z): 285.0 $[M+H]^+$. ESI-HRMS (calcd., found for $C_{16}H_{14}ClN_2O$ ($[M(^{35}Cl)+H]^+$): 285.0789, 285.0711; (calcd., found for $C_{16}H_{14}ClN_2O$ ($[M(^{37}Cl)+H]^+$): 287.0760, 287.0681.

4.1.5. Synthesis of compounds **33**-**41**

3-[(3-Chlorobenzyl)oxy]-2,6-difluorobenzamide, 33.[59] Following general procedure 4.1.1.1, compound **33** was obtained from **5** (237 mg, 1.4 mmol) and 3-chlorobenzyl bromide (0.25 mL, 2.0 mmol) as a white solid (293 mg, 89%).

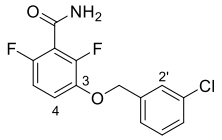

33

M.p.: 125-127 ºC (lit.[59] m.p. 121-122 °C). Rf: 0.62 (hexane/EtOAc, 3:7). IR (ATR): ν 3378, 3192 (NH), 1655 (C=O), 1594, 1492, 1455 (Ar). ^{1}H NMR (300 MHz, acetone-d_6) δ 5.23 (s, 2H, CH_2), 6.94 (td, J = 9.0, 2.0, 1H, H_5), 7.19 (br s, 1H, ½NH_2), 7.26 (td, J = 9.0, 5.0, 1H, H_4), 7.36-7.47 (m, 4H, $H_{3'}$-$H_{5'}$, ½NH_2), 7.54 (br s, 1H, $H_{2'}$). ^{13}C NMR (75 MHz, acetone-d_6) δ 71.4 (CH_2), 111.6 (dd, J_{C-F} = 23.0, 4.5, C_5), 117.2 (dd, J_{C-F} = 9.4, 2.7, C_4), 117.6 (t, J_{C-F} = 19.9, C_1), 126.9 (CH_{Ar}), 128.3 ($C_{2'}$), 129.0, 131.1 ($2CH_{Ar}$), 134.8 ($C_{3'}$), 140.1 ($C_{1'}$), 144.0 (dd, J_{C-F} = 11.0, 3.0, C_3), 150.0 (dd, J_{C-F} = 249.9, 8.0, CF), 153.8 (dd, J_{C-F} = 243.6, 6.6, CF), 162.1 ($CONH_2$). HPLC (t_R, min): 14.99. MS (ESI, m/z): 298.0 ([M(^{35}Cl)+H]$^+$, 100%), 300.0 ([M(^{37}Cl)+H]$^+$, 35%). ESI-HRMS (calcd., found for $C_{14}H_{11}ClF_2NO_2$ [M(^{35}Cl)+H]$^+$): 298.0441, 298.0453; (calcd., found for $C_{14}H_{11}ClF_2NO_2$ [M(^{37}Cl)+H]$^+$): 300.0411, 300.0424.

2,6-Difluoro-3-{[2-(trifluoromethyl)benzyl]oxy}benzamide, 34. Following general procedure 4.1.1.1, compound **34** was obtained from **5** (148 mg, 0.85 mmol) and 2-(trifluoromethyl)benzyl bromide (0.19 mL, 1.3 mmol) as a white solid (252 mg, 90%).

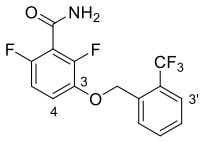

34

M.p.: 153-154 ºC. Rf: 0.43 (hexane/EtOAc, 1:1). IR (ATR): ν 3355 (NH), 1661 (C=O), 1595, 1492, 1444 (Ar). ^{1}H NMR (300 MHz, $CDCl_3$) δ 5.31 (s, 2H, CH_2), 6.02 (br s, 1H, NH), 6.06 (br s, 1H, NH), 6.86 (td, J = 9.0, 2.0, 1H, H_5), 7.01 (td, J = 9.1, 5.1, 1H, H_4), 7.45 (t, J = 7.5, 1H, $H_{4'}$), 7.59 (t, J = 7.5, 1H, $H_{5'}$), 7.70 (d, J = 7.8, 1H, $H_{3'}$), 7.75 (d, J = 7.8 1H, $H_{6'}$). ^{13}C NMR (75 MHz, $CDCl_3$) δ 68.4 (CH_2), 111.4 (dd, J_{C-F} = 23.8, 4.3, C_5), 114.2 (dd, J_{C-F} = 20.5, 16.2, C_1), 117.9 (dd, J_{C-F} = 9.8, 3.0, C_4), 124.6 (q, J_{C-F} = 273.4, CF_3), 126.2 (q, J_{C-F} = 5.6, $C_{3'}$), 127.5 (q, J_{C-F} = 3.8, $C_{2'}$), 128.3 ($C_{4'}$), 128.8 ($C_{6'}$), 132.5 ($C_{5'}$), 134.7 ($C_{1'}$), 143.4 (dd, J_{C-F} = 11.4, 3.5, C_3), 152.5 (dd, J_{C-F} = 255.1, 7.0, CF), 154.0 (dd, J_{C-F} = 247.5, 7.0, CF), 162.0 ($CONH_2$). HPLC (t_R, min): 14.80. MS (ESI, m/z): 332.0 [M+H]$^+$, 354.0 [M+Na]$^+$. ESI-HRMS (calcd., found for $C_{15}H_{11}F_5NNaO_2$ [M+Na]$^+$): 354.0529, 354.0538.

2,6-Difluoro-3-{[3-(trifluoromethyl)benzyl]oxy}benzamide, 35. Following general procedure 4.1.1.1, compound **35** was obtained from **5** (217 mg, 1.3 mmol) and 3-(trifluoromethyl)benzyl bromide (0.28 mL, 1.9 mmol) as a white solid (272 mg, 98%).

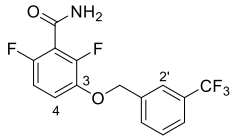

35

M.p.: 140-143 ºC. Rf: 0.60 (hexane/EtOAc, 3:7). IR (ATR): ν 3371, 3194 (NH), 1655 (C=O), 1592, 1495, 1456 (Ar). ^{1}H NMR (500 MHz, acetone-d_6) δ 5.33 (s, 2H, CH_2), 6.98 (td, J = 9.0, 2.0, 1H, H_5), 7.19 (br s, 1H, ½NH_2), 7.30 (td, J = 9.0, 5.0, 1H, H_4), 7.46 (br s, 1H, ½NH_2), 7.65-7.72 (m, 2H, $H_{4'}$, $H_{5'}$), 7.81 (d, J = 7.5 1H, $H_{6'}$), 7.85 (s, 1H, $H_{2'}$). ^{13}C NMR (125 MHz, acetone-d_6) δ 71.6 (CH_2), 111.6 (dd, $J_{C\text{-}F}$ = 23.3, 3.1, C_5), 117.3 (dd, $J_{C\text{-}F}$ = 9.5, 2.0, C_4), 117.6 (t, $J_{C\text{-}F}$ = 23.9, C_1), 125.1 (d, $J_{C\text{-}F}$ = 2.8, $C_{2'}$) 125.3 (q, $J_{C\text{-}F}$ = 271.5, CF_3), 125.7 (d, $J_{C\text{-}F}$ = 2.7, $C_{4'}$) 130.4 ($C_{5'}$), 131.2 (q, $J_{C\text{-}F}$ = 32.0, $C_{3'}$), 132.3 ($C_{6'}$), 139.1 ($C_{1'}$), 144.1 (dd, $J_{C\text{-}F}$ = 11.0, 2.0, C_3), 150.1 (dd, $J_{C\text{-}F}$ = 250.0, 8.0, CF), 153.9 (dd, $J_{C\text{-}F}$ = 243.0, 6.0, CF), 162.1 ($CONH_2$). HPLC (t_R, min): 15.10. MS (ESI, m/z): 332.0 $[M+H]^+$. ESI-HRMS (calcd., found for $C_{15}H_{11}F_5NO_2$ $[M+H]^+$): 332.0710, 332.0720.

2,6-Difluoro-3-{[4-(trifluoromethyl)benzyl]oxy}benzamide, 36. Following general procedure 4.1.1.1, compound **36** was obtained from **5** (107 mg, 0.62 mmol) and 4-(trifluoromethyl)benzyl bromide (0.14 mL, 0.92 mmol) as a white solid (252 mg, 81%).

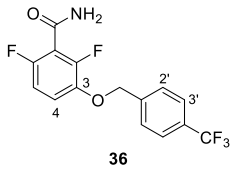

36

M.p.: 116-117 ºC. Rf: 0.40 (hexane/EtOAc, 1:1). IR (ATR): ν 3352 (NH), 1653 (C=O), 1492, 1450 (Ar). ^{1}H NMR (300 MHz, $CDCl_3$) δ 5.17 (s, 2H, CH_2), 6.04 (br s, 1H, ½NH_2), 6.29 (br s, 1H, ½NH_2), 6.86 (td, J = 9.1, 2.0, 1H, H_5), 7.01 (td, J = 9.1, 5.1, 1H, H_4), 7.54 (t, J = 7.7, 1H, $H_{2'}$, $H_{6'}$), 7.65 (d, J = 7.6, 2H, $H_{3'}$, $H_{5'}$). ^{13}C NMR (75 MHz, $CDCl_3$) δ 71.7 (CH_2), 111.4 (dd, $J_{C\text{-}F}$ = 23.8, 4.3, C_5), 114.4 (dd, $J_{C\text{-}F}$ = 20.3, 16.3, C_1), 118.0 (dd, $J_{C\text{-}F}$ = 9.8, 3.2, C_4), 124.2 (q, $J_{C\text{-}F}$ = 270.3, CF_3), 126.2 (q, $J_{C\text{-}F}$ = 3.9, $C_{3'}$, $C_{5'}$), 127.5 (q, $J_{C\text{-}F}$ = 32.6, $C_{4'}$), 128.3 ($C_{2'}$, $C_{6'}$), 140.2 ($C_{1'}$), 143.4 (dd, $J_{C\text{-}F}$ = 11.4, 3.5, C_3), 150.9 (dd, $J_{C\text{-}F}$ = 266.6, 6.2, CF), 154.1 (dd, $J_{C\text{-}F}$ = 260.2, 6.2, CF), 162.0 ($CONH_2$). HPLC (t_R, min): 15.05. MS (ESI, m/z): 332.1 $[M+H]^+$, 354.0 $[M+Na]^+$. ESI-HRMS (calcd., found for $C_{15}H_{11}F_5NNaO_2$ $[M+Na]^+$): 354.0529, 354.0523.

2,6-Difluoro-3-{2-[3-(trifluoromethyl)phenyl]ethoxy}benzamide, 37. Following general procedure 4.1.1.2 Method A, compound **37** was obtained from **5** (100 mg, 0.58

mmol) and 2-[3-(trifluoromethyl)phenyl]ethan-1-ol (118 mg, 0.58 mmol) as a white solid (95 mg, 45%).

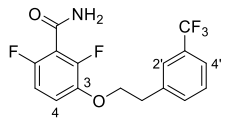

37

M.p.: 100-102 ºC. Rf: 0.44 (hexane/EtOAc, 1:1). IR (ATR): ν 3315, 3196 (NH), 1629 (C=O), 1442 (Ar). ^{1}H NMR (300 MHz, $CDCl_3$) δ 3.17 (t, *J* = 6.6, 2H, C$\underline{H}_2$Ar), 4.23 (t, *J* = 6.6, 2H, CH_2O), 6.00 (br s, 1H, ½NH_2), 6.16 (br s, 1H, ½NH_2), 6.85 (td, *J* = 9.1, 1.8, 1H, H_5), 6.95 (td, *J* = 9.0, 5.1, 1H, H_4), 7.41-7.54 (m, 4H, $H_{2'}$, $H_{4'}$-$H_{6'}$). ^{13}C NMR (75 MHz, $CDCl_3$) δ 35.7 (C$\underline{H}_2$Ar), 70.8 (CH_2O), 111.3 (dd, $J_{C\text{-}F}$ = 23.8, 4.3, C_5), 117.5 (dd, $J_{C\text{-}F}$ = 9.8, 3.2, C_4), 118.3 (t, $J_{C\text{-}F}$ = 20.3, C_1), 123.8 (q, $J_{C\text{-}F}$ = 3.8, $C_{2'}$), 124.3 (q, $J_{C\text{-}F}$ = 271.8, CF_3), 125.9 (q, $J_{C\text{-}F}$ = 3.8, $C_{4'}$), 129.2 ($C_{5'}$), 130.8 (q, $J_{C\text{-}F}$ = 32.2, $C_{3'}$), 132.7 ($C_{6'}$), 138.9 ($C_{1'}$), 143.8 (dd, $J_{C\text{-}F}$ = 11.4, 3.5, C_3), 150.4 (dd, $J_{C\text{-}F}$ = 266.4, 6.3, CF), 154.2 (dd, $J_{C\text{-}F}$ = 260.8, 6.3, CF), 162.2 ($CONH_2$). HPLC (t_R, min): 15.10. MS (ESI, m/z): 346.1 $[M+H]^+$. ESI-HRMS (calcd., found for $C_{16}H_{12}F_5NNaO_2$ $[M+Na]^+$): 368.0686, 368.0697.

2,6-Difluoro-3-{3-[3-(trifluoromethyl)phenyl]propoxy}benzamide, 38. Following general procedure 4.1.1.2 Method A, compound **38** was obtained from **5** (100 mg, 0.58 mmol) and 2-[3-(trifluoromethyl)phenyl]propan-1-ol (122 mg, 0.58 mmol) as a white solid (80 mg, 48%).

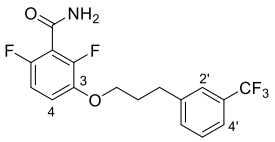

38

M.p.: 96-98 ºC. Rf: 0.56 (hexane/EtOAc, 1:1). IR (ATR): ν 3375, 3191 (NH), 1650 (C=O), 1595, 1492, 1450 (Ar). ^{1}H NMR (300 MHz, $CDCl_3$) δ 2.09-2.19 (m, 2H, CH_2), 2.89 (t, *J* = 8.4, 2H, C$\underline{H}_2$Ar), 4.00 (t, *J* = 6.1 Hz, 2H, CH_2O), 6.01 (br s, 1H, ½NH_2), 6.10 (br s, 1H, ½NH_2), 6.86 (td, *J* = 9.1, 1.7, 1H, H_5), 6.96 (td, *J* = 9.0, 5.2, 1H, H_4), 7.39-7.48 (m. 4H, $H_{2'}$, $H_{4'}$-$H_{6'}$). ^{13}C NMR (75 MHz, $CDCl_3$) δ 30.7 (CH_2), 31.9 (C$\underline{H}_2$Ar), 69.2 (CH_2O), 109.1 (t, $J_{C\text{-}F}$ = 20.3, C_1), 111.3 (dd, $J_{C\text{-}F}$ = 23.7, 4.3, C_5), 117.4 (dd, $J_{C\text{-}F}$ = 9.7, 3.4, C_4), 123.2 (q, $J_{C\text{-}F}$ = 3.9, $C_{2'}$), 124.4 (q, $J_{C\text{-}F}$ = 270.3, CF_3), 125.3 (q, $J_{C\text{-}F}$ = 3.8, $C_{4'}$), 129.1 ($C_{5'}$), 130.9 (q, $J_{C\text{-}F}$ = 32.1, $C_{3'}$), 132.1 ($C_{6'}$), 142.1 ($C_{1'}$), 144.0 (dd, $J_{C\text{-}F}$ = 11.1, 3.4, C_3), 152.1 (d, $J_{C\text{-}F}$ = 254.1, CF), 155.3 (d, $J_{C\text{-}F}$ = 258.2, CF), 162.2 ($CONH_2$). HPLC (t_R, min): 16.03. MS (ESI, m/z): 360.1 $[M+H]^+$, 382.1 $[M+Na]^+$. ESI-HRMS (calcd., found for $C_{17}H_{15}F_5NNaO_2$ $[M+Na]^+$): 382.0842, 382.0829.

3-(Dimethylamino)-1-(3-(trifluoromethyl)phenyl)propan-1-one, 43. A mixture of 1-[3-(trifluoromethyl)phenyl]ethanone (0.40 mL, 2.7 mmol), *p*-formaldehyde (215 mg, 7.2

mmol) and *N*-methylmethanamine (276 mg, 6.1 mmol) in the presence of hydrogen chloride (718 µL, 8.7 mmol) was refluxed in ethanol (5 mL) for 24 h. Afterwards, the reaction mixture was concentrated under reduced pressure, then neutralized with a 10% aqueous solution of NaOH and extracted with DCM (3 x 30 mL). The combined organic phases were dried over Na_2SO_4 and concentrated under reduced pressure. The crude was purified by flash chromatography to afford compound **43** as an oil (174 mg, 27%).

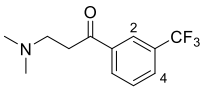

43

Rf: 0.25 (DCM/methanol, 9:1). ^{1}H NMR (300 MHz, $CDCl_3$) δ 2.30 (s, 6H, $2CH_3$), 2.85–2.67 (m, 2H, CH_2N), 3.18 (td, *J* = 7.2, 1.3, 2H, CH_2CO), 7.61 (t, *J* = 7.8, 1H, H_5), 7.82 (d, *J* = 6.8, 1H, H_4), 8.15 (d, *J* = 7.8, 1H, H_6), 8.22 (s, 1H, H_2).

3-(Dimethylamino)-1-[3-(trifluoromethyl)phenyl]propan-1-ol, 42. To a suspension of lithium aluminum hydride (30 mg, 0.80 mmol) in anhydrous THF (4 mL), a solution of β-aminoketone **43** (150 mg, 0.61 mmol) in anhydrous THF (8 mL) was added dropwise at 0 ºC and the reaction mixture was stirred at rt for 2 h. Then, the mixture was quenched with a saturated aqueous solution of $NaHCO_3$ at 0 ºC. The mixture was extracted with EtOAc (2 x 25 mL) and the combined organic phases were washed with water and brine, dried over Na_2SO_4, filtered, and concentrated under reduced pressure. The residue was purified by chromatography to afford alcohol **42** as an oil (115 mg, 76%).

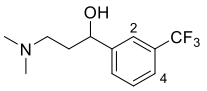

42

Rf: 0.53 (DCM/methanol, 9:1). ^{1}H NMR (300 MHz, $CDCl_3$) δ 1.71-1.91 (m, 2H, $C\underline{H}_2CH$), 2.32 (s, 6H, $2CH_3$), 2.48 (ddd, *J* = 12.6, 5.6, 3.4 Hz, 1H, ½CH_2N), 2.70 (ddd, *J* = 12.9, 9.6, 3.5, 1H, ½CH_2N), 3.48 (br s, 1H, OH), 4.99 (dd, *J* = 8.2, 3.4, 1H, CHO), 7.42-7.57 (m, 3H, H_4-H_6), 7.67 (s, 1H, H_2). ^{13}C NMR (75 MHz, $CDCl_3$) δ 34.5 ($\underline{C}H_2CH$), 45.4 ($2CH_3$), 58.5 (CH_2N), 75.4 (CHO), 122.6 (q, $J_{C\text{-}F}$ = 3.9, C_2),123.9 (q, $J_{C\text{-}F}$ = 3.8, C_4), 124.5 (q, $J_{C\text{-}F}$ = 272.8, CF_3), 128.7 (C_6), 129.1 (C_5), 130.7 (d, $J_{C\text{-}F}$ = 32.7, C_3), 146.3 (C_1). ESI-HRMS (calcd., found for $C_{12}H_{17}F_3NO$ $[M+H]^+$): 248.1262, 248.1258.

3-{3-(Dimethylamino)-1-[3-(trifluoromethyl)phenyl]propoxy}-2,6-difluoro-benzamide, 39. Following general procedure 4.1.1.2 Method A, compound **39** was obtained from **5** (69 mg, 0.36 mmol) and alcohol **42** (90 mg, 0.36 mmol) as an oil (40 mg, 50%). The free base was dissolved in dichloromethane (2 mL) and a solution of 2 M HCl in diethyl ether (2.2 mL) was added dropwise. The mixture was kept at rt for 2 h and the solvent was removed under reduced pressure.

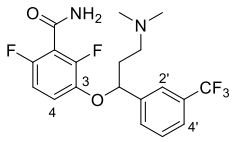

39

Rf: 0.26 (DCM/methanol, 9:1, free amine). ^{1}H NMR (300 MHz, $CDCl_3$) δ 1.90-2.03 (m, 1H, ½C<u>H</u>$_2$CH), 2.16-2.31 (m, 1H, ½C<u>H</u>$_2$CH), 2.25 (s, 6H, 2CH_3), 2.36-2.42 (m, 1H, ½CH_2N), 2.48-2.57 (m, 1H, ½CH_2N), 5.28 (dd, *J* = 8.0, 5.1, 1H, CH), 6.09 (br s, 1H, ½NH_2), 6.23 (br s, 1H, ½NH_2), 6.71 (td, *J* = 9.1, 1.7, 1H, H_5), 6.82 (td, *J* = 9.0, 5.3, 1H, H_4), 7.47 (t, *J* = 7.9, 1H, $H_{5'}$) 7.56 (d, *J* = 7.9, 2H, $H_{4'}$,$H_{6'}$), 7.63 (s, 1H, $H_{2'}$). ESI-HRMS (calcd., found for $C_{19}H_{20}F_5N_2O_2$ $[M+H]^+$): 403.1444, 403.1438.

2-{[3-(Trifluoromethyl)phenyl]amino}ethan-1-ol, 44. Following general procedure 4.1.1.10, compound **44** was obtained from 2-aminoethan-1-ol (0.18 mL, 3.0 mmol) and 1-iodo-3-(trifluoromethyl)benzene (0.43 mL, 3.0 mmol) as an off-white solid (296 mg, 48%).

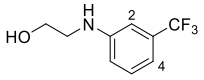

44

M.p.: 46-47 ºC. Rf: 0.35 (hexane/EtOAc, 1:1). IR (ATR): ν 3405 (OH, NH), 1616, 1598, 1454 (Ar). ^{1}H NMR (300 MHz, CD_3OD) δ 3.25 (t, *J* = 5.8, 2H, CH_2N), 3.72 (t, *J* = 5.8, 2H, CH_2O), 6.84 (app d, *J* = 8.1, 3H, H_2, H_4, H_5), 7.24 (t, *J* = 7.7, 1H, H_6). ^{13}C NMR (75 MHz, CD_3OD) δ 46.6 (CH_2N), 61.4 (CH_2O), 109.6 (q, $J_{C\text{-}F}$ = 4.0, C_2), 113.7 (q, $J_{C\text{-}F}$ = 4.0, C_4), 116.8 (C_6), 126.0 (q, $J_{C\text{-}F}$ = 271.3, CF_3), 130.7 (C_5), 132.4 (q, $J_{C\text{-}F}$ = 31.3, C_3), 150.7 (C_1). HPLC (t_R, min): 10.51. MS (ESI, m/z): 206.1 $[M+H]^+$.

2,6-Difluoro-3-(2-{[3-(trifluoromethyl)phenyl]amino}ethoxy)benzamide, 40. Following general procedure 4.1.1.2 Method A, compound **40** was obtained from **5** (80 mg, 0.46 mmol) and alcohol **44** (95 mg, 0.46 mmol) as an oil (81 mg, 49%).

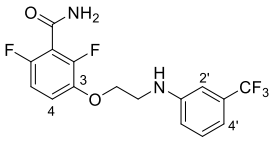

40

Rf: 0.25 (hexane/EtOAc, 1:1). IR (ATR): ν 3354, 3189 (NH), 1671 (C=O), 1614, 1490 (Ar). ^{1}H NMR (300 MHz, CD_3OD) δ 3.57 (t, *J* = 5.4, 2H, CH_2N), 4.22 (t, *J* = 5.4, 2H, CH_2O), 6.79-7.03 (m, 4H, $H_{2'}$, $H_{4'}$, $H_{6'}$, H_5), 7.18 (td, *J* = 9.2, 5.1, 1H, H_4), 7.28 (t, *J* = 7.8, 1H, $H_{5'}$). ^{13}C NMR (75 MHz, CD_3OD) δ Mixture of rotamers: 44.1 (CH_2N), 70.1 (CH_2O), 110.1 (q, $J_{C\text{-}F}$ = 4.0, $C_{2'}$), 111.9 and 112.1 (dd, $J_{C\text{-}F}$ = 23.2, 4.2, C_5), 114.4 (q, $J_{C\text{-}F}$ = 3.9, $C_{4'}$), 117.2 (br s, C_1, $C_{6'}$), 117.9 (dd, $J_{C\text{-}F}$ = 9.3, 2.8) and 119.6 (dd, $J_{C\text{-}F}$ = 9.2, 4.0, C_4), 125.9 (q, $J_{C\text{-}F}$ = 271.5, CF_3), 130.8 ($C_{5'}$), 132.5 (q, $J_{C\text{-}F}$ = 31.4, $C_{3'}$), 144.9 (dd, $J_{C\text{-}F}$ = 10.9, 3.4, C_3), 149.9

($C_{1'}$), 150.5 (dd, $J_{C\text{-}F}$ = 251.5, 7.6, CF), 154.2 (dd, $J_{C\text{-}F}$ = 243.7, 6.0, CF), 165.4 ($CONH_2$). MALDI-HRMS (calcd., found for $C_{16}H_{13}F_5N_2O_2$ $[M]^+$): 360.0897, 360.0903.

2-{[(3-Trifluoromethyl)phenyl]amino}pentan-1-ol, 45. Following general procedure 4.1.1.10, compound **45** was obtained from 2-aminopentan-1-ol (0.11 mL, 0.97 mmol) and 1-iodo-3-(trifluoromethyl)benzene (0.14 mL, 0.97 mmol) as an oil (134 mg, 56%).

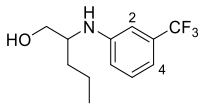

45

Rf: 0.56 (hexane/EtOAc, 1:1). IR (ATR): ν 3405 (OH, NH), 1616, 1598, 1454 (Ar). ^{1}H NMR (300 MHz, $CDCl_3$) δ 0.94 (t, J = 7.2, 3H, CH_3), 1.34-1.62 (m, 4H, $2CH_2$), 1.80 (br s, 1H, OH), 3.48-3.57 (m, 1H, CHN), 3.56 (dd, J = 10.6, 5.4, 1H, ½CH_2O), 3.76 (dd, J = 10.5, 3.7, 1H, ½CH_2O), 6.79 (dd, J = 8.2, 2.4, 1H, H_6), 6.84 (s, 1H, H_2), 6.94 (d, J = 7.7, 1H, H_4), 7.24 (t, J = 7.9, 1H, H_5). ^{13}C NMR (75 MHz, $CDCl_3$) δ 14.2 (CH_3), 19.5 ($\underline{C}H_2CH_3$), 34.3 ($\underline{C}H_2CH$), 55.0 (CHN), 64.4 (CH_2O), 109.8 (q, $J_{C\text{-}F}$ = 3.9, C_4), 114.2 (q, $J_{C\text{-}F}$ = 4.0, C_2), 116.5 (C_6), 124.4 (q, $J_{C\text{-}F}$ = 272.1, CF_3), 129.9 (C_5), 131.8 (q, $J_{C\text{-}F}$ = 31.8, C_3), 148.1 (C_1). HPLC (t_R, min): 16.78. MS (ESI, m/z): 248.1.

(*R*)-**45**. Following general procedure 4.1.1.10, compound (*R*)-**45** was obtained from (*R*)-2-aminopentan-1-ol (0.14 mL, 1 mmol) and 1-iodo-3-(trifluoromethyl)benzene (0.17 mL, 1 mmol) as an oil (128 mg, 46%). The spectroscopic data were in agreement with those described for *rac*-**45**.

(*S*)-**45**. Following general procedure 4.1.1.10, compound (*S*)-**45** was obtained from (*S*)-2-aminopentan-1-ol (0.10 mL, 0.95 mmol) and 1-iodo-3-(trifluoromethyl)benzene (0.12 mL, 0.95 mmol) as an oil (120 mg, 49%). The spectroscopic data were in agreement with those described for *rac*-**45**.

2,6-Difluoro-3-[(2-{[3-(trifluoromethyl)phenyl]amino}pentyl)oxy]benzamide, 41. Following general procedure 4.1.1.2 Method A, compound **41** was obtained from **5** (52 mg, 0.30 mmol) and alcohol **45** (75 mg, 0.30 mmol) as a colourless oil (30 mg, 45%).

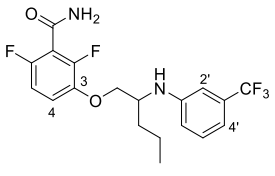

41

Rf: 0.48 (hexane/EtOAc, 1:1). IR (ATR): ν 3363 (NH), 1685 (C=O), 1491, 1445 (Ar). ^{1}H NMR (300 MHz, $CDCl_3$) δ 0.98 (t, J = 7.0, 3H, CH_3), 1.41-1.69 (m, 3H, CH_2, ½$C\underline{H}_2CH$), 1.77-1.84 (m, 1H, ½$C\underline{H}_2CH$), 3.75-3.79 (m, 1H, CHN), 4.04 (AB system, J = 9.3, 3.9, 2H, CH_2O), 5.95 (br s, 2H, NH_2), 6.77 (d, J = 8.1, 1H, $H_{6'}$), 6.82 (s, 1H, $H_{2'}$), 6.87 (dd, J = 9.1,

1.8, 1H, H_5), 6.93 (d, *J* = 8.0, 1H, $H_{4'}$), 6.96 (td, *J* = 9.1, 5.1, 1H, H_4), 7.25 (t, *J* = 7.8, 1H, $H_{5'}$). ^{13}C NMR (75 MHz, $CDCl_3$) δ 14.2 (CH_3), 19.5 ($\underline{C}H_2CH_3$), 34.4 ($\underline{C}H_2CH$), 52.5 (CHN), 72.0 (CH_2O), 109.4 (q, J_{C-F} = 3.8, $C_{2'}$), 111.4 (dd, J_{C-F} = 23.7, 4.3, C_5), 114.1 (q, J_{C-F} = 4.0, $C_{4'}$), 114.2 (q, J_{C-F} = 36.3, C_1), 116.4 ($C_{6'}$), 117.7 (dd, J_{C-F} = 9.8, 3.0, C_4), 125.2 (q, J_{C-F} = 272.4, CF_3), 130.0 ($C_{5'}$), 131.9 (q, J_{C-F} = 31.7, $C_{3'}$), 144.0 (dd, J_{C-F} = 11.4, 3.4, C_3), 147.6 ($C_{1'}$), 150.6 (dd, J_{C-F} = 254.9, 7.2, CF), 153.9 (dd, J_{C-F} = 247.2, 5.4, CF), 162.0 ($CONH_2$). ($CONH_2$). HPLC (t_R, min): 17.73. MS (ESI, m/z): 403.2 $[M+H]^+$, 425.1 $[M+Na]^+$. ESI-HRMS (calcd., found for $C_{19}H_{19}F_5N_2O_2Na$ $[M+Na]^+$): 425.1264, 425.1700.

(*R*)-41. Following general procedure 4.1.1.2 Method A, compound (*R*)-**41** was obtained from **5** (50 mg, 0.29 mmol) and alcohol (*R*)-**45** (73 mg, 0.29 mmol) as an oil (57 mg, 49%). The spectroscopic data were in agreement with those described for *rac*-**41**. $[\alpha]_D^{24}$ = + 29.0 (c = 0.15, $CHCl_3$).

(*S*)-41. Following general procedure 4.1.1.2 Method A, compound (*S*)-**41** was obtained from **5** (116 mg, 0.67 mmol) and alcohol (*S*)-**45** (150 mg, 0.61 mmol) as an oil (88 mg, 36%). The spectroscopic data were in agreement with those described for *rac*-**41**. $[\alpha]_D^{24}$ = - 28.5 (c = 0.15, $CHCl_3$).

4.2. Biochemical and biological methods

The biological evaluation of the compounds synthesized in this thesis was carried out in collaboration with the research group of Dr. José Manuel Andreu at the Centro de Investigaciones Biológicas (CIB-CSIC), Spain.

4.2.1. Protein purification and assembly conditions

BsFtsZ was overproduced and purified as described.[61] Untagged, full length BsFtsZ was overproduced in *E. coli* C41(DE3) cells, purified and its concentration measured as described.[41] BsFtsZ was eluted from the hydrophobic chromatography at 99% electrophoretic purity and the gel-filtration chromatography was omitted. Instead, BsFtsZ was equilibrated in 50 mM Tris HCl, 50 mM KCl, 1 mM ethylenediaminetetraacetic acid (EDTA), 10% glycerol at pH 7.5, employing a 5 mL HiTrap desalting column. It was concentrated to < 0.5 mL (about 1 mM BsFtsZ) and stored at -80 ºC. BsFtsZ preparations contained only 0.047 ± 0.044 guanine nucleotide bound per FtsZ, spectrophotometrically determined after perchloric acid extraction.[62] The BsFtsZ concentration was determined after subtracting the nucleotide contribution, employing a calculated extinction coefficient 2560 M^{-1} cm^{-1} at 280 nm (2 Tyr, 0 Trp residues) in 6 M guanidinium chloride. FtsZ was assembled in HEPES buffer plus 10 mM $MgCl_2$ and 1 mM GTP or 0.1 mM GMPCPP at 25ºC. FtsZ assembly was monitored by light scattering.

4.2.2. Preparation of cross-linked FtsZ polymers

FtsZ (10-15 µM) was assembled in HEPES buffer, 10 mM $MgCl_2$, 50 µM GMPCPP at 25 ºC for 10 min and then 0.15% (v/v) glutaraldehyde (distilled grade for microscopy, TAAB laboratories, UK) was added to the solution which was incubated at 25 ºC for 10 min more. (This was the minimal glutaraldehyde concentration determined to stabilize FtsZ polymers specifically binding probe UCM01). The remains of the cross-linking agent were quenched by adding 60 mM $NaBH_4$, the sample was incubated on ice for 10 min and degassed. Cross-linked polymers were centrifuged for 10 min at 8200*g* (5000 rpm) and 4 ºC in 15 mL Falcon tubes employing a Rotina 380R (Hettich) centrifuge, the supernatant was removed, and the pellet was re-suspended in the same volume of HEPES buffer, 10 mM $MgCl_2$, containing 5 µM GMPCPP.

4.2.3. Stoichiometry and affinity of binding of the fluorescent probes to FtsZ polymers

The stoichiometry of binding of (*R*)-**4** to stabilized FtsZ polymers was measured using a centrifugation assay. 10 µM FtsZ was polymerized at 25 ºC in HEPES buffer, 10 mM $MgCl_2$, 2% DMSO, 0.1 mM GMPCPP at 25 ºC in the presence of different probe concentrations, in a final volume of 0.1 mL. Samples were then centrifuged for 20 min at 100000 rpm and 25 ºC in a TLA-100 rotor. After centrifugation the supernatant was carefully withdrawn, and the pellets were resuspended in the same volume of buffer. The concentration of free probe was determined spectrophotometrically in the supernatant, employing an extinction coefficient ε_{483} = 25400 $M^{-1}cm^{-1}$ for (*R*)-**4** and the concentration of probe bound to FtsZ was calculated as the difference of the known total concentration of probe minus the free concentration. To calculate the FtsZ polymer concentration, 5 µL of the resuspended pellet were applied to SDS-12% polyacrylamide gels, stained with Coomassie blue, scanned with a CS-800 calibrated densitometer (BioRad) and the protein bands quantified with Quantity One software (BioRad).

Binding affinity of the probes to FtsZ was measured by the increase in anisotropy of the probe. Fixed concentrations of the probes (3 µM) were titrated with different FtsZ polymer concentrations (0-40 µM) in HEPES buffer with Mg^{2+}, to obtain the anisotropy increment, Δr_{max}, corresponding to the bound probe. The increase in anisotropy was plotted against FtsZ polymer concentration (calculated by subtracting from the total protein concentration the critical concentration for polymerization under the same conditions) and iteratively least-squares fitted with an isotherm of binding to one site. The estimated values of Δr_{max} were used to approximate the free FtsZ concentrations, and these new values were employed again, until an unchanging Δr_{max} value was obtained. The convergent data were used to calculate the binding constant of the fluorescent probe to FtsZ polymers

4.2.4. FtsZ affinity of ligands competing with the fluorescent probes (*S*)-**1** and (*R*)-**4**

The fluorescence anisotropy values of the different probes were acquired with a Fluoromax-4 (Horiba Jobin Yvon) photon-counting L-format spectrofluorometer using 2x10

mm cells, employing the maximum excitation and emission wavelength for each probe with 2- and 5-nm bandwidths, respectively. Competition assays were performed by measuring, through the decrease in fluorescence anisotropy, the displacement of the florescent probes from stabilized FtsZ polymers. Increasing concentrations of competing ligand were added to mixtures of cross-linked FtsZ polymers 7-8 µM FtsZ polymers with probe (*S*)-**1** (3 µM), or 2-3 µM FtsZ polymers with (*R*)-**4** (3 µM). HEPES buffer, with 10 mM $MgCl_2$ and 0.1 mM GMPCPP was employed, final volume 0.5 mL, and the anisotropy measured at 25 ºC.

4.2.5. Bacterial division phenotype

B. subtilis 168 cells were grown in cation adjusted Mueller-Hinton broth (CAMHB) at 37 °C to an absorbance 0.1-0.2 at 600 nm and then the culture was divided into new flasks containing the compound at the desired concentration. After 3 h of incubation cells were directly visualized by phase-contrast light microscopy.[63]

Fluorescent microscopy. Experiments for cell visualization with the fluorescent probes targeting the PC-binding site: *B. subtilis* 168 cells were grown in cation adjusted Mueller-Hinton broth (CAMHB) at 37 °C to an absorbance 0.1-0.2 at 600 nm then the fluorescent probes (25 µM to 100 µM) was added and after 1.5 hour of incubation, 10 µL of the sample was pipetted onto microscope slides, covered, and visualized through a 100X PlanApochromatic objective with a Zeiss Axioplan fluorescence microscope equipped with a Hamamatsu 4742-95 CCD camera. Membranes were stained with FM4-64 (1 µg/mL), which were added to the cells prior to visualization.[63]

Experiments for cell visualization with the synthesized compounds targeting the PC-binding site: A colony of *B. subtilis* strain SU570 (168 trpC2 ftsZ:ftsZ-gfp-Spec),[64,65] kindly donated by Dr. Elisabeth J. Harry, was resuspended in antibiotic medium no. 3 (Pennassay broth, Becton Dickinson) with 50 µg/mL spectinomycin and grown at 30 °C to an absorbance of 0.2 at 600 nm. Samples of the culture were mixed with an equal volume of medium containing twice the final desired concentration of compound. Aliquots (10 µL) were harvested after 1.5 h of incubation, combined with an equal volume of prewarmed Pennassay broth containing ~1% w/v agarose, and 10 µL of these samples were pipetted onto microscope slides, covered, and visualized through the previously described fluorescence microscope. Nucleoids were stained with 4,6-diamino-2-phenylindole (DAPI, 0.25 µg/mL) and membranes with FM4-64 (1 µg/mL), which were added to the cells prior to visualization.[63]

4.2.6. Antibacterial activity: MIC determination

MIC values for each compound against *B. subtilis* 168 were determined in cation-adjusted Mueller-Hinton II broth (CAMHB) (Becton Dickinson) at 37 ºC with shaking, by the broth macrodilution method according to the recommendations of the Clinical and Laboratory Standards Institute (CLSI) for which the MIC was defined as the lowest concentration inhibiting growth determined by absorbance at 600 nm.[66]

MIC values against *S. aureus* Mu50/ ATCC 700699: overnight cultures of bacteria were diluted in fresh brain-heart broth (BHB) to optical density at 600 nm, (OD_{600}) = 0.01, and 100 µL were taken to in Nunclon 96-well plates with round-shaped bottoms with 1 µL of the corresponding DMSO stock solutions of each compound at dilution ranges from 0.4 to 45 mg/L with 2% final concentration of DMSO. The samples were incubated for 12 h at 37 °C and the OD_{600} were obtained for MIC calculation. All experiments were conducted at least in triplicates, and DMSO served as control.

4.2.7. Resistant mutants of *S. aureus* Mu50

Isolation of FtsZ inhibitor resistant mutants was performed by plating 100 µL of *S. aureus* Mu50 culture (~10^8 cells/mL) into CAMHB supplemented with the corresponding FtsZ inhibitor at a concentration higher than the MIC and 2% DMSO. The plates were incubated for 24 h at 37 °C, and several colonies were picked for further analysis. Genomic DNA was extracted from each colony using the Wizard Genomic DNA Purification Kit (Promega) and was used in PCR reactions for amplification of *ftsZ* using the primers SaFtsZ-F (5' TGGCCAATAAAACTAGGAG 3') and SaFtsZ-R (5' TGTTATCTGATGATTTGTGTTG 3'). The resulting PCR products were purified using the DNA gel extraction kit (Cultek) and sequenced (Macrogen Inc. Spain). Sequence analysis was performed with BLAST (NCBI).

REFERENCES

5. REFERENCES

1. Attaibi, M.; den Blaauwen, T. An updated model of the divisome: regulation of the septal peptidoglycan synthesis machinery by the divisome. *Int. J. Mol. Sci.* **2022**, *23*, 3537.

2. den Blaauwen, T.; Hamoen, L. W.; Levin, P. A. The divisome at 25: the road ahead. *Curr. Opin. Microbiol.* **2017**, *36*, 85-94.

3. Oliva, M. A.; Trambaiolo, D.; Löwe, J. Structural insights into the conformational variability of FtsZ. *J. Mol. Biol.* **2007**, *373*, 1229-1242.

4. Adams, D. W.; Errington, J. Bacterial cell division: assembly, maintenance and disassembly of the Z ring. *Nat. Rev. Microbiol.* **2009**, *7*, 642-653.

5. Bi, E.; Lutkenhaus, J. FtsZ ring structure associated with division in *Escherichia coli*. *Nature* **1991**, *354*, 161-164.

6. Ortiz, C.; Natale, P.; Cueto, L.; Vicente, M. The keepers of the ring: regulators of FtsZ assembly. *FEMS Microbiol. Rev.* **2016**, *40*, 57-67.

7. Tripathy, S.; Sahu, S. K. FtsZ inhibitors as a new genera of antibacterial agents. *Bioorganic Chem.* **2019**, *91*, 103169.

8. Anderson, D. E.; Gueiros-Filho, F. J.; Erickson, H. P. Assembly dynamics of FtsZ rings in *Bacillus subtilis* and *Escherichia coli* and effects of FtsZ-regulating proteins. *J. Bacteriol.* **2004**, *186*, 5775-5781.

9. Bisson-Filho, A. W.; Hsu, Y. P.; Squyres, G. R.; Kuru, E.; Wu, F.; Jukes, C.; Sun, Y.; Dekker, C.; Holden, S.; VanNieuwenhze, M. S.*; et al.* Treadmilling by FtsZ filaments drives peptidoglycan synthesis and bacterial cell division. *Science* **2017**, *355*, 739-743.

10. Yang, X.; Lyu, Z.; Miguel, A.; McQuillen, R.; Huang, K. C.; Xiao, J. GTPase activity-coupled treadmilling of the bacterial tubulin FtsZ organizes septal cell wall synthesis. *Science* **2017**, *355*, 744-747.

11. Squyres, G. R.; Holmes, M. J.; Barger, S. R.; Pennycook, B. R.; Ryan, J.; Yan, V. T.; Garner, E. C. Single-molecule imaging reveals that Z-ring condensation is essential for cell division in *Bacillus subtilis*. *Nat. Microbiol.* **2021**, *6*, 553-562.

12. Silber, N.; Matos de Opitz, C. L.; Mayer, C.; Sass, P. Cell division protein FtsZ: from structure and mechanism to antibiotic target. *Future Microbiol.* **2020**, *15*, 801-831.

13. Barrows, J. M.; Goley, E. D. FtsZ dynamics in bacterial division: What, how, and why? *Curr. Opin. Cell Biol.* **2021**, *68*, 163-172.

14. McQuillen, R.; Xiao, J. Insights into the structure, function, and dynamics of the bacterial cytokinetic FtsZ-ring. *Annu. Rev. Biophys.* **2020**, *49*, 309-341.

15. Lowe, J.; Amos, L. A. Crystal structure of the bacterial cell-division protein FtsZ. *Nature* **1998**, *391*, 203-206.

16. Nogales, E.; Wolf, S. G.; Downing, K. H. Structure of the alpha beta tubulin dimer by electron crystallography. *Nature* **1998**, *391*, 199-203.

17. Erickson, H. P. FtsZ, a prokaryotic homolog of tubulin. *Cell* **1995**, *80*, 367-370.

18. Läppchen, T.; Pinas, V. A.; Hartog, A. F.; Koomen, G. J.; Schaffner-Barbero, C.; Andreu, J. M.; Trambaiolo, D.; Löwe, J.; Juhem, A.; Popov, A. V.*; et al.* Probing FtsZ and tubulin with C8-substituted GTP analogs reveals differences in their nucleotide binding sites. *Chem. Biol.* **2008**, *15*, 189-199.

19. Fujita, J.; Maeda, Y.; Mizohata, E.; Inoue, T.; Kaul, M.; Parhi, A. K.; LaVoie, E. J.; Pilch, D. S.; Matsumura, H. Structural flexibility of an inhibitor overcomes drug resistance mutations in *Staphylococcus aureus* FtsZ. *ACS Chem. Biol.* **2017**, *12*, 1947-1955.

20. Steinmetz, M. O.; Prota, A. E. Microtubule-targeting agents: strategies to hijack the cytoskeleton. *Trends Cell Biol.* **2018**, *28*, 776-792.

21. Lowe, J. Crystal structure determination of FtsZ from *Methanococcus jannaschii*. *J. Struct. Biol.* **1998**, *124*, 235-243.

22. Scheffers, D. J.; de Wit, J. G.; den Blaauwen, T.; Driessen, A. J. M. GTP hydrolysis of cell division protein FtsZ: evidence that the active site is formed by the association of monomers. *Biochemistry* **2002**, *41*, 521-529.

23. Martin-Galiano, A. J.; Buey, R. M.; Cabezas, M.; Andreu, J. M. Mapping flexibility and the assembly switch of cell division protein FtsZ by computational and mutational approaches. *J. Biol. Chem.* **2010**, *285*, 22554-22565.

24. Kusuma, K. D.; Payne, M.; Ung, A. T.; Bottomley, A. L.; Harry, E. J. FtsZ as an antibacterial target: status and guidelines for progressing this avenue. *ACS Infect. Dis.* **2019**, *5*, 1279-1294.

25. Casiraghi, A.; Suigo, L.; Valoti, E.; Straniero, V. Targeting bacterial cell division: a binding site-centered approach to the most promising inhibitors of the essential protein FtsZ. *Antibiotics-Basel* **2020**, *9*.

26. Han, H.; Wang, Z.; Li, T.; Teng, D.; Mao, R.; Hao, Y.; Yang, N.; Wang, X.; Wang, J. Recent progress of bacterial FtsZ inhibitors with a focus on peptides. *Febs J.* **2021**, *288*, 1091-1106.

27. Pradhan, P.; Margolin, W.; Beuria, T. K. Targeting the Achilles heel of FtsZ: the interdomain cleft. *Front. Microbiol.* **2021**, *12*, 732796.

28. Andreu, J. M.; Huecas, S.; Araújo-Bazán, L.; Vázquez-Villa, H.; Martín-Fontecha, M. The search for antibacterial inhibitors targeting cell division protein FtsZ at its nucleotide and allosteric binding sites. *Biomedicines* **2022**, *10*, 1825.

29. Stokes, N. R.; Sievers, J.; Barker, S.; Bennett, J. M.; Brown, D. R.; Collins, I.; Errington, V. M.; Foulger, D.; Hall, M.; Halsey, R.*; et al.* Novel inhibitors of bacterial cytokinesis identified by a cell-based antibiotic screening assay. *J. Biol. Chem.* **2005**, *280*, 39709-39715.

30. Margalit, D. N.; Romberg, L.; Mets, R. B.; Hebert, A. M.; Mitchison, T. J.; Kirschner, M. W.; RayChaudhuri, D. Targeting cell division: small-molecule inhibitors of FtsZ GTPase perturb cytokinetic ring assembly and induce bacterial lethality. *Proc. Natl. Acad. Sci. U. S. A.* **2004**, *101*, 11821-11826.

31. Läppchen, T.; Hartog, A. F.; Pinas, V. A.; Koomen, G. J.; den Blaauwen, T. GTP analogue inhibits polymerization and GTPase activity of the bacterial protein FtsZ without affecting its eukaryotic homologue tubulin. *Biochemistry* **2005**, *44*, 7879-7884.

32. Schaffner-Barbero, C.; Gil-Redondo, R.; Ruiz-Avila, L. B.; Huecas, S.; Läppchen, T.; den Blaauwen, T.; Diaz, J. F.; Morreale, A.; Andreu, J. M. Insights into nucleotide recognition by cell division protein FtsZ from a *mant*-GTP competition assay and molecular dynamics. *Biochemistry* **2010**, *49*, 10458-10472.

33. Ruiz-Avila, L. B.; Huecas, S.; Artola, M.; Vergoñós, A.; Ramírez-Aportela, E.; Cercenado, E.; Barasoain, I.; Vázquez-Villa, H.; Martín-Fontecha, M.; Chacón, P.*; et al.* Synthetic inhibitors of bacterial cell division targeting the GTP-binding site of FtsZ. *ACS Chem. Biol.* **2013**, *8*, 2072-2083.

34. Artola, M.; Ruiz-Avila, L. B.; Vergoñós, A.; Huecas, S.; Araujo-Bazán, L.; Martín-Fontecha, M.; Vázquez-Villa, H.; Turrado, C.; Ramírez-Aportela, E.; Hoegl, A.*; et al.* Effective GTP-replacing FtsZ inhibitors and antibacterial mechanism of action. *ACS Chem. Biol.* **2015**, *10*, 834-843.

35. Plaza, A.; Keffer, J. L.; Bifulco, G.; Lloyd, J. R.; Bewley, C. A. Chrysophaentins A-H, antibacterial bisdiarylbutene macrocycles that inhibit the bacterial cell division protein FtsZ. *J. Am. Chem. Soc.* **2010**, *132*, 9069-9077.

36. Keffer, J. L.; Hammill, J. T.; Lloyd, J. R.; Plaza, A.; Wipf, P.; Bewley, C. A. Geographic variability and anti-staphylococcal activity of the chrysophaentins and their synthetic fragments. *Mar Drugs* **2012**, *10*, 1103-1125.

37. Ohashi, Y.; Chijiiwa, Y.; Suzuki, K.; Takahashi, K.; Nanamiya, H.; Sato, T.; Hosoya, Y.; Ochi, K.; Kawamura, F. The lethal effect of a benzamide derivative, 3-methoxybenzamide, can be suppressed by mutations within a cell division gene, ftsZ, in *Bacillus subtilis*. *J. Bacteriol.* **1999**, *181*, 1348-1351.

38. Brown, D. R. C., I.; Czaplewski, L. G; Haydon, D. J. Antibacterial agents. WO2007/107758 A1, 2007.

39. Czaplewski, L. G.; Collins, I.; Boyd, E. A.; Brown, D.; East, S. P.; Gardiner, M.; Fletcher, R.; Haydon, D. J.; Henstock, V.; Ingram, P.*; et al.* Antibacterial alkoxybenzamide inhibitors of the essential bacterial cell division protein FtsZ. *Bioorg. Med. Chem. Lett.* **2009**, *19*, 524-527.

40. Haydon, D. J.; Bennett, J. M.; Brown, D.; Collins, I.; Galbraith, G.; Lancett, P.; Macdonald, R.; Stokes, N. R.; Chauhan, P. K.; Sutariya, J. K.*; et al.* Creating an antibacterial with in vivo efficacy: synthesis and characterization of potent inhibitors of the bacterial cell division protein FtsZ with improved pharmaceutical properties. *J. Med. Chem.* **2010**, *53*, 3927-3936.

41. Andreu, J. M.; Schaffner-Barbero, C.; Huecas, S.; Alonso, D.; Lopez-Rodriguez, M. L.; Ruiz-Avila, L. B.; Núñez-Ramírez, R.; Llorca, O.; Martín-Galiano, A. J. The antibacterial cell division inhibitor PC190723 is an FtsZ polymer-stabilizing agent that induces filament assembly and condensation. *J. Biol. Chem.* **2010**, *285*, 14239-14246.

42. Haydon, D. J.; Stokes, N. R.; Ure, R.; Galbraith, G.; Bennett, J. M.; Brown, D. R.; Baker, P. J.; Barynin, V. V.; Rice, D. W.; Sedelnikova, S. E.*; et al.* An inhibitor of FtsZ with potent and selective anti-staphylococcal activity. *Science* **2008**, *321*, 1673-1675.

43. Stokes, N. R.; Baker, N.; Bennett, J. M.; Berry, J.; Collins, I.; Czaplewski, L. G.; Logan, A.; Macdonald, R.; MacLeod, L.; Peasley, H.*; et al.* An improved small-molecule inhibitor of FtsZ with superior in vitro potency, drug-like properties, and in vivo efficacy. *Antimicrob. Agents Chemother.* **2013**, *57*, 317-325.

44. Kaul, M.; Mark, L.; Zhang, Y.; Parhi, A. K.; Lyu, Y. L.; Pawlak, J.; Saravolatz, S.; Saravolatz, L. D.; Weinstein, M. P.; LaVoie, E. J.*; et al.* TXA709, an FtsZ-targeting benzamide prodrug with improved pharmacokinetics and enhanced in vivo efficacy against methicillin-resistant *Staphylococcus aureus*. *Antimicrob. Agents Chemother.* **2015**, *59*, 4845-4855.

45. Lepak, A. J.; Parhi, A.; Madison, M.; Marchillo, K.; VanHecker, J.; Andes, D. R. In vivo pharmacodynamic evaluation of an FtsZ inhibitor, TXA-709, and its active metabolite, TXA-707, in a murine neutropenic thigh infection model. *Antimicrob. Agents Chemother.* **2015**, *59*, 6568-6574.

46. *Taxis Pharmaceuticals Pipeline*. 2020. https://www.taxispharma.com/research-development/our-pipeline/ (accessed Dec 2022).

47. Tan, C. M.; Therien, A. G.; Lu, J.; Lee, S. H.; Caron, A.; Gill, C. J.; Lebeau-Jacob, C.; Benton-Perdomo, L.; Monteiro, J. M.; Pereira, P. M.*; et al.* Restoring methicillin-resistant *Staphylococcus aureus* susceptibility to beta-lactam antibiotics. *Sci. Transl. Med.* **2012**, *4*, 126ra135-126ra135.

48. Elsen, N. L.; Lu, J.; Parthasarathy, G.; Reid, J. C.; Sharma, S.; Soisson, S. M.; Lumb, K. J. Mechanism of action of the cell-division inhibitor PC190723: modulation of FtsZ assembly cooperativity. *J. Am. Chem. Soc.* **2012**, *134*, 12342-12345.

49. Artola, M.; Ruíz-Avila, L. B.; Ramírez-Aportela, E.; Martínez, R. F.; Araujo-Bazán, L.; Vázquez-Villa, H.; Martín-Fontecha, M.; Oliva, M. A.; Martín-Galiano, A. J.; Chacón, P.*; et al.* The structural assembly switch of cell division protein FtsZ probed with fluorescent allosteric inhibitors. *Chem. Sci.* **2017**, *8*, 1525-1534.

50. Díaz, J. F.; Buey, R. M. Characterizing ligand-microtubule binding by competition methods. *Methods Mol. Med.* **2007**, *137*, 245-260.

51. Śliwińska, A.; Zwierzak, A. Regioselective aminobromination of terminal alkenes. *Tetrahedron* **2003**, *59*, 5927-5934.

52. Garcin, E. D.; Arvai, A. S.; Rosenfeld, R. J.; Kroeger, M. D.; Crane, B. R.; Andersson, G.; Andrews, G.; Hamley, P. J.; Mallinder, P. R.; Nicholls, D. J.*; et al.* Anchored plasticity opens doors for selective inhibitor design in nitric oxide synthase. *Nat. Chem. Biol.* **2008**, *4*, 700-707.

53. Bartoli, G.; Bosco, M.; Carlone, A.; Locatelli, M.; Melchiorre, P.; Sambri, L. Asymmetric catalytic synthesis of enantiopure N-protected 1,2-amino alcohols. *Org. Lett.* **2004**, *6*, 3973-3975.

54. Huecas, S.; Araujo-Bazan, L.; Ruiz, F. M.; Ruiz-Avila, L. B.; Martinez, R. F.; Escobar-Pena, A.; Artola, M.; Vazquez-Villa, H.; Martin-Fontecha, M.; Fernandez-Tornero, C.*; et al.* Targeting the FtsZ allosteric binding site with a novel fluorescence polarization screen, cytological and structural approaches for antibacterial discovery. *J. Med. Chem.* **2021**, *64*, 5730-5745.

55. Anderson, D. E.; Kim, M. B.; Moore, J. T.; O'Brien, T. E.; Sorto, N. A.; Grove, C. I.; Lackner, L. L.; Ames, J. B.; Shaw, J. T. Comparison of small molecule inhibitors of the bacterial cell division protein FtsZ and identification of a reliable cross-species inhibitor. *ACS Chem. Biol.* **2012**, *7*, 1918-1928.

56. Bhattacharya, A.; Jindal, B.; Singh, P.; Datta, A.; Panda, D. Plumbagin inhibits cytokinesis in *Bacillus subtilis* by inhibiting FtsZ assembly--a mechanistic study of its antibacterial activity. *Febs J.* **2013**, *280*, 4585-4599.

57. Hwang, D.; Lim, Y.-H. Resveratrol antibacterial activity against *Escherichia coli* is mediated by Z-ring formation inhibition via suppression of FtsZ expression. *Sci. Rep.* **2015**, *5*, 10029.

58. Sun, N.; Zheng, Y.-Y.; Du, R.-L.; Cai, S.-Y.; Zhang, K.; So, L.-Y.; Cheung, K.-C.; Zhuo, C.; Lu, Y.-J.; Wong, K.-Y. New application of tiplaxtinin as an effective FtsZ-targeting chemotype for an antimicrobial study. *MedChemComm* **2017**, *8*, 1909-1913.

59. Qiang, S.; Wang, C.; Venter, H.; Li, X.; Wang, Y.; Guo, L.; Ma, R.; Ma, S. Synthesis and biological evaluation of novel FtsZ-targeted 3-arylalkoxy-2,6-difluorobenzamides as potential antimicrobial agents. *Chem. Biol. Drug Des.* **2016**, *87*, 257-264.

60. Haneda, S.; Okui, A.; Ueba, C.; Hayashi, M. An efficient synthesis of 2-arylimidazoles by oxidation of 2-arylimidazolines using activated carbon–O_2 system and its application to palladium-catalyzed Mizoroki–Heck reaction. *Tetrahedron* **2007**, *63*, 2414-2417.

61. Ruiz-Avila, L. B.; Huecas, S.; Artola, M.; Vergoñós, A.; Ramírez-Aportela, E.; Cercenado, E.; Barasoain, I.; Vázquez-Villa, H.; Martín-Fontecha, M.; Chacón, P.*; et al.* Synthetic inhibitors of bacterial cell division targeting the GTP-binding site of FtsZ. *ACS Chem. Biol.* **2013**, *8*, 2072-2083.

62. Rivas, G.; Lopez, A.; Mingorance, J.; Ferrandiz, M. J.; Zorrilla, S.; Minton, A. P.; Vicente, M.; Andreu, J. M. Magnesium-induced linear self-association of the FtsZ bacterial cell division protein monomer - The primary steps for FtsZ assembly. *J. Biol. Chem.* **2000**, *275*, 11740-11749.

63. Araújo-Bazán, L.; Ruiz-Avila, L. B.; Andreu, D.; Huecas, S.; Andreu, J. M. Cytological profile of antibacterial FtsZ inhibitors and synthetic peptide MciZ. *Front. Microbiol.* **2016**, *7*.

64. Levin, P. A.; Kurtser, I. G.; Grossman, A. D. Identification and characterization of a negative regulator of FtsZ ring formation in *Bacillus subtilis*. *Proc. Natl. Acad. Sci. USA* **1999**, *96*, 9642-9647.

65. Strauss, M. P.; Liew, A. T. F.; Turnbull, L.; Whitchurch, C. B.; Monahan, L. G.; Harry, E. J. 3D-SIM super resolution microscopy reveals a bead-like arrangement for FtsZ and the division machinery: implications for triggering cytokinesis. *Plos Biol.* **2012**, *10*, e1001389.

66. Nilsson, B. M.; Ringdahl, B.; Hacksell, U. Derivatives of the muscarinic agent *N*-methyl-*N*-(1-methyl-4-pyrrolidino-2-butynyl)acetamide. *J. Med. Chem.* **1988**, *31*, 577-582.